NASA CR-54674

00024

N.T.

LIQUID MERCURY CATHODE ELECTRON-BOMBARDMENT ION THRUSTERS

CONTRACT NO. NAS 3-6262

FACILITY FORM 602

N68-26310 (ACCESSION NUMBER) (THRU)

111 (PAGES) 1 (CODE)

CR-54674 (NASA CR OR TMX OR AD NUMBER) 28 (CATEGORY)

prepared for

NATIONAL AERONAUTICS AND SPACE ADMINISTRATION

GPO PRICE $ _____

CFSTI PRICE(S) $ _____

Hard copy (HC) 3.00

Microfiche (MF) .65

ff 653 July 65

HUGHES RESEARCH LABORATORIES
A DIVISION OF HUGHES AIRCRAFT COMPANY
3011 MALIBU CANYON ROAD
MALIBU, CALIFORNIA 90265

JUN 1968
RECEIVED
NASA STI FACILITY
INPUT BRANCH

NOTICE

This report was prepared as an account of Government sponsored work. Neither the United States, nor the National Aeronautics and Space Administration (NASA), nor any person acting on behalf of NASA:

A.) Makes any warranty or representation, expressed or implied, with respect to the accuracy, completeness, or usefulness of the information contained in this report, or that the use of any information, apparatus, method, or process disclosed in this report may not infringe privately owned rights; or

B.) Assumes any liabilities with respect to the use of, or for damages resulting from the use of any information, apparatus, method or process disclosed in this report.

As used above, "person acting on behalf of NASA" includes any employee or contractor of NASA, or employee of such contractor, to the extent that such employee or contractor of NASA, or employee of such contractor prepares, disseminates, or provides access to, any information pursuant to his employment or contract with NASA, or his employment with such contractor.

Requests for copies of this report should be referred to

National Aeronautics and Space Administration
Office of Scientific and Technical Information
Attention: AFSS-A
Washington, D.C. 20546

SUMMARY REPORT

LIQUID-MERCURY CATHODE ELECTRON-BOMBARDMENT ION THRUSTERS

by

W. O. Eckhardt, H. J. King, J. A. Snyder, J. W. Ward,
G. Hagen, W. D. Myers, and R. C. Knechtli

prepared for

NATIONAL AERONAUTICS AND SPACE ADMINISTRATION

Contract NAS 3-6262
1 August 1964 through 31 October 1966

Technical Management
NASA-Lewis Research Center
Cleveland, Ohio
Spacecraft Technology Division
R. R. Nicholls

HUGHES RESEARCH LABORATORIES
A Division of Hughes Aircraft Company
3011 Malibu Canyon Road
Malibu, California

PRECEDING PAGE BLANK NOT FILMED.

TABLE OF CONTENTS

LIST OF ILLUSTRATIONS

I. INTRODUCTION AND SUMMARY

During the period covered by this report the LM cathode invented* at Hughes Research Laboratories as a solution to the cathode life problem of electron-bombardment ion thrusters has been developed from a crude laboratory device+ to a highly efficient and reliable unit. (The LM cathode is basically a gravity-independent, force-fed version of the mercury pool cathode used for many years in mercury rectifiers and other discharge tubes.) Furthermore, the LM cathode has been integrated successfully into complete Kaufman-type thrusters, and the cathode durability has been demonstrated by a life test which has exceeded 5250 hours, with over 4000 hours of in-thruster operation. An ion source efficiency‡ of 75% at a specific impulse of 6400 sec (67% at 3400 sec) was reliably attained. Automatic startup and closed-loop operation have been demonstrated during the last 1000 hours of the life test with a prototype mercury feed system which is suitable for use in a flight-type propulsion system. For the last 500 hour test increment the thruster was also equipped with an LM cathode neutralizer.

The most important test results can be summarized as follows:

1. No cathode degradation after > 5250 hours of operation
2. Absolute stability of thruster characteristics over > 4000 hours of test duration
3. Extrapolated accelerator lifetime of > 10,000 hours
4. Complete insensitivity of thruster and cathode to intermittent operation and exposure to air (even by catastrophic vacuum failure)
5. Demonstration of 85% mass utilization at a power expenditure of 393 eV/Hg ion.

---

* W. O. Eckhardt, Liquid-Metal Arc Cathode; patent applied for.

\+ Described in W. O. Eckhardt, J. A. Snyder, H. J. King, and R. C. Knechtli, "A New Cathode for Mercury Electron-Bombardment Thrusters," AIAA Paper No. 64-690, Philadelphia, Pa., 1964; and in Summary Report, Contract NAS 3-4118.

‡ The ion source efficiency is defined as the thruster efficiency, excluding accelerator drain power, feed system power, neutralizer power, and magnet power.

It should be noted that this thruster performance was achieved during the life test extensions of the contract without the support of a systematic performance improvement program, and that experimental and theoretical results obtained since the termination of the life test have led to further substantial increases in mass utilization and power efficiency.

In parallel with the main effort a study of the LM cathode electron-bombardment discharge was carried out, with results which have proved to be of benefit to electron-bombardment thrusters in general.

II. LM CATHODES

A. Principle of the LM Cathode

With all liquid-metal cathodes, the discharge is operated in the liquid-metal pool arc mode to cause electrons to be emitted from the surface. In addition to emitting electrons at the arc spot, the liquid metal surface also emits atoms of the liquid metal, as a result of local heating (and possibly sputtering) by ion bombardment and by radiation from the dense spot plasma. An additional efflux of atoms from the liquid results from evaporation from the inactive part of the cathode surface.

Our force-fed version of the liquid-metal cathode is gravity independent. The volume of liquid metal which is exposed to the discharge is sufficiently small that it is able to maintain its integrity by cohesive forces, and it is held in place by adhesive attachment to the pool-keeping structure.* In the ion thruster application of this cathode, the removal of metal atoms from the liquid metal surface is used to feed the expellant into the discharge chamber. The most favorable results were obtained with pool-keeping structures of divergent-nozzle geometry, as shown in Fig. 1. A major advantage of the divergent geometry is that it automatically stabilizes the liquid metal surface at that level in the pool-keeping structure at which the rate of removal of metal atoms from the pool surface is exactly balanced by the expellant feed rate to the pool, which is set at the value desired for thruster operation. Should the surface move downstream of its equilibrium position, the increased area of the pool surface results in an increased rate of evaporation of metal atoms, thereby returning the exposed surface toward its equilibrium position. Should the level recede from its equilibrium value, the resultant decreased rate of evaporation likewise acts to stabilize the level.

If surface evaporation constitutes the major mechanism for removal of metal atoms from the pool surface, both the electron and the atom flux emanating from an LM cathode are separately and independently variable so long as the cathode is operated at a constant temperature. The electron current is set to the desired value by adjusting the power supply which drives the discharge. The atomic flux is set independently to its desired value, which is equal to the liquid metal feed rate. In the ion thruster application, the ratio K_e/K_a of electron to atom flux can be set to that value which optimizes the performance of the entire thruster system.

---

* For brevity, we refer to this gravity-independent, force-fed liquid-metal cathode in general as the Liquid-Metal or LM cathode; for reference to a particular liquid metal, its chemical symbol is added in parenthesis, e.g., LM (Hg) cathode, in the case of mercury.

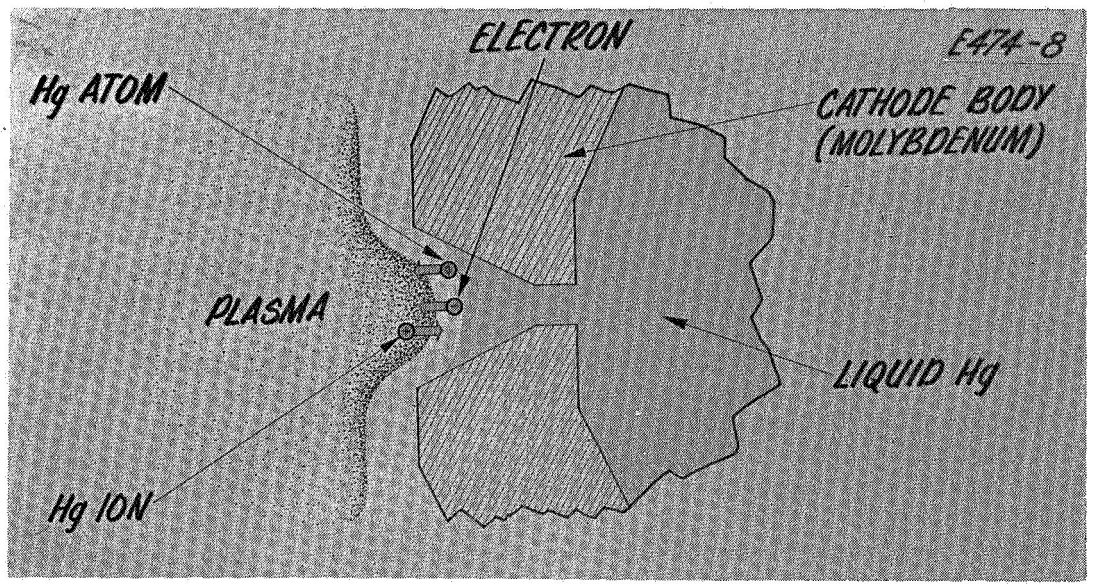

Fig. 1. Particle flow at surface of LM (Hg) cathode.

In order to optimize the usefulness of the LM cathode for electron-bombardment thrusters, the possible performance-limiting mechanisms had to be first identified and then eliminated. The following problems were found to require attention: (a) the necessity of avoiding a thermal instability at high current and low heat rejection rates, (b) the reduction of feed rate fluctuations, and (c) the prevention of arc spot interaction with the magnetic field in the discharge chamber. These problems and their solutions are described in detail in the following sections.

The cathode designs which evolved following the elimination of the detrimental effects (a), (b), and (c) have yielded electron-to-atom emission ratios one order of magnitude above those of conventional pool cathodes and far exceeding those required for optimum thruster operation. Thus it became possible to use the LM cathode not only as a long-life cathode in the main discharge chamber, but also as a sputter-resistant and efficient neutralizer.

B. Identification of Performance-Limiting Mechanisms

1. Temperature-Area Dependence

An LM cathode will be stable against small perturbations of feed rate or discharge current if the total evaporation rate decreases when the exposed liquid-metal surface decreases (and vice versa). However, this correlation (decrease of the total evaporation rate resulting from a decrease of the exposed area) will prevail only if the effect of a decrease of the exposed surface area is not overcompensated by a large increase in evaporation rate per unit area. Therefore, the stability requirement means that any change in surface temperature which accompanies a change in surface area must be either in the favorable direction or sufficiently small.

It should be recalled that the arc spot changes its position very rapidly along the circumference of the exposed liquid-metal surface, spending approximately equal times at any portion of this circumference.* Therefore, the density of thermal power flow into the exposed liquid-metal surface (and, consequently, its temperature and evaporation rate per unit area) will increase when the perimeter of the exposed liquid-metal surface area decreases. This means that the temperature-area dependence is in the unfavorable direction and, if not kept sufficiently small by a suitable

* In the case of mercury, this statement holds within the range of the ratio (cathode current)/(length of circumference of exposed mercury surface), which is of interest for thruster applications.

thermal design, will render the cathode unstable.

A related problem is that of thermal overload. Under operating conditions in which the current is too high for a given cathode or, equivalently, the heat rejection is too low for a given current, it has been observed experimentally that the liquid level is driven to zero and the arc extinguishes. Temperature measurements with an annular thermocouple surrounding the pool-keeping structure fully verified that this instability is indeed of thermal origin.

2. Feed Rate Fluctuations

Even when the thermal design of a liquid-metal cathode permits stable operation in the presence of small perturbations of feed rate or discharge current, the permissible amplitude of these perturbations is limited by the range of variability of the exposed liquid-metal surface area which the particular cathode geometry can accommodate.

Visual observation of an LM(Hg) cathode with a nozzle geometry as shown in Fig. 2 (operated within its range of thermal stability) showed that, under various operating conditions, rather regular short-term fluctuations of the mercury surface position indeed existed with an amplitude which was not contained by the nozzle cone of 0.76 mm maximum diameter. It was decided that this problem should be approached both by increasing the amplitude which can be contained by the nozzle geometry and by locating and reducing the effects causing the fluctuation.

A possible cause of short-term fluctuations was seen in the existence of a large plenum chamber between flow impedance and orifice (see Fig. 2). Especially in conjunction with a cathode operating close to the limit of thermal stability, the liquid metal contained in the plenum volume will change its temperature, and hence its density, as a function of the surface position in the cone, as discussed above. Because of the direction of the correlation between surface position, temperature, and liquid metal density, this situation can give rise to a nonlinear oscillation of the surface position. Such an oscillation is equivalent to a feed rate fluctuation and can exist even when the actual feed rate through the flow impedance remains constant.

3. Magnetic Field Interaction

The arc spot behavior of an LM cathode can be influenced considerably by the presence of an axial magnetic field, as was revealed by visual observation of an LM cathode operating in a Penning discharge chamber. A magnetic field of sufficient intensity causes the arc spot pattern to rotate around the circumference of the exposed mercury surface. When the mercury surface is located in a divergent nozzle, the centrifugal force acting on a rotating arc spot causes the arc spot to move to a location

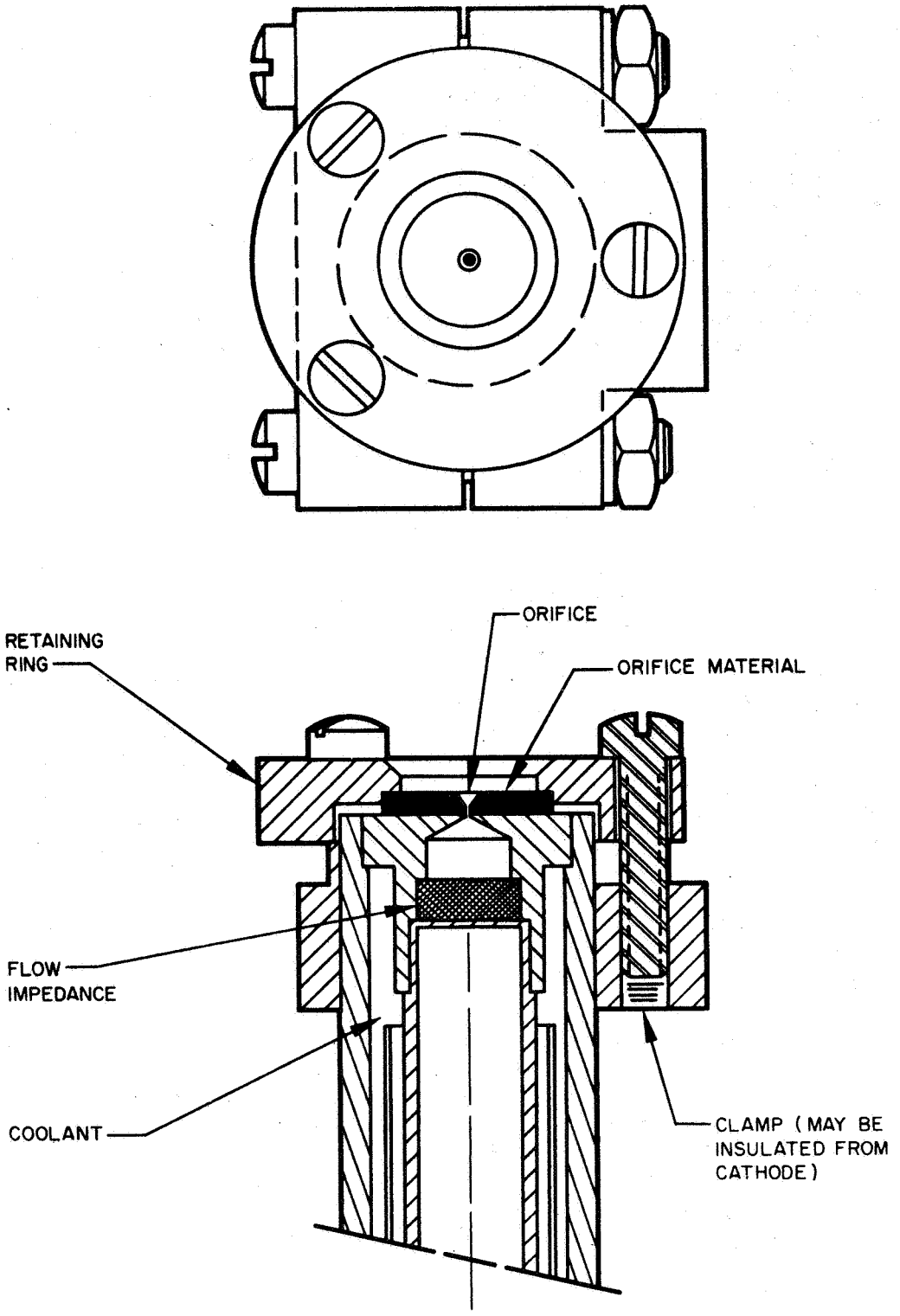

Fig. 2. Early experimental LM cathode design.

of larger radial position (i.e., downstream in the nozzle cone). In moving, the arc spot pulls the circumference of the exposed mercury surface along, and the surface continuity will be disrupted if the force exerted by the interaction of the arc spot with the applied magnetic field exceeds the surface tension force. This will result in arc instability, and therefore determines an upper limit for the magnetic field which can be tolerated on the cathode axis.

The maximum permissible magnetic field, as determined by this mechanism, may (especially for thrusters of relatively small diameter) be well below the field required for optimum thruster performance. Therefore, if this were permitted to occur, a performance limitation would result.

C. Design Considerations for Optimum Performance

1. Design for Thermal Stability

Once the mechanism of thermal instability had been identified, it became possible to design cathodes which are stable up to any desired maximum current. The most crucial design objective is to prevent thermal overload. This is achieved by maximizing the thermal conductance to the heat sink from the minimum cross section region of the pool-keeping structure. Although this increased conductance near the throat of the pool-keeping structure raises the threshold for instability of a given cathode to above its normal operating limits, the thermal destabilizing influence still persists so long as the thermal conductance decreases with decreasing liquid level. In response to flow perturbations, this persisting thermal destabilization results in larger excursions in liquid level from its equilibrium value than would result in the isothermal case. The amplitude of these excursions can be diminished, however, by actually reducing the thermal conductance to the heat sink from the downstream end of the pool-keeping structure. This reduces the dependence of the temperature on liquid level, and thus reduces the destabilizing effect.

2. Design for Steady Liquid-Metal Flow

In order to minimize the effect of thermal expansion of the liquid-metal volume bounded on the upstream side by the flow impedance and on the downstream side by the free surface in the orifice, the plenum chamber created by a separation between flow impedance and nozzle throat (as shown in Fig. 2) should be made as small as possible. The lower limit for this minimization is given by the requirement that the entire cross section of the flow impedance be utilized.

3. Design for Magnetic Stability

Two basically different possibilities exist for keeping the magnetic field in the cathode nozzle region small, relative to the field inside the discharge chamber: (1) magnetic shielding by a high-permeability field shunt, or (2) creation of a cusp-shaped field configuration and placement of the cathode orifice in the vicinity of the saddle point. Both of these approaches have relative advantages, and the choice depends strongly on the discharge-chamber field geometry. We have used both approaches successfully in electron-bombardment thrusters employing either solenoids or permanent magnets.

Figure 3(a) shows an embodiment of the high-permeability shunt concept as applied to a solenoidal field configuration. Lines of magnetic field which would otherwise have passed through the cathode are redirected to pass instead through the shunt, thereby placing the LM cathode in a region of low magnetic field. The same result is accomplished, as shown in Fig. 3(b) by placing the LM cathode in the vicinity of a saddle point created by a permanent magnet field generating configuration. Field lines emanate from both sides of the magnetic end plate in opposite directions, again resulting in a region of low magnetic field in the vicinity of the cathode.

D. Design of Life-Tested Main Thruster Cathode

Based on the considerations listed above, a cathode design has been evolved which is shown in schematic cross section in Fig. 4. Fig. 5 is an overall view of this cathode with all major components of the assembly clearly visible; the cathode is mounted inside a magnetic shield for use on a solenoid-type thruster. A closeup of the pool-keeping structure and the surrounding stainless-steel insert is shown in Fig. 6.

For convenience in experimentation with this laboratory-type cathode, it was designed for liquid cooling; flight versions will use heat conduction to the thruster shell and radiation cooling. Throughout the life test, cooling water was used to keep the cathode at a temperature of $\approx 35^{\circ}C$. With oil cooling, a cathode of the same geometry has permitted satisfactory thruster operation at a temperature of $\approx 135^{\circ}C$. (For details concerning this test and high-temperature LM cathodes see Section V-F.)

E. Design of LM Cathode Neutralizer

Simultaneously with tests performed on the main thruster cathode, the feasibility of an LM cathode capable of operation at typical neutralizer currents for a 20 cm diameter thruster had been demonstrated under Company funding. The contract requirements were then modified to include operation

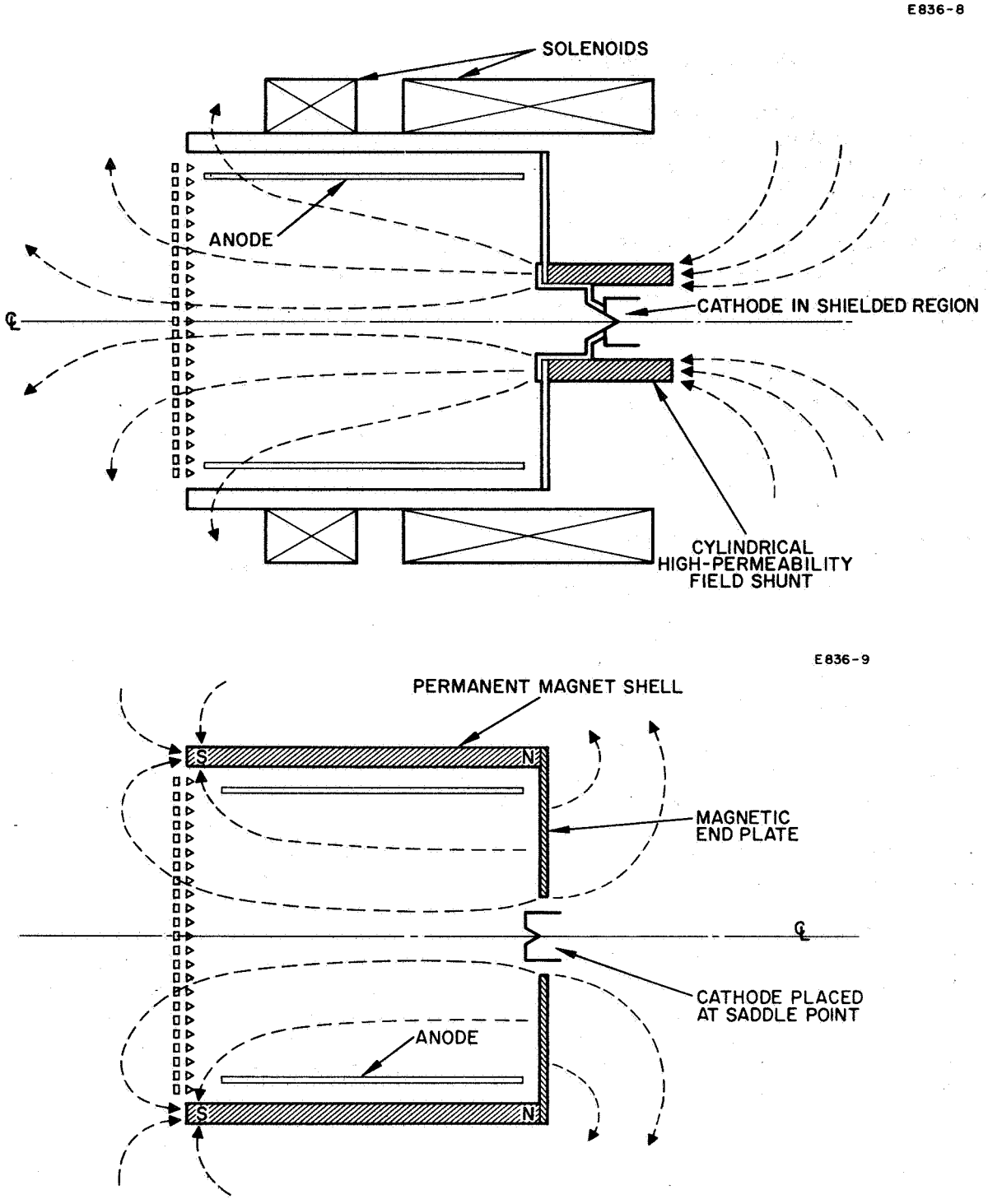

Fig. 3. Two techniques for placing cathode in a field-free region. (a) High-permeability field shunt. (b) Cusp-shaped field configuration.

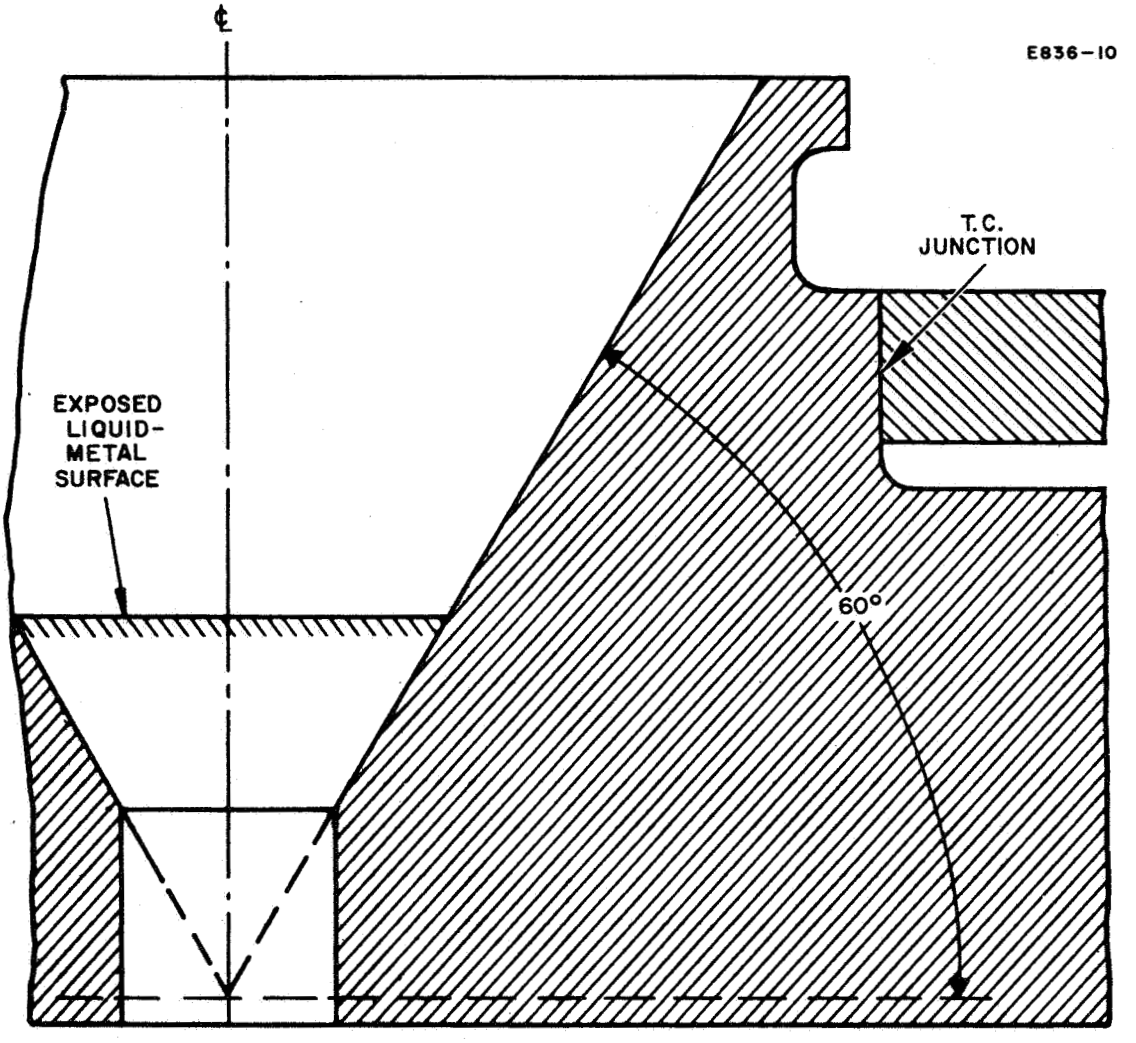

Fig. 4. Schematic cross section of life-tested LM cathode design (not to scale).

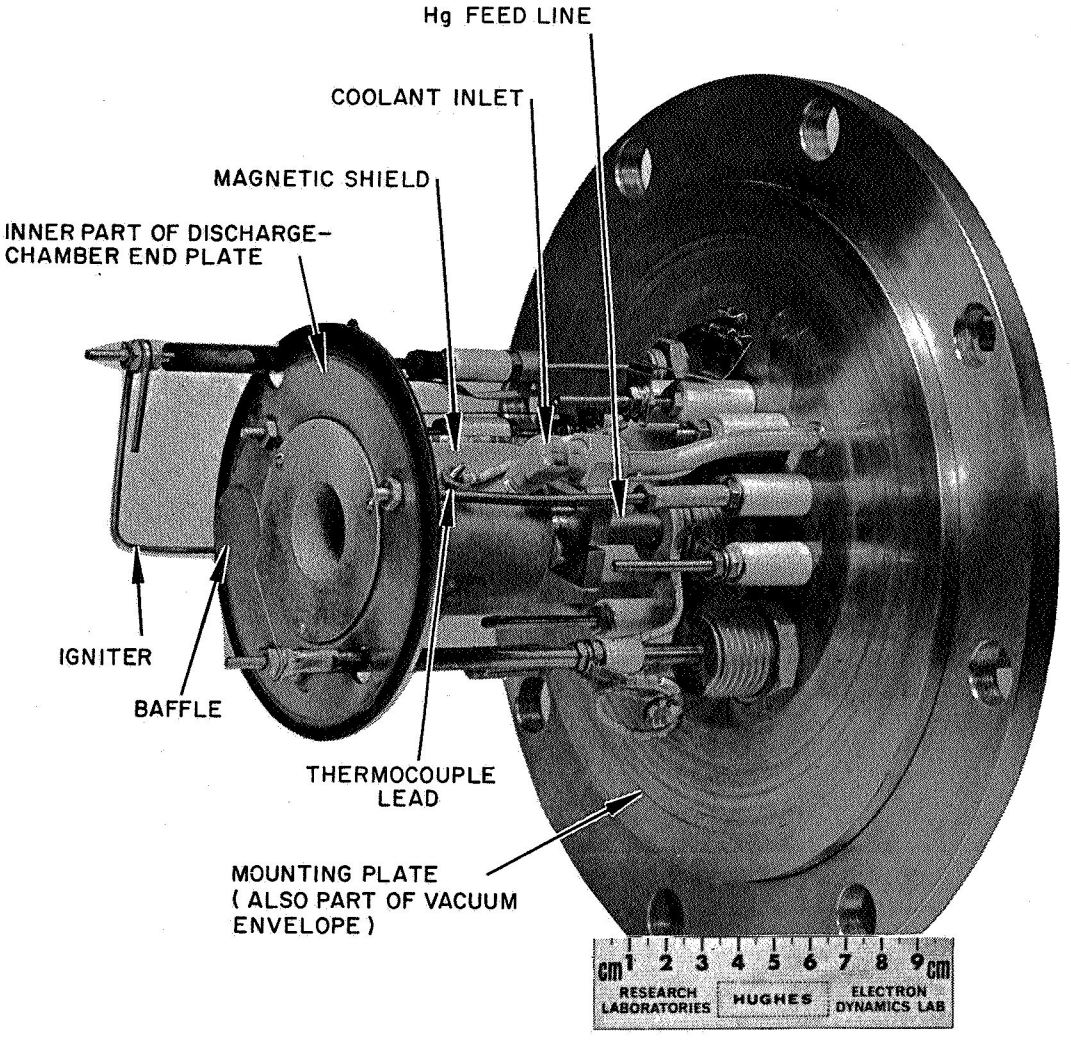

Fig. 5. LM(Hg) life-test cathode on mounting plate.

M 4210

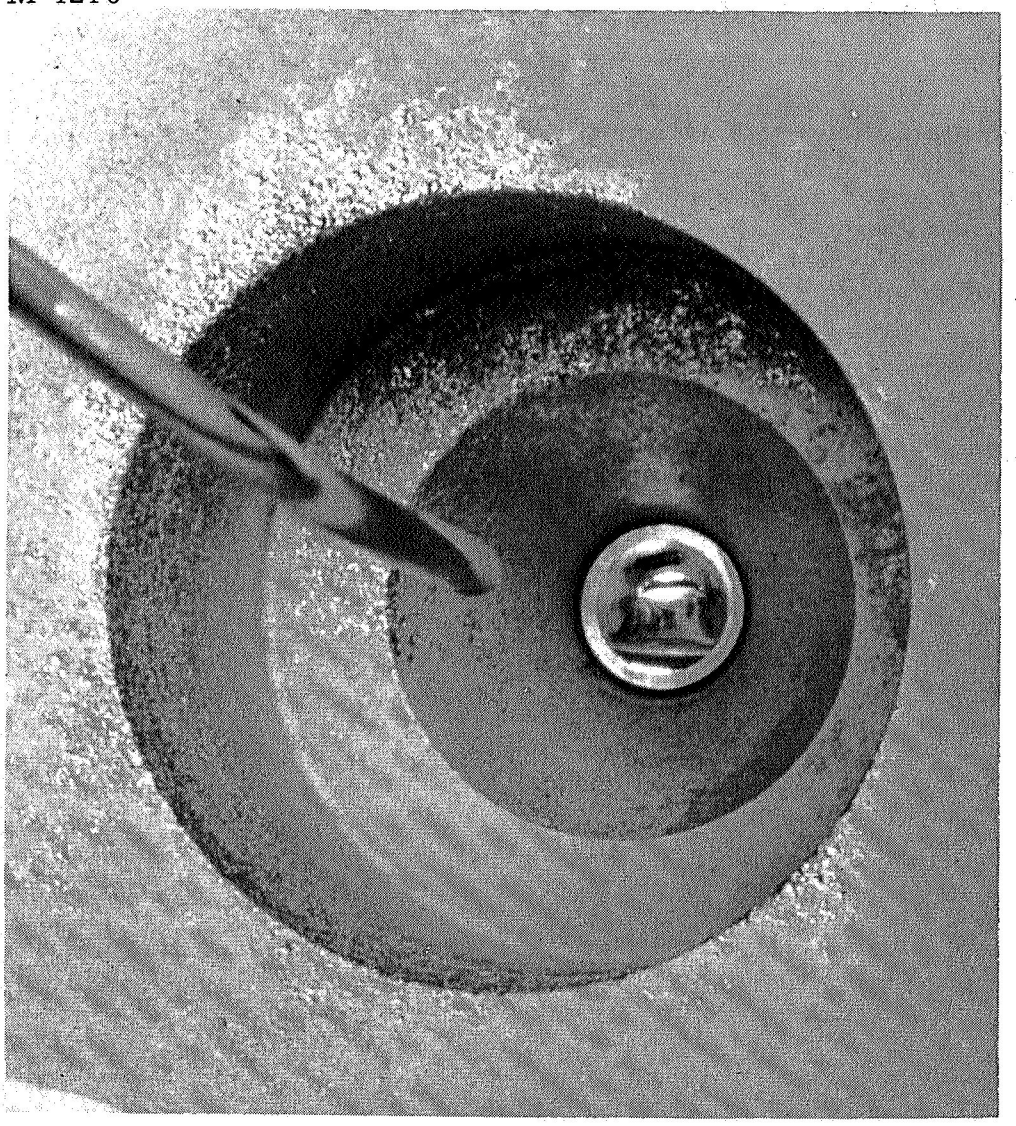

Fig. 6. Closeup of life-test cathode.

of a cathode of this type as a neutralizer for the beam of the life-test thruster during the last 500 hour increment of the life test.

The design of this neutralizer cathode is illustrated by Fig. 7. The main difference (other than size) between the neutralizer pool-keeping structure and that of the main thruster cathode is in the use of a bi-metal structure for the neutralizer. The upstream portion consists of a metal which is permanently wettable by mercury (such as copper or platinum), while the downstream portion is made of a refractory metal (such as molybdenum or tungsten) which requires the presence of an arc spot for each rewetting after consumption of a previous mercury layer. This combination results in the ability to contain a large amplitude feed rate fluctuation, while limiting the arc spot pattern excursions under normal operating conditions to the upstream proximity of the dividing line between the two materials, thereby maximizing the obtainable electron-to-atom emission ratio.

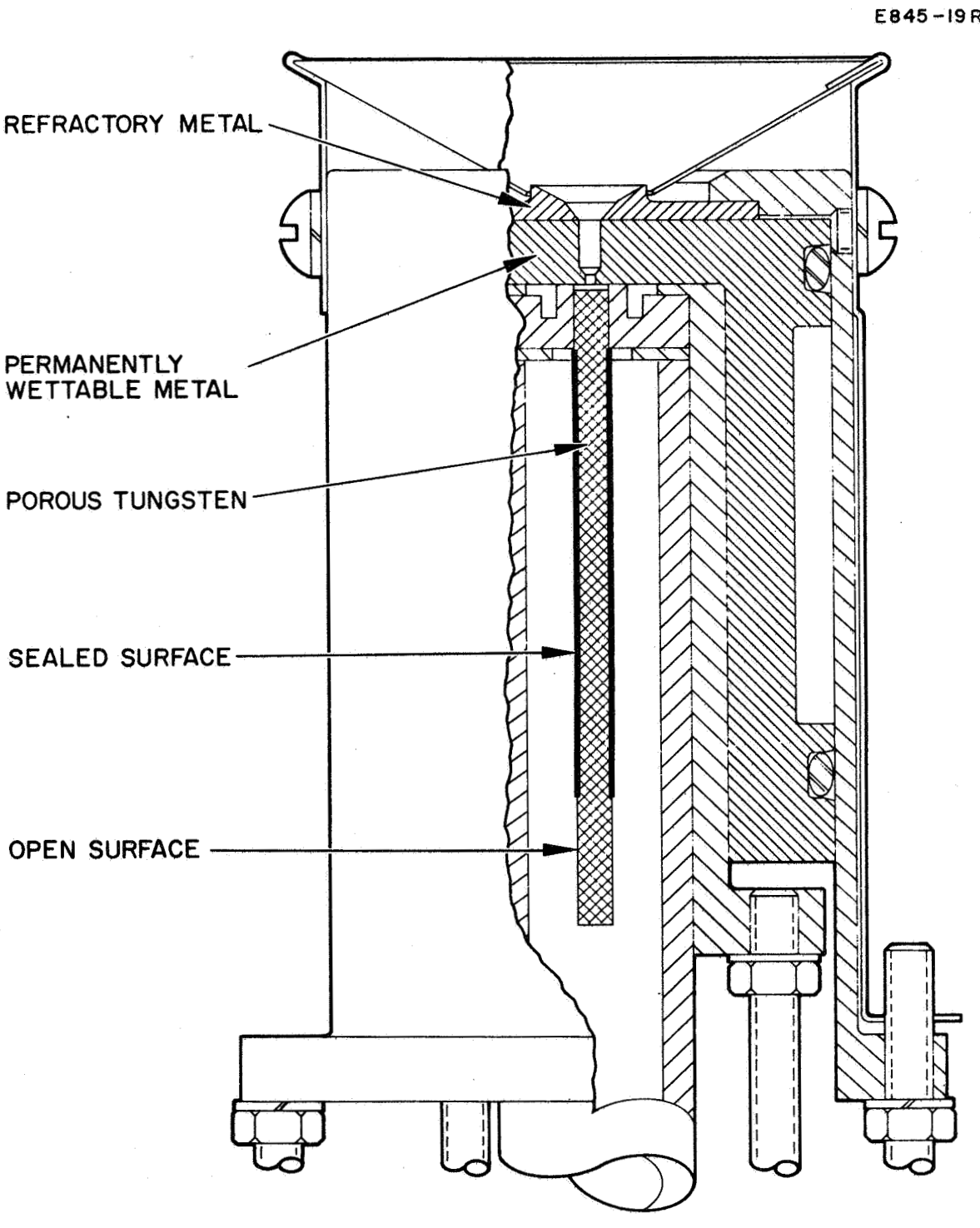

Fig. 7. Schematic cross section of LM cathode neutralizer (not to scale).

PRECEDING PAGE BLANK NOT FILMED.

III. FEED SYSTEMS

A. Gas Pressure Feed System

With an LM cathode, liquid mercury can be fed directly to the cathode from the storage reservoir; hence, the propellant feed system can be very simple. One of the systems which has been utilized to feed mercury to the cathode is shown in Fig. 8. This system, developed under a previous contract,* was used for the main thruster cathode throughout most of this contract period, and it was also used exclusively to feed the neutralizer. The delivery mechanism consists of a piston which drives mercury out of a cylinder, through a delivery tube, and thence through a porous tungsten flow impedance to the cathode. The piston itself is driven by a constant pressure of gas furnished through a regulator from a standard tank of nitrogen. A dial indicator mounted to indicate the movement of the piston stem is used to monitor flow rate. The feed rate can be controlled over a wide range by adjusting the driving pressure.

B. Vapor Pressure Feed System

A design requirement for LM cathode feed systems applicable to space use is the provision for a pressurizing system which continuously regulates the pressure without requiring a large high-pressure gas storage vessel, as would be required with a conventional relief-valve type of a system which can reduce pressure only by venting gas.

A propellant feed system which satisfies this requirement is shown in Fig. 9. The piston is sealed to the cylinder wall with a rolling diaphragm, thus providing a low friction seal which requires no lubricant. The force on the piston is provided by a pressurizer unit which consists of a bellows sealed inside a housing. The space between bellows and housing is filled with a liquid – in this case distilled water. By heating, some of the water is changed to vapor. Thus the pressure in the system is a function of temperature, accurately following the saturated vapor pressure curve. The double piston arrangement is necessary to provide thermal isolation between pressurizer and reservoir, thus minimizing the response time constant of the system. If the water was simply placed on the opposite side of the rolling diaphragm from the mercury, so that the two were in intimate thermal contact, it would be necessary to temperature control the entire volume of mercury (which could be greater than 100 lb) and the response would be very sluggish.

---

* NAS 3-4118.

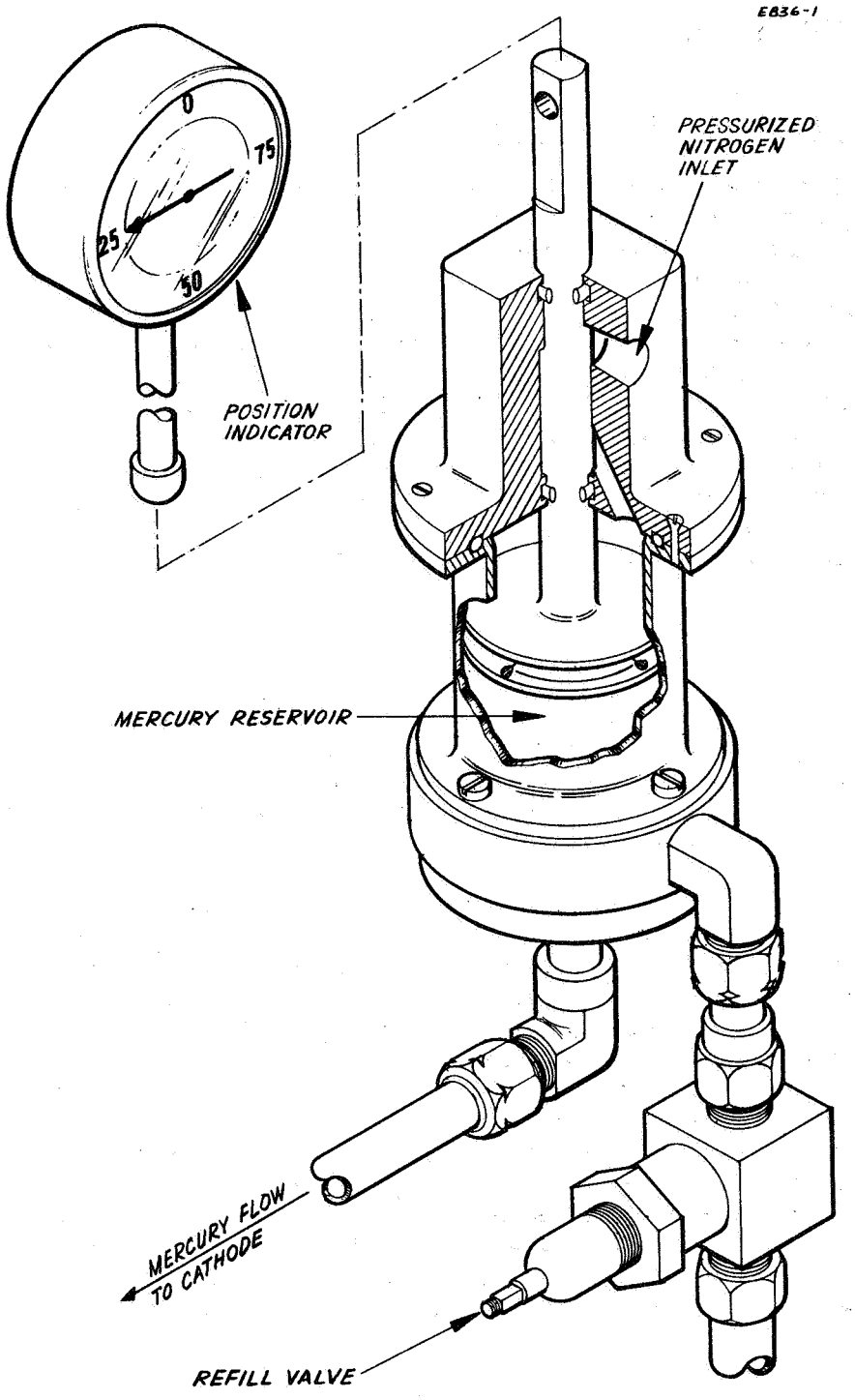

Fig. 8. Gas pressure mercury feed system.

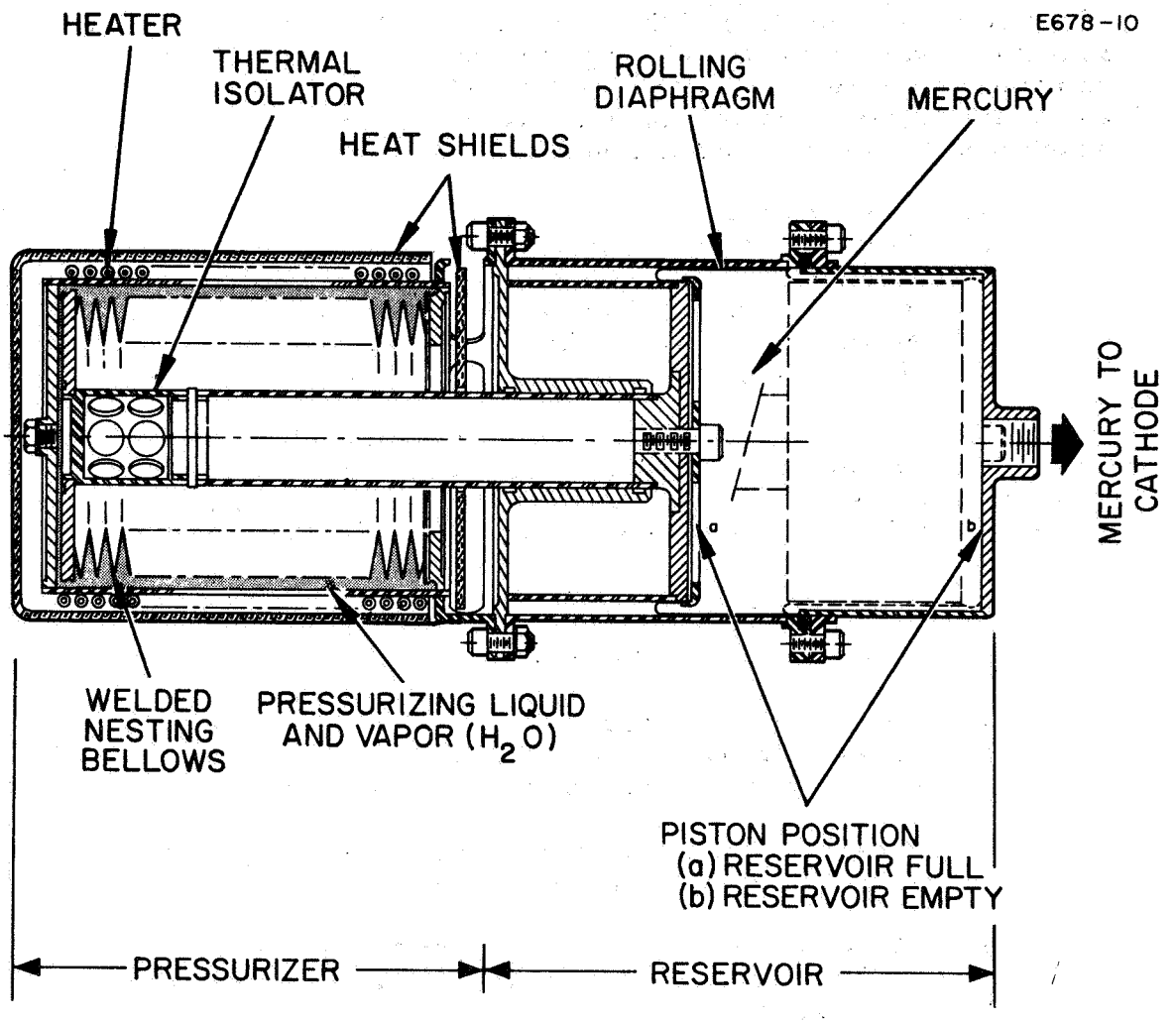

Fig. 9. Vapor pressure feed system.

C. Refilling System

During the early part of the contract period, including the beginning of the life test, refilling of the gas pressure feed system entailed the following sequence: extinguishing the arc; removing the reservoir pressure cap and piston; refilling with liquid metal by hand; reassembling and evacuating system; restarting arc. A system was devised subsequently which has the following advantages:

1. continuous arc
2. feed system is not disassembled
3. constant positive pressure on mercury applied by piston
4. no possibility of liquid metal becoming contaminated
5. elimination of air bubbles in liquid metal
6. time saving.

Figure 10 is a schematic cross section of this refilling system.* The storage chamber is filled manually with liquid metal, which is then continuously degassed by a forepump. When needed, liquid metal is transferred to the feed system of an operating LM cathode by the following procedure:

1. Piston of main pressure chamber is lifted to top of cylinder into wider diameter section

2. Liquid metal in storage chamber is then emptied into the main pressure chamber, appropriate valves are closed, and piston is reinserted into narrow portion of cylinder

3. Connection is made to the cathode by means of a transfer hose. This line is evacuated by the forepump.

4. The feed valve on the main pressure chamber is opened, and the hose is filled with liquid metal up to the refill valve of the feed system

5. A nitrogen pressure is applied to the top of the piston of the main pressure chamber which is slightly greater than the pressure on the piston of the feed system. The refill valve is opened and the feed system reservoir is filled

6. After filling, the refill valve is closed and the refilling system is removed.

All the above steps are accomplished without exposing the liquid metal to air and while the arc is continuously running.

---

* Described in T. A. Planz, "Liquid Metal Propellant Refill System," HAC Patent Disclosure 67064, 1967. The same basic transfer method can be used with ion engine arrays, employing small individual tanks on each engine which are refilled periodically from a main propellant reservoir.

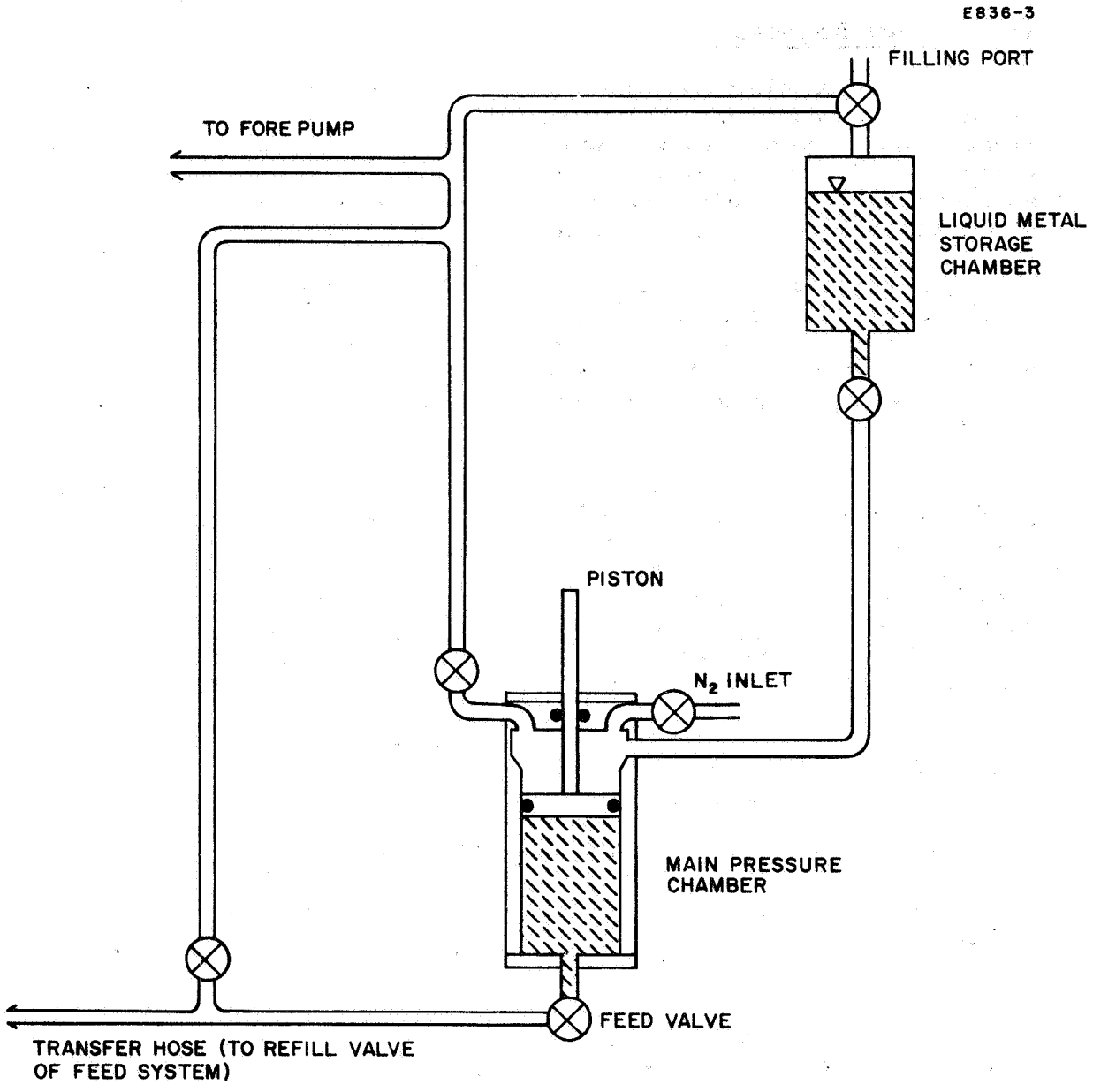

Fig. 10. Liquid-metal propellant refilling system.

D. Flow Impedance

The final element of an all-liquid-phase feed system for LM cathodes is the flow impedance. This consists of a porous tungsten plug which is electron-beam welded into a coaxial molybdenum holder. Early in the contract period this holder was an integral extension of the cathode itself, as shown in Fig. 2; later, however, an independent holder such as that shown in Fig. 7 was used for ease of interchangeability.

Early in the use of such an impedance it was recognized that the flow characteristics were neither linear nor well reproducible after depressurization. Consequently, efforts were initiated to find an impedance which would give reproducible results, and at the same time allow the original porous tungsten version to be tested for long life at constant pressure.

The other types of impedances which have been flow tested (at pressures ranging from 1.5 to 150 psia) included glass capillary bundles,* single capillaries of glass (0.005 in. i.d.) and stainless steel (0.004 in. i.d.), and stainless steel capillary bundles.+ The tests on all of these have shown unsatisfactory flow characteristics, such as several hours of time lag between pressure application and equilibrium or steady flow, and extreme sensitivity to gases or water vapor entrained in the mercury stream from organic hoses.

On the other hand, the long-duration tests with porous tungsten showed that the observed nonlinearity and shifts in flow rate after depressurization are not detrimental in actual use. These tests culminated in three successive runs for a total of 1012 hours, with a porous tungsten impedance of 7 μm nominal pore size, 75% density, 0.150 in. diameter, and 0.060 in. thickness.‡ The test was discontinued when the mercury in the reservoir was depleted on the third run. The results are summarized in Table I.

---

* Arrays of capillary glass tubes sintered together and sliced into wafer form with uniformly sized passages perpendicular to the surfaces from Permeonics Corporation, Cambridge, Massachusetts. Pore sizes obtained for test as feed system impedances ranged from 3 to 100 μm; the bundles had 0.150 in. diameter and were 0.100 in. long.

\+ Seamless stainless steel tubes, 0.150 in. i.d., packed with capillary tubes 0.009 in. o.d., 0.0025 in. wall, from Pacific Tube Company, 5710 Smithway Street, Los Angeles, California.

‡ Supplied by Semicon Associates, Inc., P. O. Box 832, Lexington, Kentucky.

TABLE I
Flow Stability

Run Number	Duration, hours	Pressure Applied, psia	Average Normalized Rate of Piston Displacement, 10^{-6} in/hour-psia	Maximum Deviation from Average, %	Reason for Interruption
1	150	80	93.8	1.3	Mercury depleted
2	387	70	16.3	2.5	Modification of test facility for reasons outside this test
3	475	70	11.8	1	Mercury depleted

The measurements conclusively demonstrated that during any uninterrupted run the fluctuations in flow rate at constant pressure were small enough to require only occasional readjustment in long thruster runs or, alternatively, to be easily compensated by a feedback loop, as described in Section V-D-2.

Similar results were obtained with porous tungsten impedances produced at Hughes Research Laboratories. These had a more uniform pore size distribution centered at 2.7 μm, 80% density, and the same dimensions as mentioned above. This impedance type exhibits a smooth flow-pressure dependence in the flow range required for main thruster cathodes and was used in all subsequent experiments with such cathodes.

For the neutralizer flow impedance it was necessary to shift the range where the smooth flow-pressure dependence exists to lower flow values by a factor of ≈ 40. This was accomplished by increasing the thickness of the flow-impeding layer by a factor of 20, and by reducing its cross-sectional area by a factor of 4. Porous tungsten produced at HRL with 4 μm nominal pore size and 85% density was used, and most of the surface was sealed by electron-beam washing, as indicated in Fig. 7.*

* The technique for producing these impedances is described in J. A. Snyder, "Large Length to Diameter Ratio Filter or Impedance," HAC Patent Disclosure 67063, 1967.

E. Electrolytic Feed Systems

One of the requirements for feeding an LM cathode at the proper rate is the ability to measure the flow rate, which is typically < 1 cm^3/hour. For the main thruster cathode, this problem was solved by establishing a close correlation between flow rate and beam current, and using the beam current as a measure for the flow rate. (This is discussed in detail in Section V-D-2.) For the neutralizer cathode it now appears possible to use an observed correlation between the flow rate and the small variations in the discharge voltage in a similar way, but this had not yet been demonstrated during the contract period. Both of these methods for determining flow rates provide an instantaneous electrical readout, but they are both indirect. During the early part of the contract period it was believed that a direct flow measuring technique giving instantaneous electrical rate readout would be desirable; because electrolytic feed systems are capable of filling this need, some effort was devoted to their development.

Electrolysis can be employed in one of two ways in mercury feed systems: (1) as a means for both producing a flow and measuring its rate, and (2) as a means for measuring the flow rate and producing a signal which controls a feed system, as described in Section III-B.

The basic embodiment of scheme (1) is illustrated by Fig. 11. Here an insulating-wall section of the feed line contains an electrolyte between two porous membranes which are permeable for the electrolyte, but not for liquid mercury (at the pressure differentials required in the system). If the mercury on the upstream side is held under a constant pressure by the reservoir in order to confine the electrolyte to the space between the membranes, application of a voltage between the two mercury columns results in electrolytic transfer of mercury at a rate exactly proportional to the instantaneous electrolysis current.*

Because all electrolytic devices employing membranes are limited in current density by polarization effects within the membrane pores, relatively large membrane areas were provided by using concentric glass frit cylinders. Typical frit wall thickness ranged from 1.8 to 4.7 mm. Current densities obtained were 1.5 to 0.5 mA cm^{-2}, respectively. The tests demonstrated that mercury could be electrolytically pumped against at least a 2 atm pressure differential. They also showed that continuous pumping for a very long time was feasible against a constant head of 600 Torr, with no degradation after 570 hours.

In another experiment the electrolyte was held only within the pores of a single frit cylinder by capillary action. This scheme showed no improvement over a double cylinder with the equivalent wall thickness. It

---

* This approach was invented and its principle demonstrated prior to the subject contract. It is described in W. O. Eckhardt, "Gravity-Independent Mercury Flow Control and Metering Device," HAC Patent Disclosure 6081, 1964.

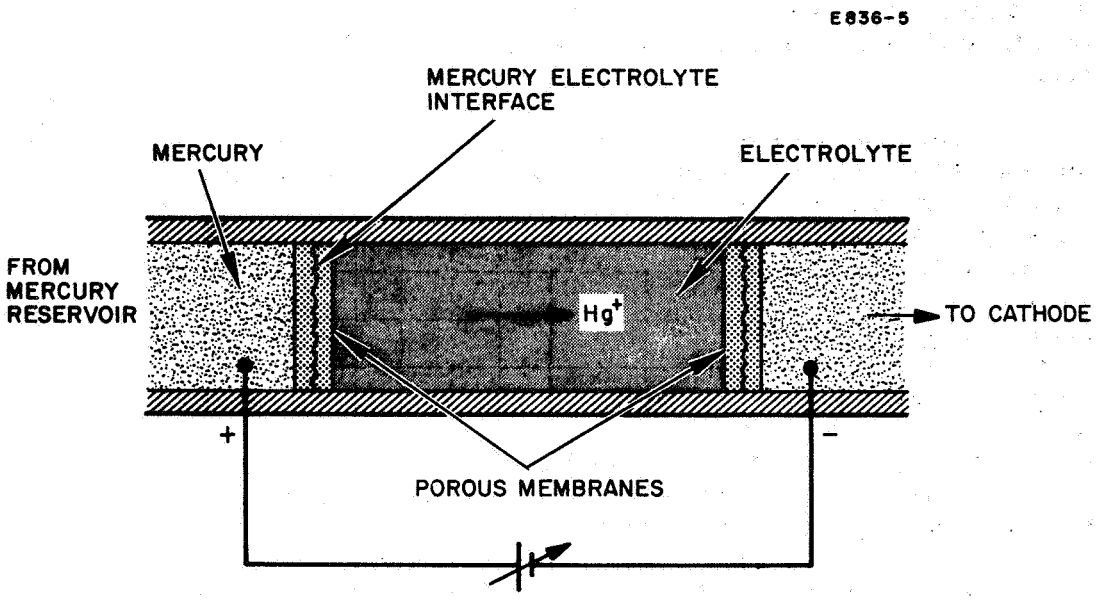

Fig. 11. Electrolytic mercury feed system.

was observed generally with glass frit cylinders that there was a noticeable nonuniformity of pore size from one part of the cylinder to another. This could lead to nonuniform response because the smaller pore sizes would saturate quickly and gas, as a result of overload. Various large organic sheet membranes were also investigated as possible barriers in a mercury electrolytic cell, but showed less capability (0.3 mA cm^{-2}) than the glass frits.

The glass capillary arrays mentioned in Section III-D have been shown to be a very suitable membrane or cell separator. Using a flat, thin disk of this material (0.030 in. thick, 0.150 in. diameter), a current density of 4 mA cm^{-2} was maintained for several days, and the accuracy of the metering method was demonstrated to be $\approx 1\%$ when operating against a constant pressure. In this configuration, the electrolyte is held in the glass matrix itself by capillary action and the mercury is against both surfaces of the disk. However, loss of electrolyte on a microscale basis during severe vibrations could impair the current carrying capacity with this geometry. Accordingly, a double membrane cell as shown in Fig. 11 holds more promise for a long-life electrolyte unit. Glass bundles of 0.010 in. thickness were tested at the close of the contract, but they suffered damage during processing.

The most obvious embodiment of scheme (2) simply omits the porous membranes in Fig. 11 and uses some sensing device to determine the location of the electrolyte bubble.* This approach permits current densities several orders of magnitude higher than the membrane systems, but in its simplest form requires sensing methods which are rather complicated because the electrolyte is positioned in a cylindrical tube, thus making the properties of the electrolytic transfer gap intrinsically independent of axial position. In addition, a cylindrical tube does not prevent escape of the electrolyte out of the permissible range of axial shift in case of a temporary overload or malfunctioning of the control system.

These disadvantages are eliminated by the embodiment shown in Fig. 12.+ The various numbered zones have the following functions: In normal operation, the gap is in the conical zone IV, where the voltage across the gap (at constant impressed current) is a strong function of the cross-sectional

---

* This approach was also invented and its principle demonstrated prior to the subject contract. It is described in H. J. King, "Metering System for Liquid Mercury," HAC Patent Disclosure 6084, 1964.

\+ This device was invented and demonstrated during a Company-supported effort carried out simultaneously with the life-test extensions of the subject contract. It is described in H. J. King, W. O. Eckhardt, and J. A. Snyder, "Liquid-Mercury Flow Meter," HAC Patent Disclosure 7025, 1966.

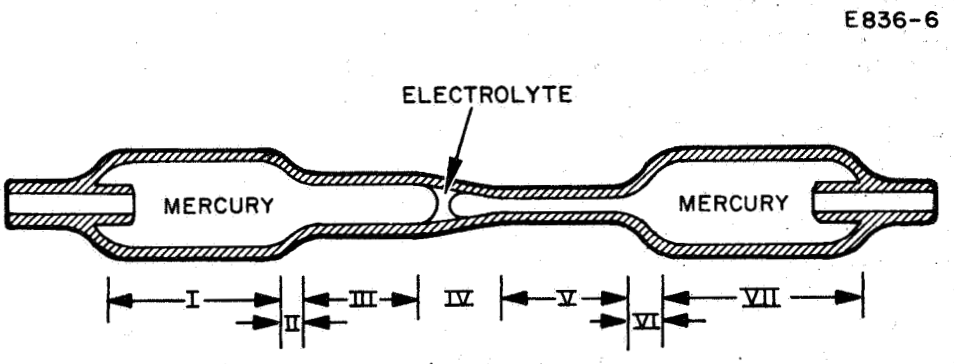

Fig. 12. Electrolytic mercury flow meter.

area (and hence the axial position). At constant electrolysis current and varying mercury flow rate, the gap position will shift upstream or downstream, and the deviation of the gap voltage from its value at the center position can be used as the error signal in a control loop adjusting the mercury feed rate. If the gap is shifted to either of the extreme positions in zone IV by a gross discrepancy between the actual flow rate and the intended flow rate (as determined by the impressed electrolysis current), the maximum error signal will be maintained even if the discrepancy persists for a while because the gap can move for some time without changing its cross section in zones III and V, respectively. These zones should be made long enough to accommodate the normal response time of the control loop. Should the intended flow rate not be reestablished for some reason when the gap reaches the outer ends of zones III or V, escape of the electrolyte is prevented by zones II and VI. Their operation is based on the fact that a liquid bubble which wets the tube walls cannot be expanded to arbitrary diameters when bounded by a liquid which does not wet the tube walls; instead, in order to maximize its attachment area to the wettable wall, the bubble will jump into an asymmetric position (thus permitting the two mercury columns to short out) when it is pushed into a cross section of such diameter that the asymmetric position results in a smaller value of the surface energy. However, because an even smaller surface energy is available in the symmetric position at a smaller diameter, the asymmetric bubble will subsequently creep back into zone III or V, respectively, and re-form a gap between the mercury columns. Zones I and VII, finally, are provided to trap the electrolyte positively within the flow meter; the surface-energy argument shows that the electrolyte bubble cannot enter the reentrant sections of the mercury lines.

Experiments with this type of flow meter have shown that an adequate voltage excursion for control purposes (e.g., a ratio of 1.5:1) is easily obtained. A flow meter of this type could be used for measuring the flow rate to an LM cathode neutralizer; it would have a power consumption of less than 50 mW/A of neutralizer current.

F. Mercury Purity

All mercury used was supplied by Bethlehem Apparatus Company, Inc., Front and Depot Streets, Hellertown, Pa., as "instrument grade, triply distilled mercury" in 5 lb glass bottles. The general claim for this mercury is less than 1 ppm impurities. A certificate of analysis was furnished with each shipment, showing nonvolatile residue by weight to be less than 0.1 ppm.

A sample from the vendor, subjected to spectrographic analysis by a local firm, showed silicon and calcium content to be ≈ 0.45 and ≈ 0.27 ppm, respectively. This was considered entirely adequate because the emission mechanism of LM cathodes is very insensitive to contamination, as was demonstrated when a cathode was accidentally operated with macroscopically dirty mercury.

IV. LM CATHODE TESTING IN DIODE AND PENNING DISCHARGE CHAMBERS

The cathode design described in Section II-D was subjected to extensive testing in diode and Penning discharge operation, and the life tested cathode in particular was operated both before and between thruster tests for an additional cumulative total of over 1250 hours. The purposes of these tests were

1. To establish that the design provided stability against all perturbing effects, as discussed in Section II-B and II-C

2. To demonstrate the ability to operate at and above the currents and electron-to-atom emission ratios required for efficient operation of a 20-cm diameter thruster

3. To accumulate additional operating time in support of our contention that LM cathodes represent a solution to the cathode life problem of mercury electron-bombardment thrusters.

Figure 13 shows an LM cathode operating in a Penning discharge test setup. The magnet coil shown in this figure was capable of producing fields up to several hundred gauss for testing the effectiveness of the cathode's magnetic shield. An end-on view of the life-tested cathode in operation is shown in Fig. 14; it was photographed (through a glass window facing the cathode) in a similar setup with the aid of an external light source after 650 operating hours. Figure 15 shows the same cathode after 3000 hours of operation, photographed in the light of its own discharge only. The life-tested cathode was also photographed after all mercury had been removed from the pool-keeping structure by shutting off the mercury flow and operating the discharge until it starved out; Fig. 16 is such a view after 3000 hours, and Fig. 17 is after 5250 hours of operation. (In both figures, small mercury droplets are visible in or near the throat of the pool-keeping structure; these had passed the throat after the discharge had starved out.) The difference in appearance is caused by a change in surface texture also observed after a few hours of operation on all LM cathodes used at high current densities. There is no macroscopic erosion; within measuring accuracy, the dimensions of the pool-keeping structure, including the throat, remained unchanged during the full 5250 hour duration of the tests.

The following typical measured data illustrate the capability of the life-tested cathode to operate stably at currents up to and above the required level, at electron-to-atom ratios considerably above the optimum for

M 3534

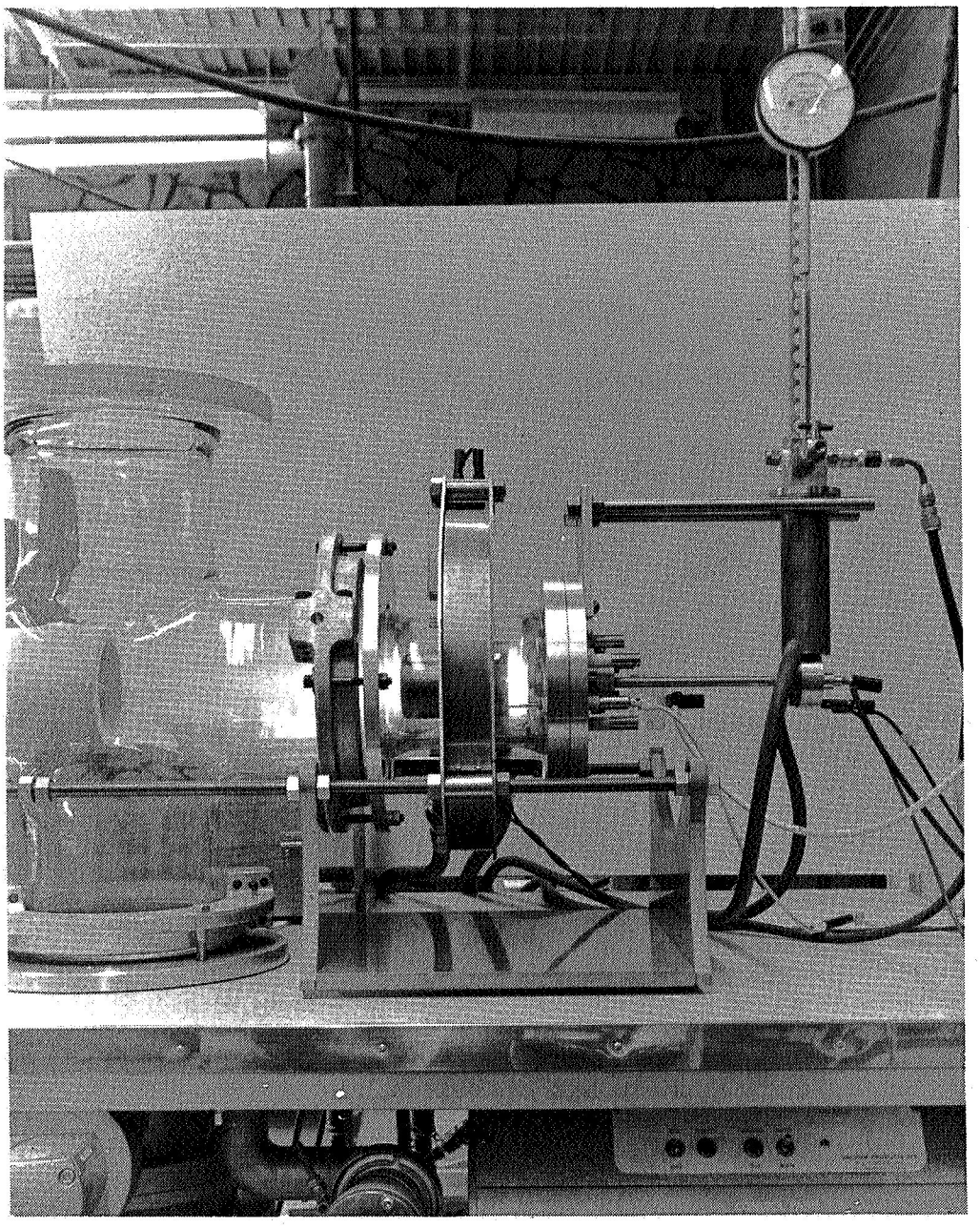

Fig. 13. LM cathode arc in Penning discharge chamber.

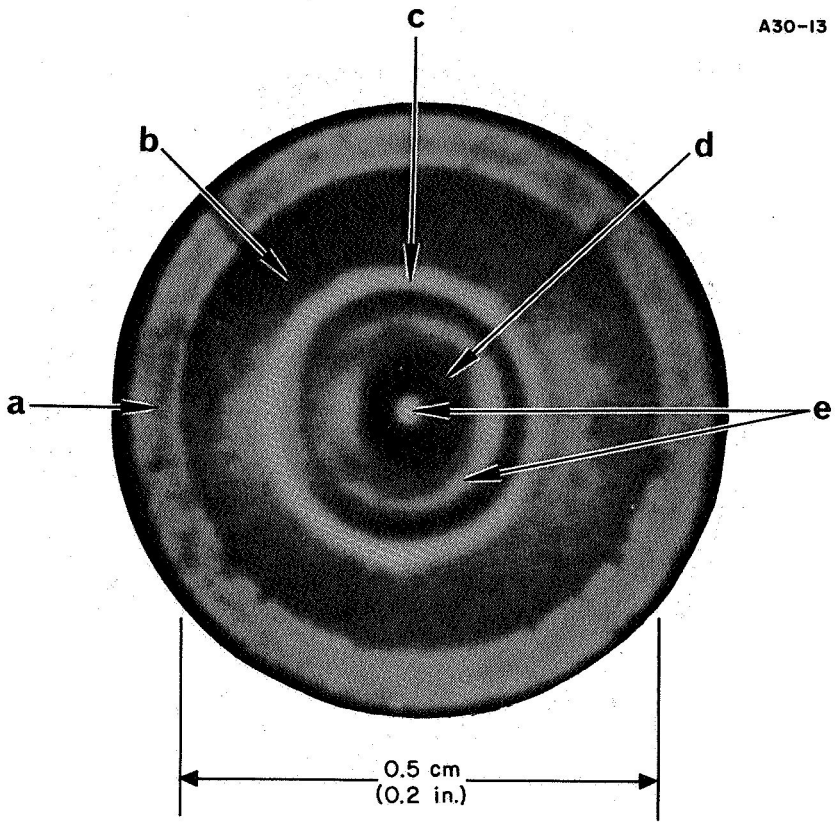

Fig. 14. LM (Hg) cathode in operation, viewed along the axis of symmetry. a = rim of divergent nozzle; b = exposed nozzle surface; c = circular arc-spot pattern at edge of exposed mercury surface; d = exposed mercury surface; e = reflections of external light source in concave mercury surface.

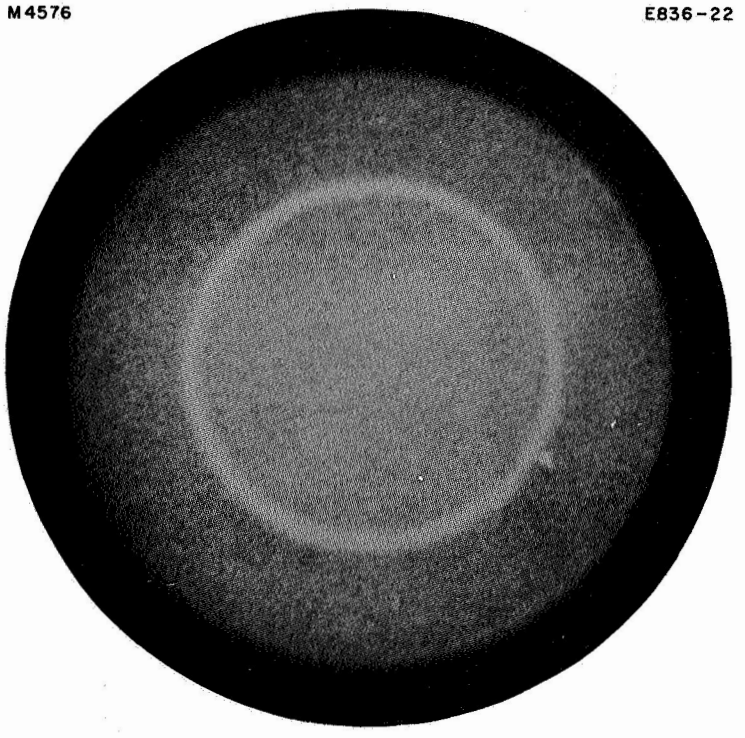

Fig. 15. LM (Hg) cathode in operation, viewed along the axis of symmetry without external light source.

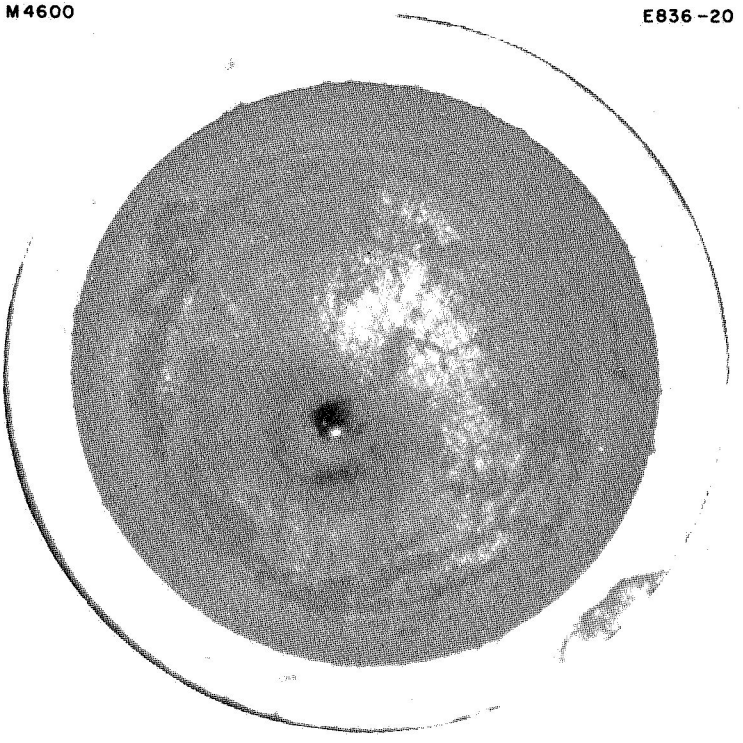

Fig. 16. Pool-keeping structure of LM cathode after 3000 hours of operation.

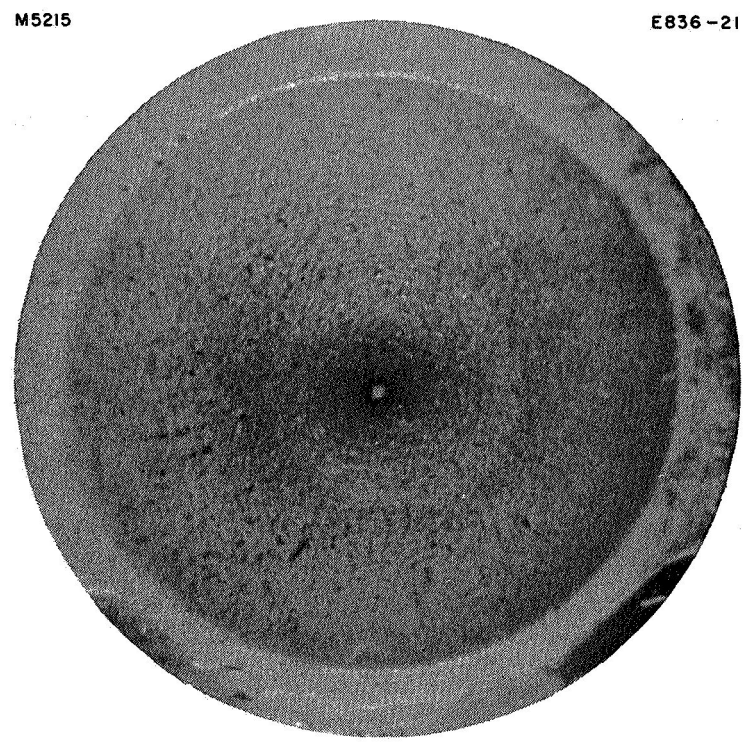

Fig. 17. Pool-keeping structure of LM cathode after 5250 hours of operation

efficient thruster operation:

50 electrons/atom at 12.3 A,

40 electrons/atom at 20 A.

For comparison, the performance required for the thruster life test was

12···20 electrons/atom at 9···14 A.

PRECEDING PAGE BLANK NOT FILMED.

V. THRUSTER TESTING OF LM CATHODES

A. General Conditions

The primary objective of the original contract was to develop LM cathodes suitable for use under actual thruster conditions, and to test these cathodes in a thruster supplied by NASA-LeRC which was to be modified only to the extent required for compatibility with the LM cathode. The crucial test was to be a cathode life test of 750 hour cumulative operation with beam extraction and without cathode change or modification. Performance optimization of this thruster was not a goal of the contract.

After the 750 hour test had been completed successfully in every respect, the contract was modified to prolong the test period in 1000 hour increments to a total of 3750 hours. During these increments, a new contract from NASA Headquarters* and Company-supported programs led to the availability or to feasibility demonstrations of several important items which were subsequently included in the thruster test. As a result, the thruster operated during the last test periods with drastically improved efficiency; it was also equipped with a flight-type feed system, an LM cathode neutralizer, and an automatic control system.

The various modifications were possible without invalidating the cathode life test because LM cathodes are totally insensitive to air exposure. The tests required for incorporation of the additional components resulted in an increase of the total cumulative thruster operating time to 4009 hours.

B. Modified LeRC Thruster

The 20-cm diameter thruster supplied by NASA-LeRC was modified by removing the expellant distributor and providing an opening in the rear of the thruster to accept the LM cathode assembly. The magnet coil was replaced by 500 turns of high-temperature insulated wire to permit operation at magnetic fields up to 200 G. (After the latest discharge chamber modifications described below, only 10 to 20 G were required.)

The NASA ion-optical system was replaced by a unit in which the screen was countersunk on the plasma side. The center spacing between screen and accel was 0.13 cm, and the spacing at the anode radius was

---

* NASW-1404

0.37 cm. The closer spacing in the center provided a quasi-matching of perveance and current density. The optics had a hexagonal close-packed array of 1027 holes with a nominal diameter of 4.76 mm on 6.35 mm centers drilled in 1.58-mm-thick molybdenum plates. The total hole area is 177 cm^2, corresponding to an open area of 56%. Figure 18 is a schematic cross section of this thruster; Fig. 19 shows it before mounting; and Fig. 20 shows it mounted inside its shielding enclosure (without neutralizer).

C. Vacuum Facility

A vacuum chamber of 3 m length and 1.2 m diameter was modified for the thruster tests by installing an easily cleanable liquid-nitrogen cooled stainless steel cryowall, with approximately 4.6 m^2 of surface area. Three baffle apertures were used to protect the cryowall from erosion by the incident ion beam. A liquid-nitrogen cooled baffle was installed between the chamber and the 25-cm diameter oil diffusion pump to prevent mercury from entering the pump. Typical operating pressure with the thruster running was 10^{-6} Torr. The collector was built up from 3.2 mm thick stainless steel fins, individually water cooled and mounted at a small incidence angle to reduce the fraction of sputtered material returning to the engine. Figure 21 is a photograph of the vacuum tank, showing cryowall, collector, and baffle mounting brackets.

D. Electrical Test and Control Circuits

The schematic of the thruster test circuits shown in Fig. 22 represents the final stage of evolution. The notation used is explained by Table II. The test was begun without neutralizer, automatic feed system, interlock sequencer, and automatic igniter. However, the basic circuit was such that all these auxiliary circuits could simply be added when they became available, without requiring any major changes in the existing circuitry. While all circuits were intimately interconnected (and hence are all shown in one diagram to indicate possible interactions), their functions can be explained rather independently. One general principle will be appreciated by inspection of Fig. 22: extensive instrumentation was used to guard against spurious currents (caused, for example, by backsputtered material shorting out components) going undetected, and to provide cross checks on the basis of the following continuity equations:

$$I_A + I_{IK} = I_K + I_B = I_D \qquad \text{(always)},$$

$$I_{Ac} + I_{C'} + I_C = I_B \qquad \text{(without neutralizer)},$$

$$I_{Ac} + I_N + I_{IN} + I_{Sk} + I_{C'} + I_C = I_B \qquad \text{(with neutralizer, in general)},$$

$$\left.\begin{aligned} I_{Ac} + I_N &= I_B \\ I_{Sk} &= 0 \\ -I_{C'} &= I_C \end{aligned}\right\} \qquad \text{[with neutralizer, in normal operation } (I_{L1} = 0 = I_{L2})\text{]}$$

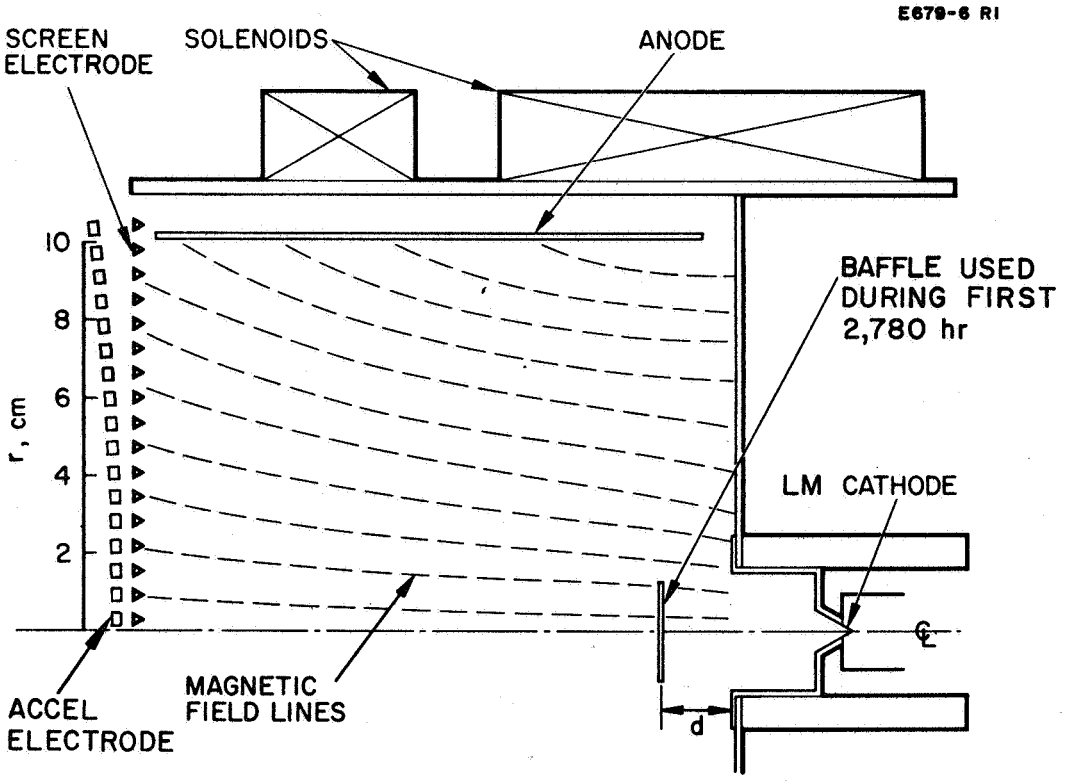

Fig. 18. Schematic cross section of modified LeRC life test thruster.

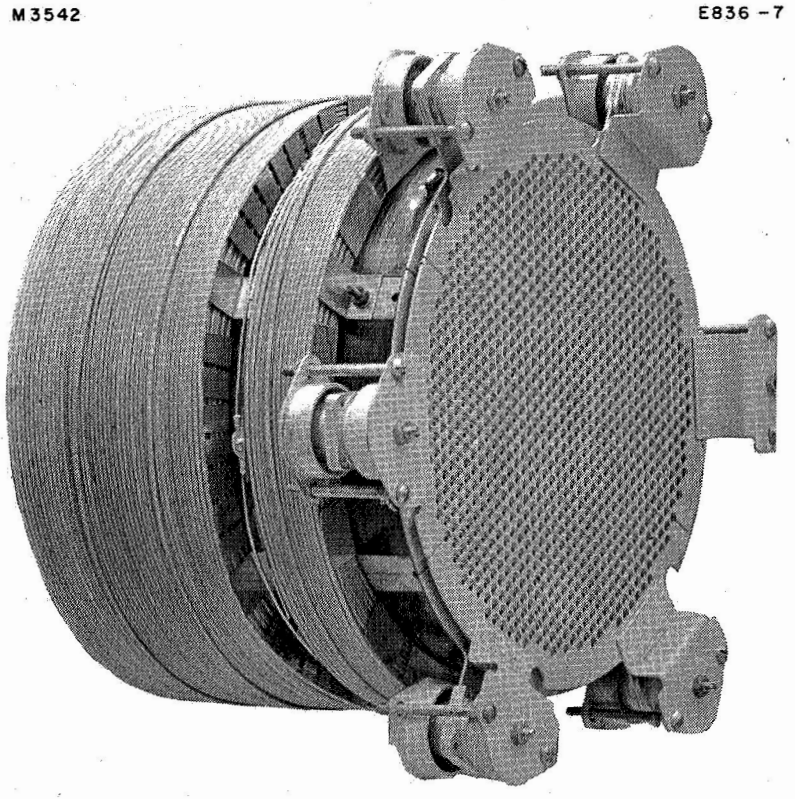

Fig. 19. Modified LeRC thruster before mounting.

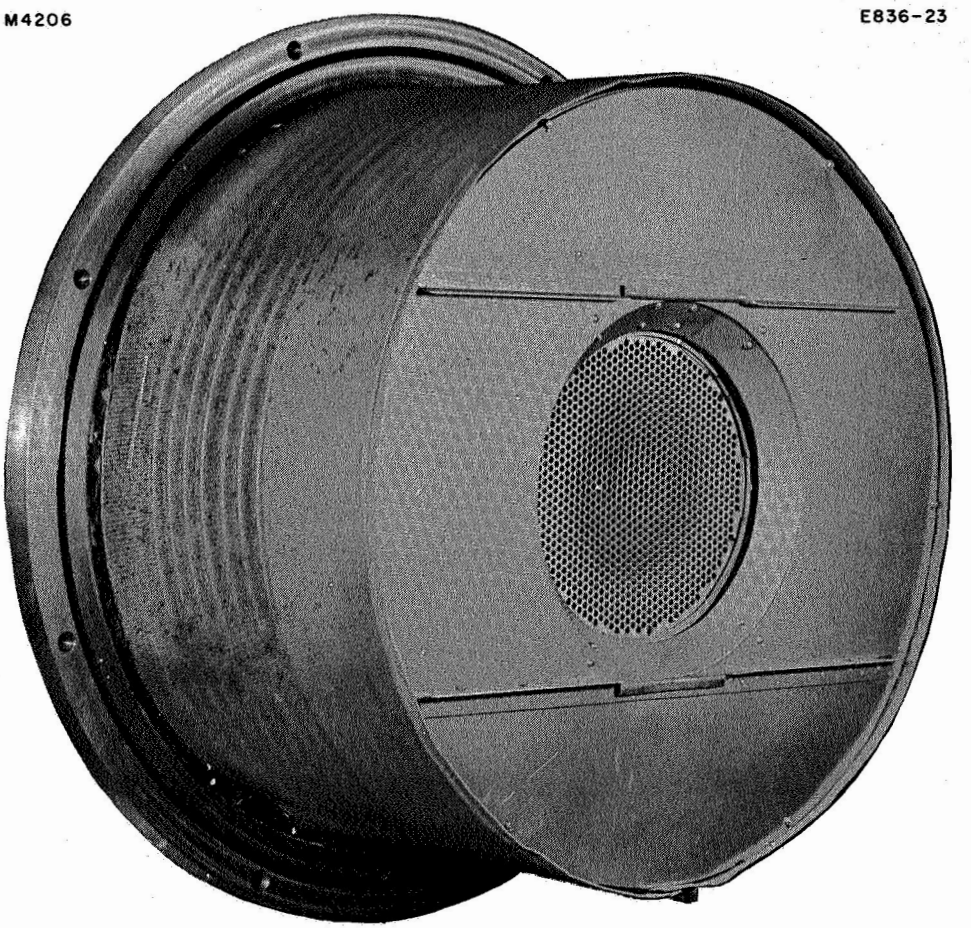

Fig. 20. Life test thruster with shields, mounted on vacuum chamber end plate.

M 3579

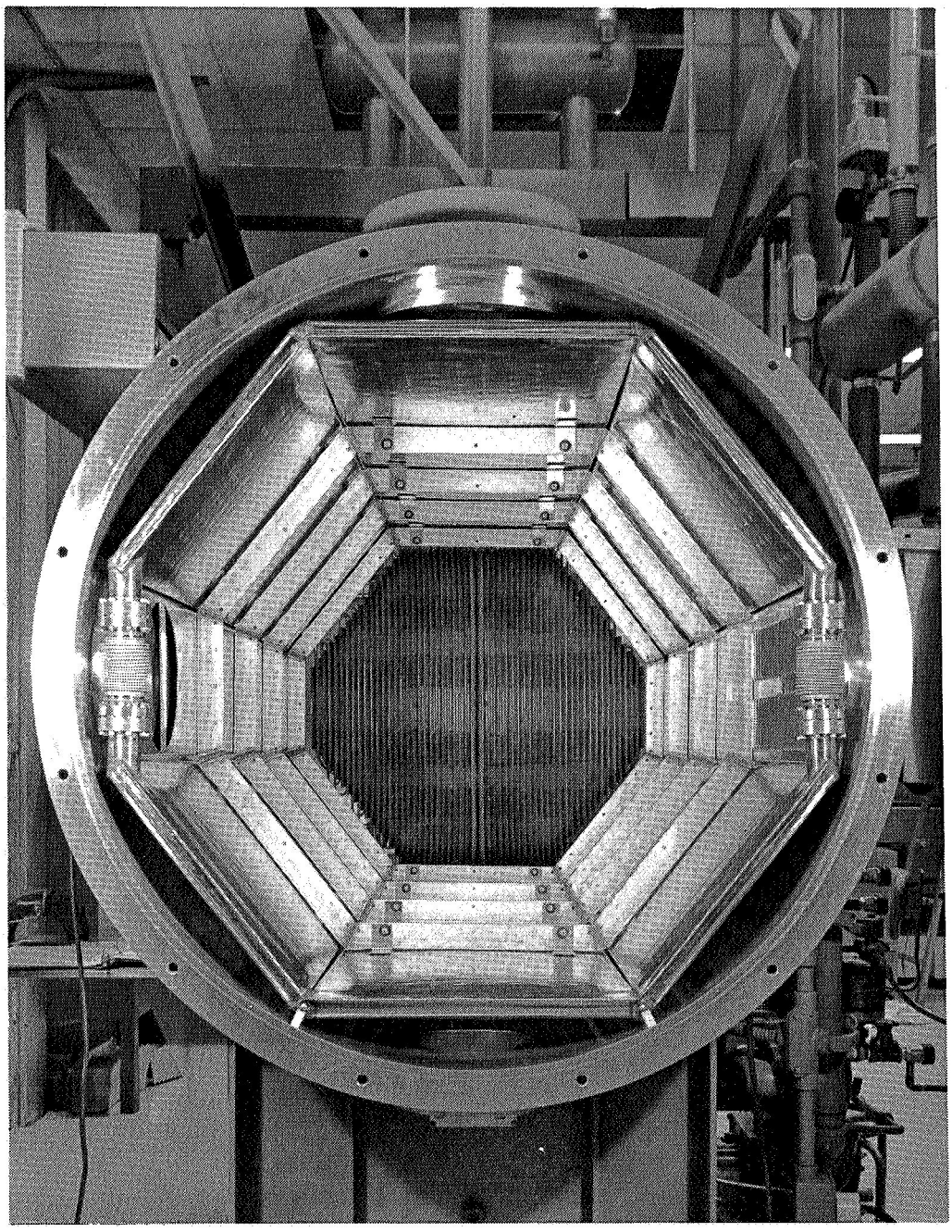

Fig. 21. Test chamber (1.2 m diameter) with cryowall and collector.

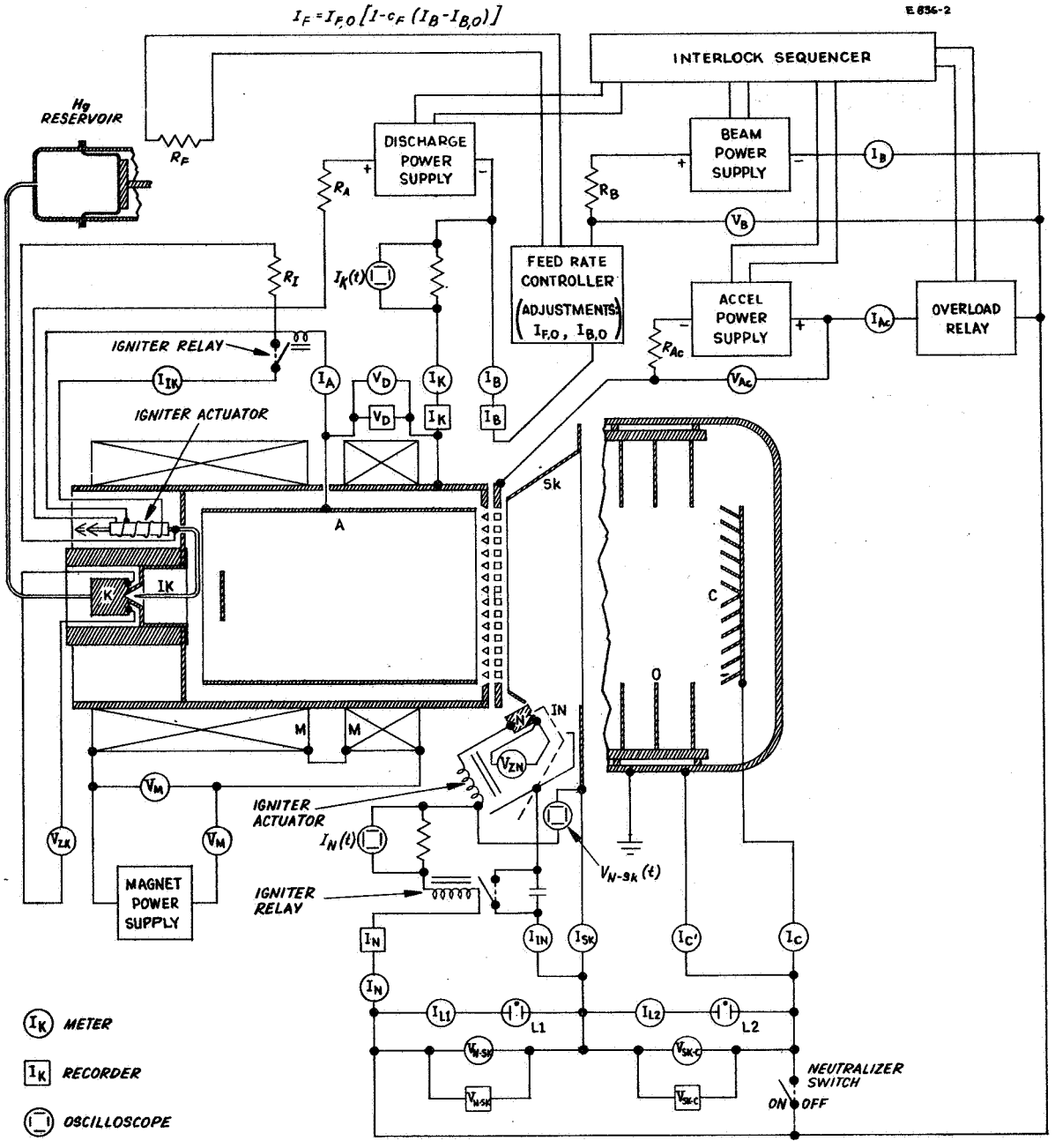

Fig. 22. LM cathode thruster test circuits (see Table II for notation).

TABLE II

Notation Used for Physical Quantities and for Components of Test Setup

Physical Quantities

I	≡	current
P	≡	power
V	≡	voltage

Components

A	≡	anode
B	≡	beam
C	≡	collector
C′	≡	tank, cryowall, baffles
D	≡	discharge
F	≡	feed system
I	≡	igniter (IK = igniter for main thruster cathode. IN = igniter for neutralizer)
K	≡	cathode
L	≡	voltage limiter
M	≡	magnet
N	≡	neutralizer
R	≡	resistor
Z	≡	thermocouple
Ac	≡	accel electrode
Sc	≡	screen electrode
Sk	≡	spacecraft skin

The current-limiting resistors R_B and R_{Ac} were provided to protect the thruster from the high short-circuit currents available from the laboratory-type high voltage supplies used. They are not required in a flight-type system.

1. Ion Source Circuits

The discharge power supply and the magnet power supply consisted of three-phase full-wave silicon diode rectifiers fed by ganged variacs. Before the automatic feed system was introduced they were fed directly from the power line and operated without filters; with automatic systems they were fed through magnetic voltage regulators and equipped with ripple filters. The relatively large (8 Ω) series resistance R_A converts the effective discharge supply characteristics from constant-voltage to (essentially) constant-current.*

To ignite the discharge, a mechanically movable igniter electrode (tungsten tip) was first dipped into the mercury held in the cathode pool-keeping structure and then retracted. This caused an arc discharge between cathode and igniter which transferred immediately to the anode, because of the lower impedance in the anode circuit. Actuation of the igniter was first manual (this was permissible because the discharge never extinguished except when intentionally turned off) and later automatic, as shown in Fig. 22.

With the automatic circuit, the igniter current was passed through the entire igniter actuator solenoid, which pulled the igniter out of the mercury against a spring force. When the discharge had transferred to the anode, the igniter was held in the "out" position by the "holding" portion of the actuator solenoid, and the igniter was disconnected by the igniter relay. Both this relay and the "holding" winding had very low impedances, so that the hold power was negligible ($\approx$ 0.5 W). The system was simple and reliable and required no external logic or additional power supply.

It has since been demonstrated that arc initiation can be accomplished equally well without any moving parts, using a stationary igniter electrode placed in front of the cathode. In order to start the discharge, an automatic circuit applies high voltage pulses ($\gtrsim$ 20 kV) in rapid sequence between igniter and cathode. After a short interruption of normal discharge operation, usually only one pulse is needed to restart the arc. The electrical pulse

* It was demonstrated, however, that the loss associated with R_A is nonessential, and that equal results can be obtained using $R_A = 0$ and an electronically controlled (variable-reactance) constant-current supply.

ignition system is fully applicable to thruster operation. A flight-type system will use a vacuum-potted pulse transformer (also demonstrated) and silicon controlled rectifiers to derive the pulse power directly from the discharge power supply.

2. Feed Rate Control

During most thruster tests, including most of the life test period, the feed rate was controlled by manual gas pressure adjustment, using a feed system such as that shown in Fig. 8. The feed rate was measured by taking periodic readings of the piston position indicator.

When the vapor pressure feed system (Fig. 9) became available, automatic closed-loop control was provided as follows (see Fig. 22): The actual beam current I_B was compared electronically with a manually set level $I_{B,O}$, and the rms value of the ac current through the feed system heater I_F was made to follow the relation

$$I_F = I_{F,O} \left[1 - c_F (I_B - I_{B,O}) \right]$$

by phase-angle control, using silicon controlled rectifiers. (In the equation above, $I_{F,O}$ is the manually adjusted normal level of I_F, and c_F is a design constant of the control circuit, chosen to provide the proper sensitivity.)

This method of feed rate control was feasible because of the time invariance of the LM cathode thruster characteristics observed during the life test. For a given magnetic field and discharge current, the ratio of beam current to propellant flow rate is a constant, independent of time. Thus the mass flow rate may be accurately determined by monitoring the beam current.

The vapor pressure feed system was also equipped with a position indicator (not shown in Fig. 9), which was read periodically in order to obtain absolute flow rate measurements.

3. Neutralizer Circuit

The LM neutralizer cathode has the basic advantage of requiring no additional power supply; it has no heater, and the power required to transfer the neutralizing electrons from the cathode into the beam, as well as that required to ignite the neutralizer arc, can both be furnished by the beam supply.

We have simulated the conditions expected in actual space operation for a thruster with LM cathode neutralizer by the circuit arrangement shown in Fig. 22. To this end, we have distinguished between the function of the "spacecraft skin" (represented by the shield plate surrounding the downstream end of the thruster) and the function of "space" (represented by the

sum of all beam collecting surfaces, i.e., collector, cryowall, and baffles.)

To appreciate this distinction, consider what will happen in space when a thruster is turned on (the beam supply being connected between thruster and neutralizer) and the neutralizer does not yet emit electrons: First, the entire spacecraft will charge negatively until its potential with respect to space just exceeds the beam voltage. This condition will then prevent further escape of the ion beam; hence the beam will be forced to return to the spacecraft skin. If neutralizer were directly connected to this skin, no voltage difference could arise between neutralizer and skin, nor could the fact that an ion current is returning to the skin be distinguished from the desired condition where an equal electron current is emitted by the neutralizer. Therefore, no signal would be available to initiate the neutralizer discharge. However, by the simple expedient of connecting the neutralizer to the skin through a voltage-limiting device, capable of carrying temporarily the full beam current, the voltage across this limiter (and a maximum power equal to beam current times limited voltage) can be used to start the neutralizer. In our tests a bank of 100 V glow discharge tubes (L1 in Fig. 22) served in the limiter capacity; a flight-type system would use Zener diodes instead. Neutralizer arc initiation was accomplished during the entire contract period by connecting, in parallel to the limiter, an electromechanical igniter similar to that used on the main thruster cathode; again, automatic ignition by a stationary electrical pulse igniter suitable for space application has since been demonstrated.

The part of the circuit described to this point would also be required in space, while the remainder of the circuit was necessary only for testing with a laboratory-type beam power supply. Had the neutralizer extinguished while no current return path existed between the thruster and the grounded collecting surfaces in the vacuum chamber, the continued emission of ions by the thruster would have caused the negative terminal of the beam power supply to float up to slightly more than the full beam voltage with respect to ground,* while normally (when the neutralizer is operating or the neutralizer circuit is shorted out by the neutralizer switch shown in Fig. 22), the positive terminal of the beam supply is at beam voltage with respect to ground. Because our beam power supply design permitted only relatively small deviations of the negative terminal from ground potential, it was necessary to connect the "spacecraft skin" through a second voltage limiter (also capable of carrying the full beam current) to the collecting surfaces. Another bank of 100 V glow discharge tubes was used for this purpose in our tests (L2 in Fig. 22). So long as the neutralizer was operating, the floating voltage between skin and collector was only a few volts and the glow tubes acted as insulators. When the neu-

* This potential distribution corresponds to that in space described in the preceding paragraph.

tralizer was not emitting electrons, the glow tubes ignited and completed the beam current loop. Figure 23 illustrates qualitatively the ranges of variability of all pertinent voltages in this circuit.

4. Automatic Sequencer

The automatic igniter described in Section V-D-1 made it possible to use the following extremely simple start-up procedure:

1. Turn on (simultaneously, if desired) feed-rate controller, beam power supply, accel power supply, discharge power supply, magnet power supply (if electromagnets are used), and neutralizer feed system. With no mercury in the cathode pool-keeping structure, the igniter tip remains $\approx$ 1 mm from the cathode throat without making contact.

2. When mercury starts to flow, it completes the igniter circuit, and the automatic igniter starts the discharge, thereby immediately producing an ion beam.

   Since the high voltages are applied before the discharge is ignited, the plasma can never diffuse out of the discharge chamber; hence, the accel interception current is always kept low, thus permitting the use of a low-power accel supply.

3. The automatic neutralizer igniter, actuated by the presence of beam current, begins with attempts to ignite the neutralizer arc; these attempts succeed as soon as mercury starts to flow through the neutralizer cathode. (If the neutralizer flow has started before the main thruster cathode flow, the first attempt will succeed.)

When high-voltage breakdown occured between the accel and screen electrodes or between accel electrode and "spacecraft skin," the overload relay in the accel circuit triggered the automatic interlock sequencer, which then performed the following operations (with time delays as required to accommodate the power supply time constants):

1. Turn off beam supply, accel supply, and discharge supply

2. Turn on beam supply and accel supply

3. Turn on discharge supply. (Automatic igniters restart discharge, and hence beam and neutralizer.)

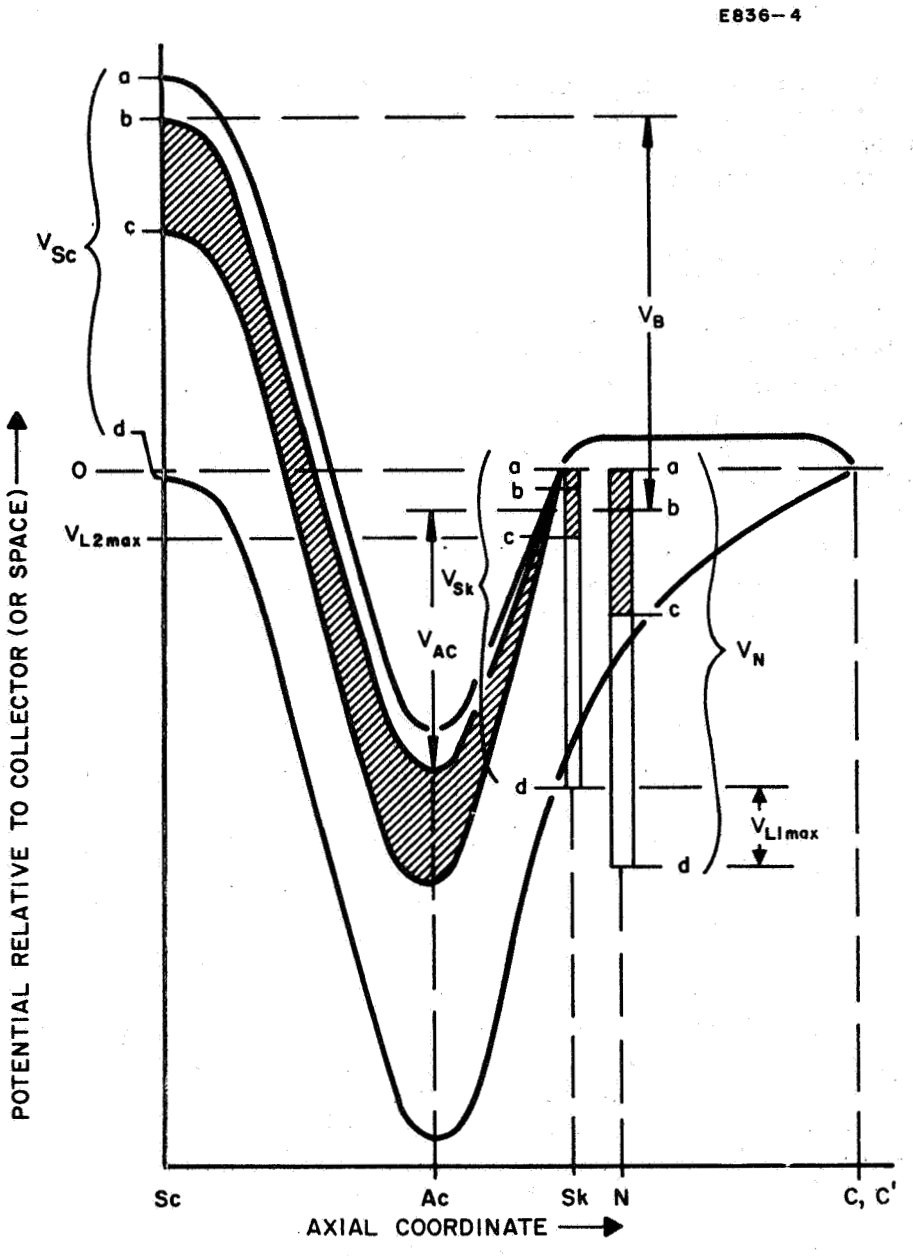

Fig. 23.
Qualitative potential distributions on beam axis, and potential ranges of "spacecraft skin" and neutralizer. (Voltage symbol without arrows denotes voltage between the respective point and collector or space; voltage symbol with arrows denotes voltage between arrow tips.) Operating conditions: (a) neutralizer circuit shorted out by neutralizer switch, (b) normal operation with neutralizer, (c) maximal excursion with neutralizer circuit during tests, limited by L1 and L2, (d) maximal excursion with neutralizer circuit in space (or during test without L2), limited by L1 only. The shaded region indicates the potential range accessible to the system during the tests. V_B and V_{Ac} are potential differences impressed by power supplies and remain the same under all operating conditions.

When high-voltage breakdown occurred between the thruster and ground, an internal overload relay of the beam power supply turned this supply off. This resulted immediately in an accel overload, thus triggering the same sequence as above.

E. 4,000 hour Test

The most important test result obtained under the subject contract is the demonstration of essentially unlimited cathode life. The problem of cathode life had previously threatened the usefulness of mercury bombardment thrusters for missions of 10^4 hours or longer.* The goal of the test was to establish the cathode lifetime in a working thruster by testing the complete unit for a cumulative total of 3750 hours under specified conditions. Not only has this requirement been satisfied, but a total of 4009 hours with beam extraction had been recorded and the total operating time of the cathode had exceeded 5250 hours at the end of the reporting period, with both thruster and cathode continuing to be used for diagnostic and comparative tests, with no degradation.

1. Long-Term Thruster Performance

Table III shows the operating parameter ranges for the life test. As stated in Section V-A, thruster optimization was not required under the contract, which specified only the test conditions listed on line I of this table. Lines I, II, and III show, however, that the test was already started with considerably better performance than required, and that there was no degradation over the 2780 hour period where the thruster was left unchanged.

The time invariance of the thruster characteristics also is illustrated in Fig. 24, which shows the reproducibility of the mass utilization and discharge voltage (at constant discharge current) at various times during the test. The spread in the measured points is less than $\pm 1\%$ over 2780 hours. As described in Section V-D, this part of the test was conducted with an open-loop control system; this was possible because of the inherent stability of the cathode and thruster characteristics.

Throughout the test the accel interception current remained stable at $\approx 0.5\%$. The interception current goes through a broad minimum at accel-decel ratios between 1.2 and 1.5, as discussed below. During the life test, a ratio of approximately 1.3 was maintained.

The maximum accel erosion occurred on the central downstream side of the accel electrode in triangular-shaped pits between apertures. Adjacent pits were interconnected by shallower troughs of erosion. A photograph of the downstream side of the accel electrode after 2780 hours is shown in Fig. 25. These pits were formed by slow charge-exchange ions created in the

---

* W. R. Kerslake, "Cathode Durability in the Mercury Electron-Bombardment Ion Thruster," AIAA Paper No. 64-683, Philadelphia, Pa., 1964.

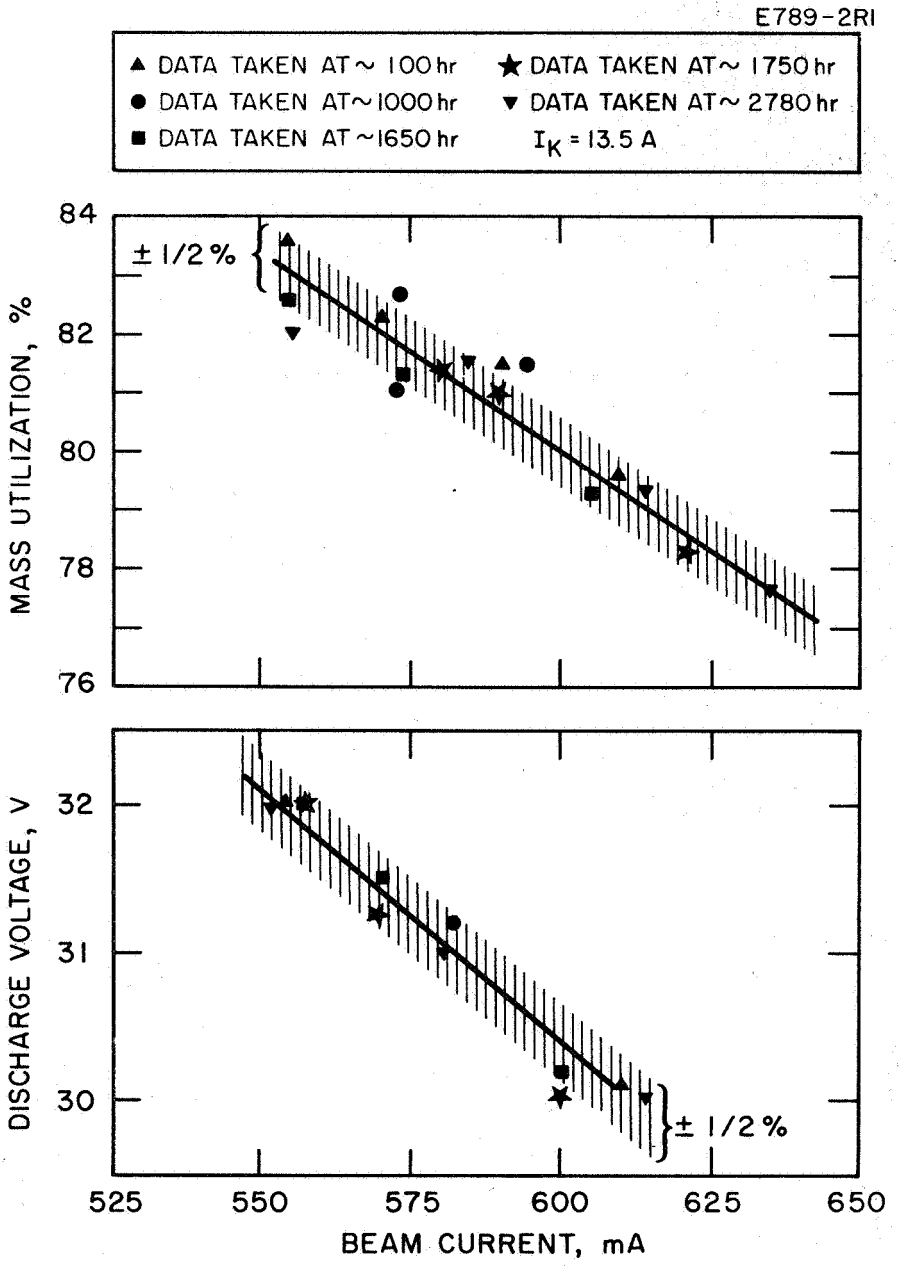

Fig. 24.
Thruster characteristics for constant discharge current during first 2780 hours of test. Primary independent variable is the mercury feed rate (in open-loop operation) on the beam current setting of the feed-rate controller (in closed-loop operation).

E679-I

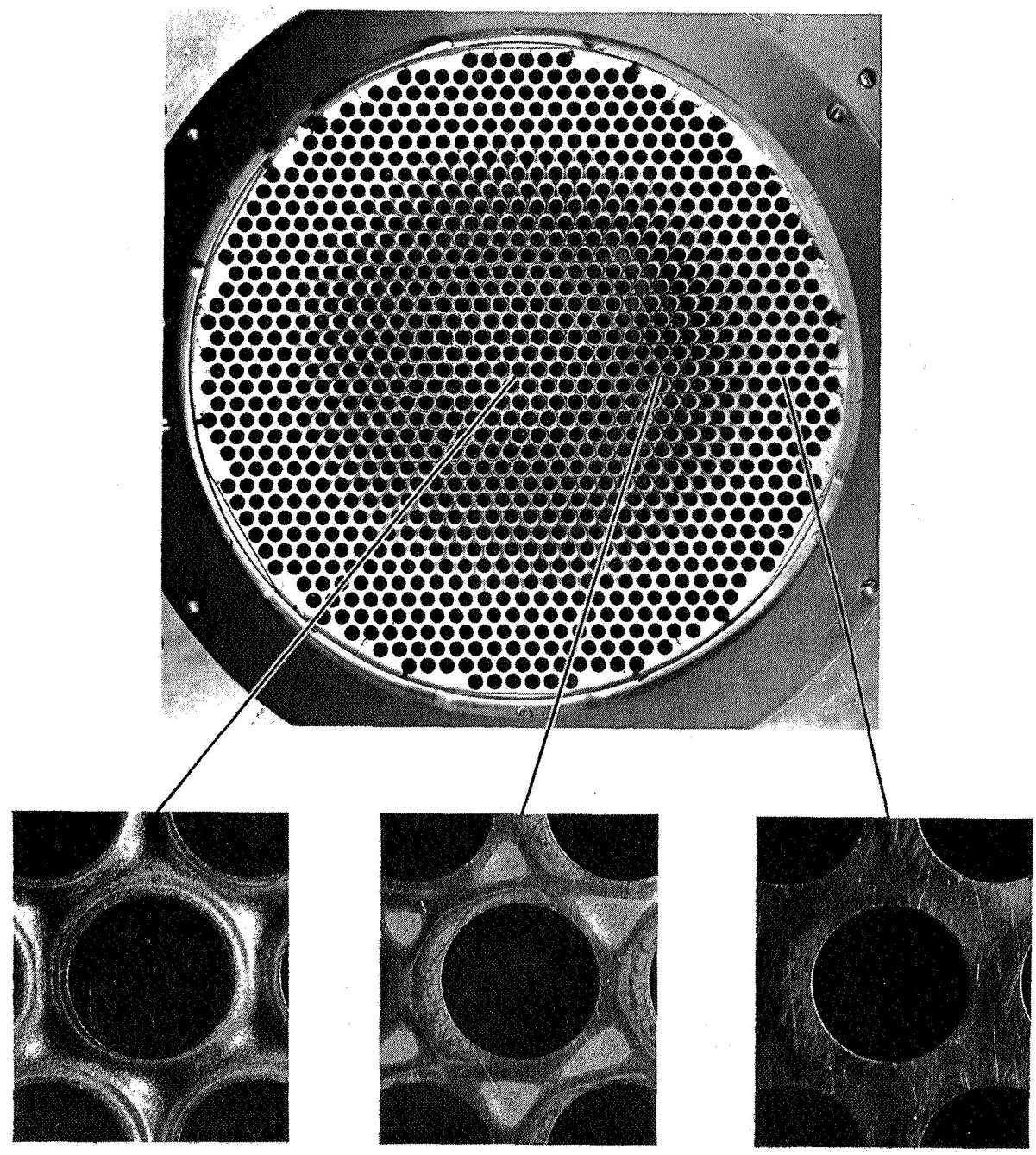

Fig. 25. Accel electrode after 2780 hours of test.

TABLE III

Thruster Performance Summary

		Beam Current, mA	Beam Power, kW	Effective I_{sp}, sec	Mass Utilization %	Source Energy per ion, eV/ion	Accel Current, mA	Magnetic Field at Screen, G
I	50-hour average required by contract	600± 10%	≥3	6000 ± 15%	>80	<1000	-	-
II [a]	50-hour averages at 150 hours	589	3.66	6370	80.8	729	2.9	26
III [a]	50-hour average at 2700 hours	588	3.65	6380	81.0	724	2.8	26
IV [a]	Average for first 2780 hours	588	3.65	6380	81.0	725	2.8	26
V [b]	500-hour average at 3400 hours	575	3.56	6370	80.9	567	2.5	10
VI [c]	500-hour aver. age at 4000 hours	605	3.69	6350	81.0	472	2.7 w/o neutr. 3.4 w. neutr.	16.5
VII [d]	6-hour average at 3500 hours	600	3.72	6700	85	393	3.6 w. neutralizer	15
VIII [d]	Low-I_{sp} test at 3500 hours	595	0.95	3360	84	413	4.5	16

[a] Central baffle as shown in Fig. 18

[b] Baffle consisting of single annular opaque zone

[c] Baffle consisting of central opaque zone plus an annular opaque zone

[d] Same baffle as for line VI, all operating parameters optimized for this thruster geometry.

beam plasma and focused by the concave part of the plasma meniscus which separates the downstream plasma from the nonplasma region.*

In addition to this erosion by charge-exchange ions, some enlargement of the accel holes is caused by the small percentage of ions which are extracted from the plasma but are not focused through the accel apertures. The radial dependence of the erosion on the downstream face of the accel electrode and the enlargement of the accel apertures is plotted in Fig. 26.

The peak in the aperture enlargement at approximately r = 2.5 cm, observed after 2780 hours, resulted from the combined effects of the reduction in perveance with increasing radius (which, by itself, is not sufficient to explain the observation) and of an annular peak in the plasma density caused by the effects of the baffle. The increased plasma density in this annular region has also been observed visually. It was caused by electrons streaming out around the baffle and following magnetic field lines which intersect the screen electrode at approximately r = 2.5 cm, the radius of maximum aperture enlargement (see Fig. 18).

On the basis of the erosion measurements and the observed electron concentration, the baffle geometry was modified in steps after 2780 hours from a single disk to annular open and opaque zones, in order to spread the electrons more evenly over the discharge-chamber cross section. The final baffle configuration is shown in Fig. 27. As a result, the annular peak in the aperture enlargement disappeared (see Fig. 26, 4009-hour direct-interception curve),+ and the thruster performance was improved drastically, as shown in Table III and Fig. 28. An additional benefit of the improved electron distribution was the lowering of the magnetic field required for optimum efficiency. With a field of 16G in the plane of the screen electrode, the magnet power consumption was 25W.

Both curves for charge-exchange erosion in Fig. 26 are peaked at the center. Because the local charge-exchange ion production rate is directly proportional to the product of beam current density and neutral

---

* W. O. Eckhardt, J. Hyman, Jr., G. Hagen, C. R. Buckey, and R. C. Knechtli, "Research Investigation of Ion Beam Formation from Electron-Bombardment Ion Sources," HRL Final Report for Contracts NAS 3-2511 and 3-3564, March 1964. Also S. L. Eilenberg, W. Seitz, and E. Caplinger, "Evaluation of Electrode Shapes for Ion Engines," AIAA J. 3, 866 (1965).

\+ At present we have no explanation for the fact that the total diameter increase measured after 4009 hours is less than that measured after 2780 hours for the central portion of the accel electrode. Both measurements were carefully repeated by independent methods; the effect is considerably larger than the statistical spread of the measurements, and backsputtering is insufficient to explain the observation by about an order of magnitude.

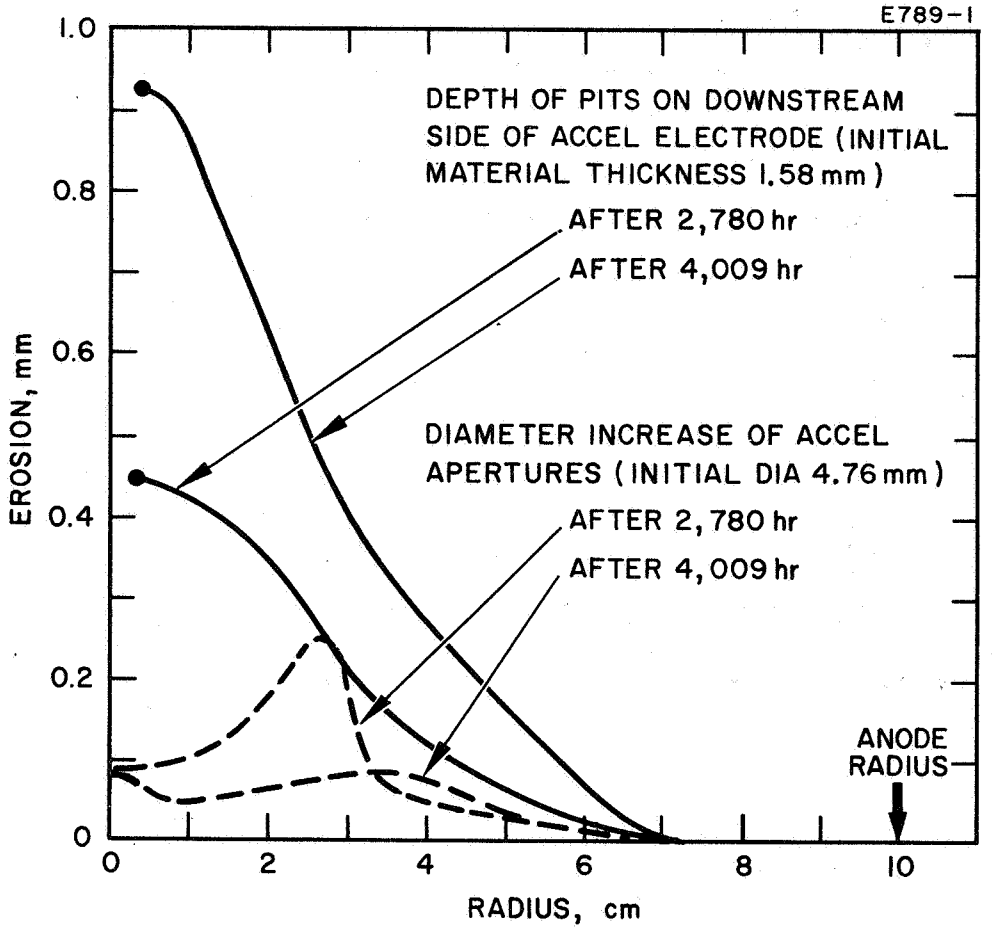

Fig. 26. Charge-exchange and direct interception erosion of accelerator. (Note that the deep pits are not limiting the electrode life, as explained in text.)

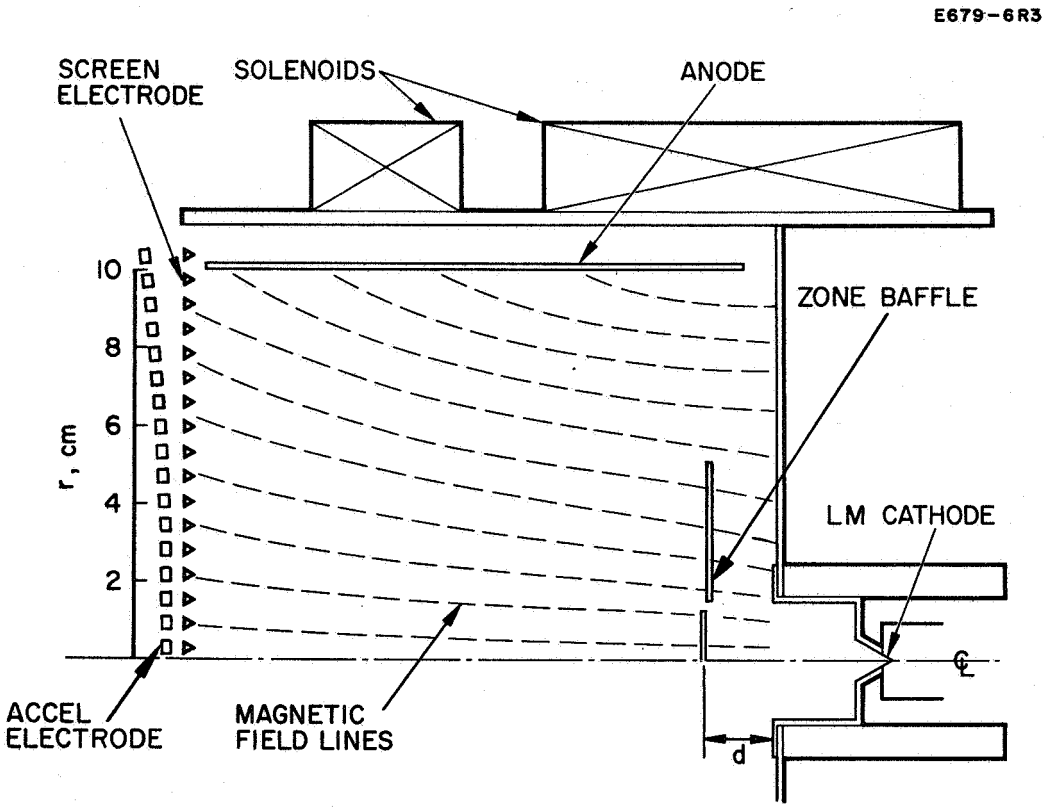

Fig. 27. Schematic cross section of life test thruster with final baffle configuration.

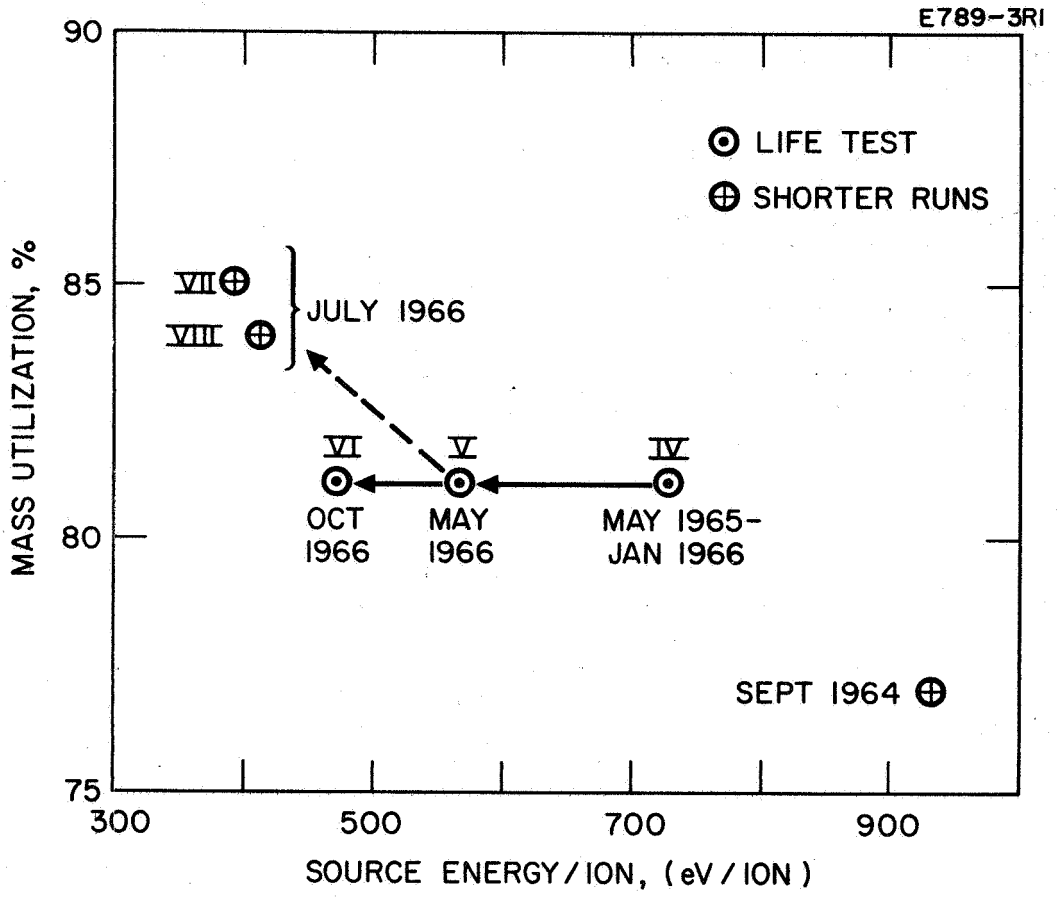

Fig. 28. Thruster performance improvements. (Roman numerals refer to items in Table III, p. 53.)

efflux density, the neutral efflux must have been peaked in the center by a sufficient amount to compensate for the central dip in beam current density which existed during the first 2780 hour period. This conclusion is further supported by the increased steepness of the 4009-hour charge-exchange erosion curve, after the annular peak in the beam current density profile was eliminated.

Our erosion measurements led to the following predictions for the useful life of the ion extraction system: The critical erosion mechanism is charge-exchange erosion; however, this is not because of the deep triangular pits which will eventually result in additional holes in the accel electrode (these holes are permissible from both an electrical and a mechanical point of view), but rather because of the shallower troughs connecting the pits. It is when these troughs break through in the region of maximum erosion of the accel electrode that the electrode starts to disintegrate. Therefore, the useful lifetime of the ion-optical system is taken as the extrapolated breakthrough time for the deepest troughs. Based on the erosion rate prevailing during the last 1229 hours, the ion extraction system used in this test should have a useful life of 10,500 hours.

The thruster test history during the 3750 hours of operation under specified conditions is summarized in Fig. 29. It shows the 50-hour averages of the relevant operating parameters and of the high-voltage arcing rate, and it indicates when the major interruptions or changes in the test occurred. Note that the arcing rate was significantly higher after the cryo-wall baffle material had been changed from copper to stainless steel, because of different peeling characteristics of the thin metal layers formed on the exposed thruster components by sputter deposition.

2. Thruster Performance Mapping

After the first 1000 hours of the life test, the thruster performance was mapped* under direction of the contract monitor, Mr. R. R. Nicholls. The results are summarized below.

The beam current and hence the mass utilization and source energy per ion are strong functions of the neutral flow rate, the discharge current, and the magnetic field, and they are weak functions of the total accelerating voltage and the baffle position. It is always advantageous to operate the thruster at the maximum mass utilization and minimum source energy per ion. We describe here one method of optimizing thruster performance by measuring the beam current as a function of magnetic field for different cathode currents. A typical set of curves at a fixed neutral flow equivalent of I_a = 630 mA is shown in Fig. 30. Characteristic of these curves is the very rapid rise in beam current as the magnetic field is increased from zero to $\approx$ 10 G (at screen); the curve gradually becomes flatter as the field is raised past $\approx$ 20 G. Increasing the discharge current raises the curve without changing its shape. From these curves an optimum operating point

* It should be noted that all performance mapping was done before the baffle modifications and the resulting performance improvements.

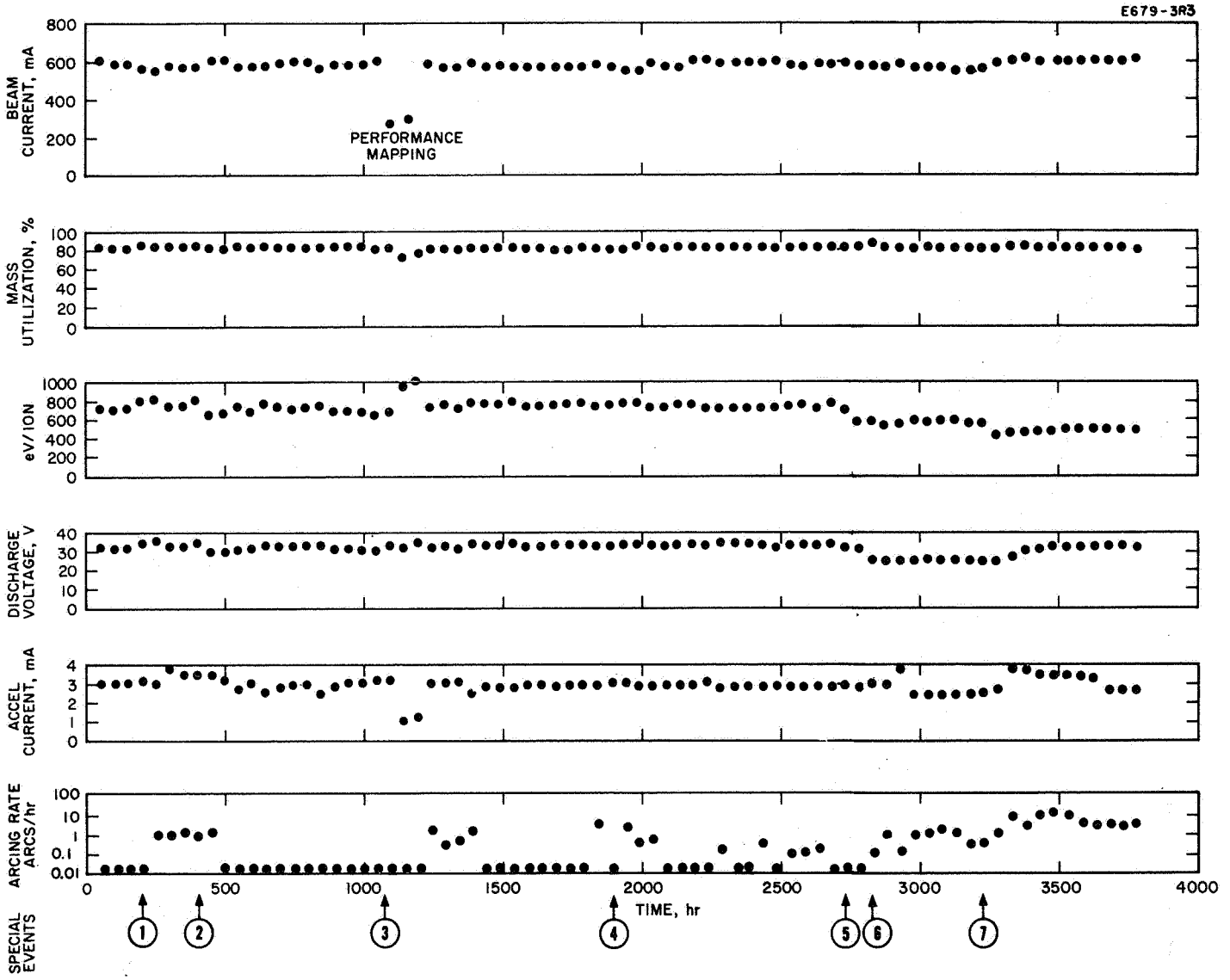

Fig. 29. Relevant parameters (50-hour averages) during thruster life test. Special events: (1) Optics cleaned. (2) Vacuum chamber cleaned. (3) Optics and vacuum chamber cleaned. (4) Optics and vacuum chamber cleaned. (5) Baffle consisting of single annular opaque zone installed in discharge chamber; copper baffles in vacuum chamber replaced by stainless steel baffles. (6) Start of automatic feed-rate control; optics and vacuum chamber cleaned. (7) Baffle consisting of central opaque zone plus annular opaque zone installed in discharge chamber; continuous neutralizer operation started; optics and vacuum chamber cleaned.

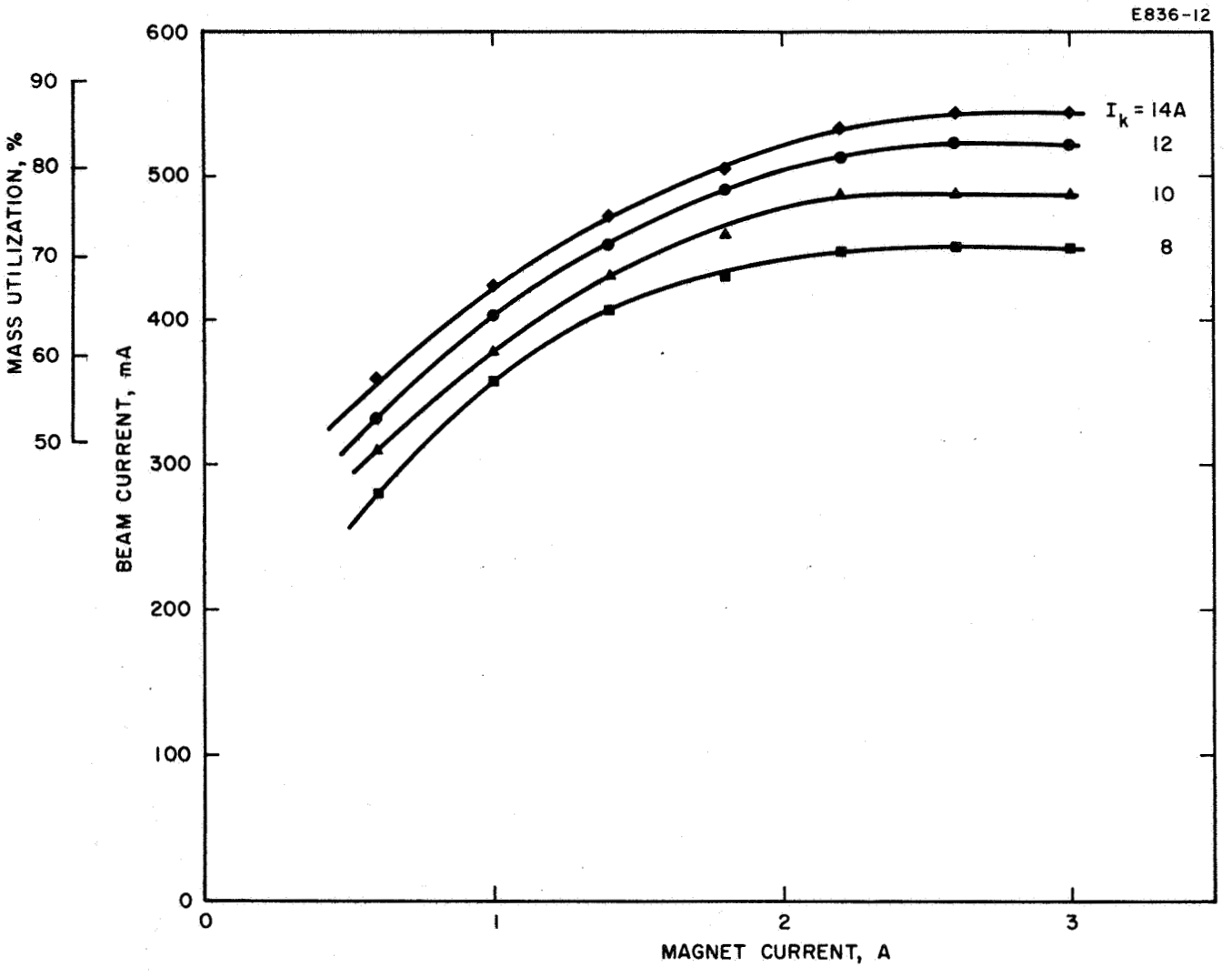

Fig. 30.
Beam current and mass utilization versus magnet current at fixed mass flow rate (I_a = 630 mA). Parameter: cathode current. (Magnetic field versus magnet current calibration: 10 G/A at screen, 20 G/A at upstream end plate.)

can be found for a given mass utilization; for example, if a mass utilization of ≥ 80% is desired, the curves in Fig. 30 show that the cathode current must be ≥ 11A and the magnet current ≥ 2A. Table IV shows the tradeoff between mass utilization and source energy per ion as a function of arc current and magnetic field. Figure 31 shows these points plotted on a graph of mass utilization versus source energy per ion, with arc current as the parameter. When this laborious process is repeated at other neutral flow rates, the data are found to fit on a universal curve with a fairly narrow spread, as shown in Fig. 32. The data include the flow rate equivalent (≈720 mA) at which most of the life test was run.

The dependence of the accel current on the accel-decel ratio is shown in Fig. 33. This graph shows that for the extraction system and current density distribution used, the minimum accel current occurs at an accel-decel ratio between 1.25 and 1.50. Throughout the life test the accel-decel ratio was maintained near the minimum of this curve at approximately $\frac{6.2 + 2}{6.2} = 1.32$.

During the performance mapping experiments the baffle consisted of a 2.5 cm diameter tantalum disk which could be moved downstream from a stop approximately 0.5 cm from the end of the magnetic shield which enclosed the LM cathode. Figure 34 shows the dependence of both beam current and discharge voltage on the baffle position. There is a definite maximum of the beam current at a baffle position ~2 cm downstream from the shield. The discharge voltage increased from ~28 V to ~31 V as the baffle was moved toward this optimum position from a downstream distance of 5 cm. (For the effect of the baffle position on the beam current density profile, see Section VI-C.)

3. Neutralizer Performance

The LM cathode neutralizer described in Section II-E was operated with the life-test thruster during the last 500 hour test increment. The neutralizer was held at a temperature of ≈20°C by water cooling. The mass flow rate was set by manual adjustment of the feed pressure; no automatic feedback loop existed, and manual readjustments were usually made only once daily. The circuit used is described in Section V-D-3. As noted in that section, the neutralizer was equipped with an electromechanical automatic igniter consisting of a solenoid-actuated tungsten tip which dipped into the exposed liquid mercury when the arc current was interrupted; it was subsequently pulled out in order to restrike the discharge.

While this type of igniter performed satisfactorily on the main thruster cathode during the life test, its use on the neutralizer was less successful. Because the igniter and neutralizer pool-keeping structure had approximately equal diameters, the mechanical action caused splashing of a considerable fraction of the small amount of liquid mercury contained in the pool-keeping

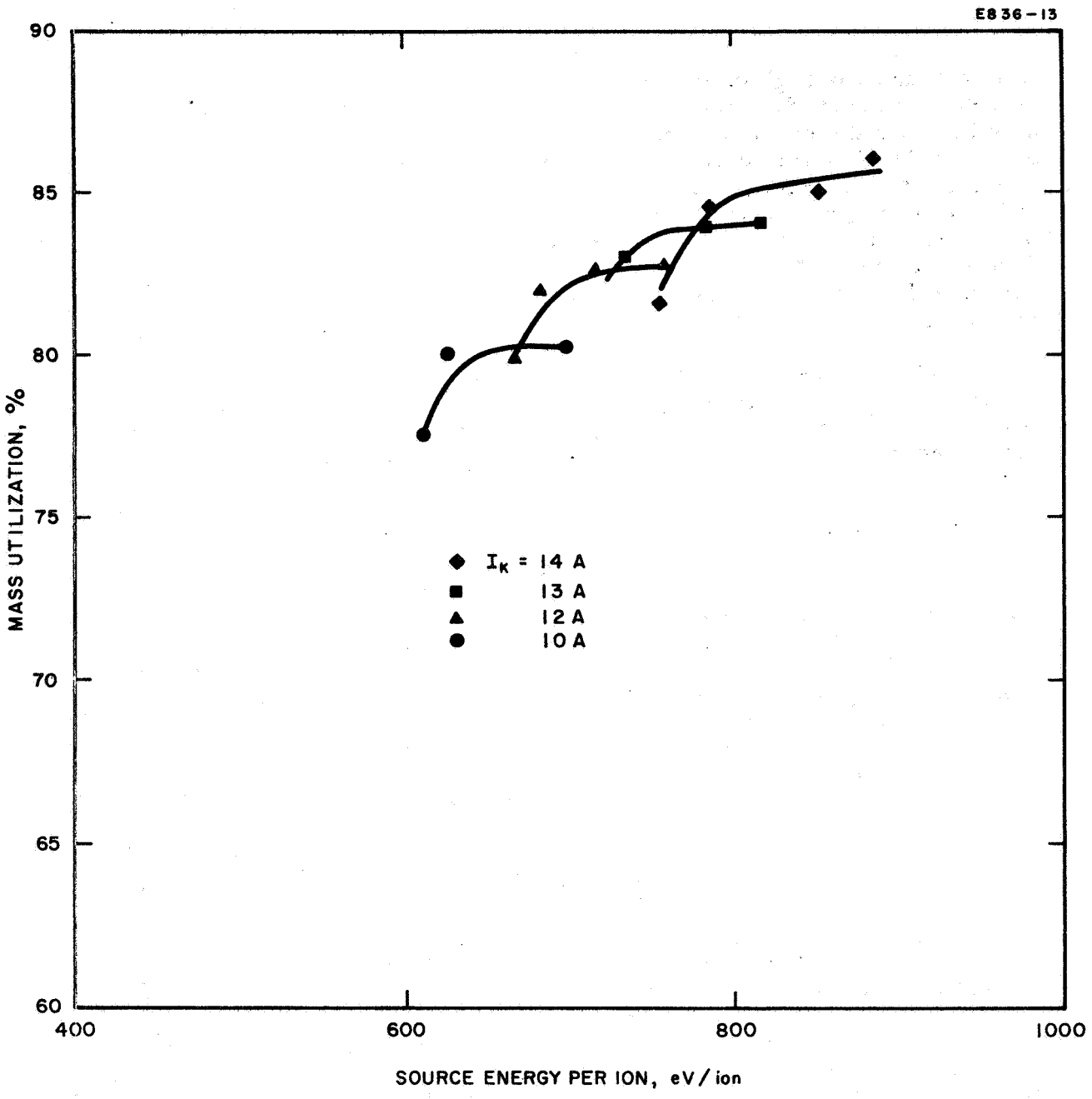

Fig. 31. Mass utilization versus source energy per ion for optimized magnetic field and fixed mass flow rate (I_a = 630 mA). Parameter: cathode current.

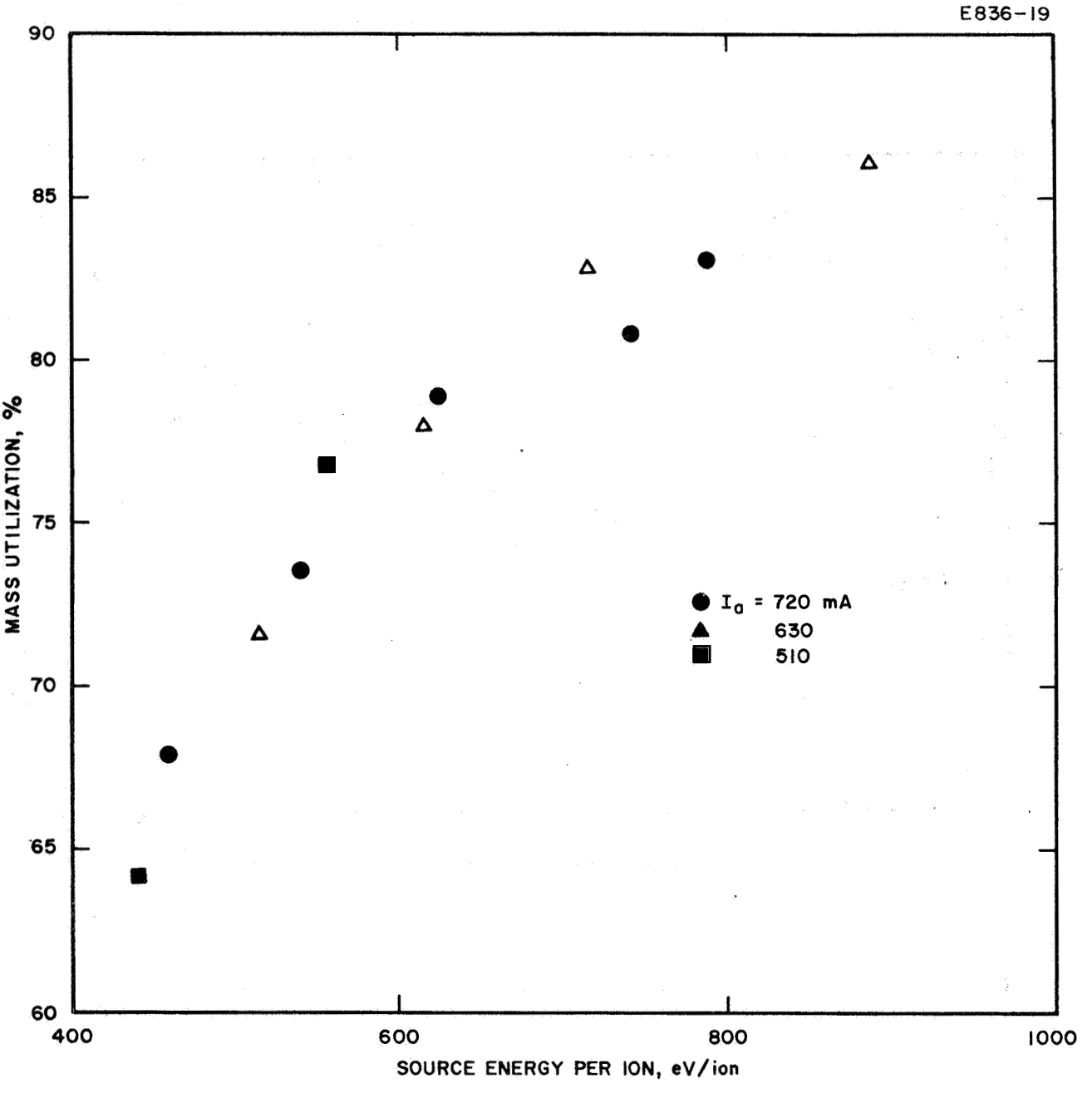

Fig. 32. Mass utilization versus source energy per ion for optimized magnetic field. Parameter: mass flow rate.

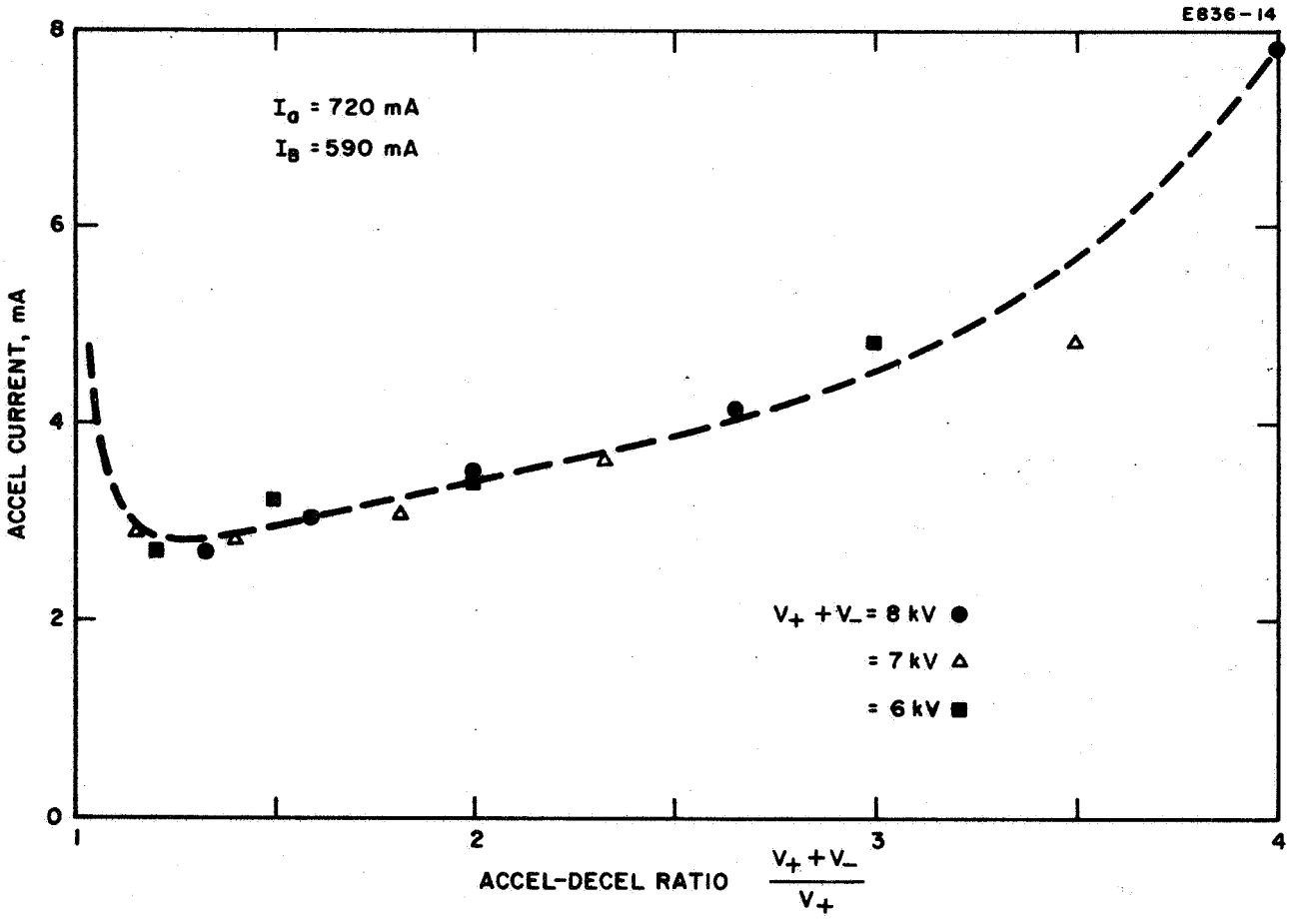

Fig. 33. Accelerator electrode current versus accel-decel ratio. Parameter: total accelerating voltage.

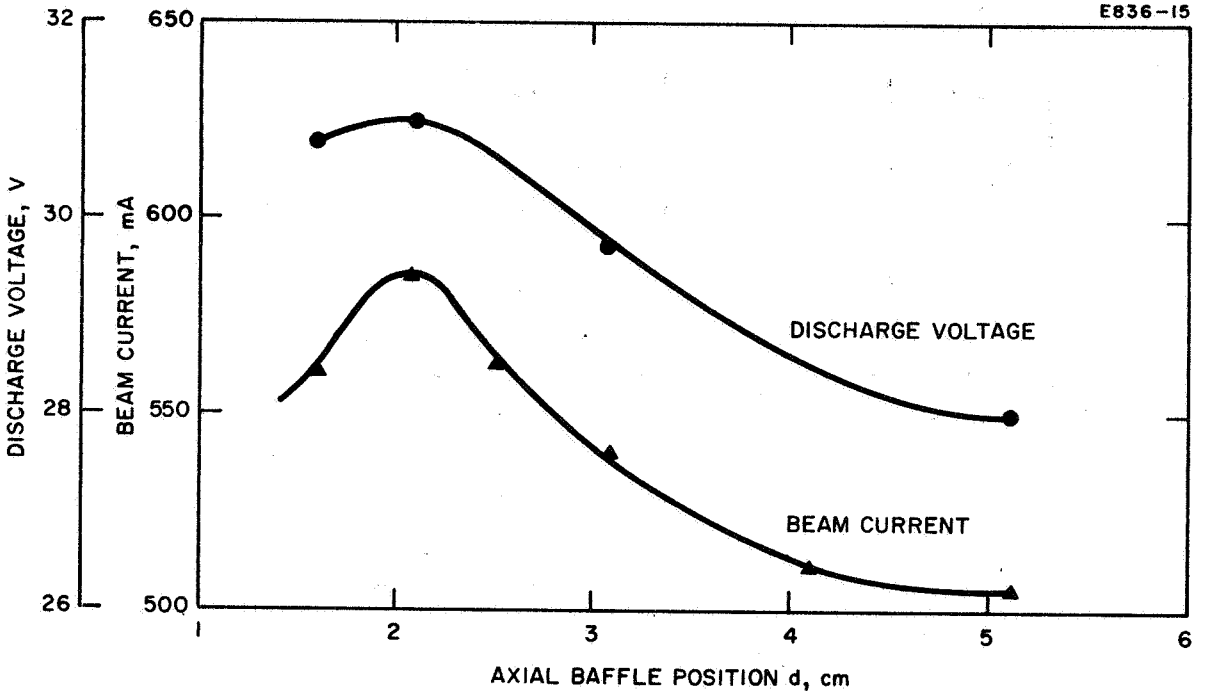

Fig. 34. Beam current and discharge voltage versus baffle position at fixed mass flow rate (I_a = 720 mA) and fixed cathode current (I_K = 13 A).

TABLE IV

Mass Utilization η_m and Source Energy per Ion V_S as a Function of Magnet Current I_M and Cathode Current I_K for a Flow Rate Equivalent I_a = 630 mA

I_M, A	I_K, A	V_S, eV/ion	η_m, %
3.0	11	698	80.3
	12	760	82.7
	13	815	84.2
	14	887	86.0
2.6	11	664	80.3
	12	714	82.5
	13	784	84.2
	14	852	85.0
2.2	11	627	80.0
	12	685	82.0
	13	735	83.0
	14	788	84.5
2.0	11	615	77.5
	12	670	80.0
	13	715	80.8
	14	753	81.5

structure when operating at the high electron-to-atom ratios (K_e/K_a) and low currents needed for neutralizer service. This had two detrimental effects: (1) It permitted the arc to run on the splashed mercury globules outside the pool-keeping structure, resulting in frequent arc extinctions (followed by more splashing by the igniter, thus perpetuating the situation); (2) It limited the obtainable effective electron-to-atom emission ratio to a level far below the design value (even though the latter had been confirmed in experiments using careful manual ignition.* The average effective operating time (on-time) of the neutralizer was reduced to a certain fraction of the total operating time by these frequent extinctions and the time required for reignition; this fraction was measured by observing oscilloscope traces of neutralizer current and voltage versus time.

The problem of neutralizer arc extinction when running on splashed mercury globules was alleviated somewhat when an auxiliary power supply was connected between the neutralizerand its igniter (serving as an auxiliary anode), providing an open circuit voltage of 1250 V and an auxiliary discharge current of 50 mA when the neutralizer was operating; the auxiliary discharge voltage was approximately equal to the voltage between neutralizer and collector, and hence the auxiliary discharge power was < 9% of the neutral-

---

* To confirm the contention that the predominant mercury loss mechanism was igniter splashing rather than evaporation, the neutralizer cathode was operated under the subsequent Contract NASW-1404 with the mechanical igniter at temperaures ranging from 20 to 90°C. (The operating temperature of an LM cathode neutralizer in space is expected to be in the vicinity of 100°C, assuming that it can radiate waste heat only from its exposed face.) While the vapor pressure of mercury changes by two orders of magnitude over this temperature range, the temperature increase to 90°C resulted in a reduction of the obtainable effective electron-to-atom emission ratio by only a small factor ($\lesssim 2$), as expected. At currents of 600 to 700 mA (corresponding to typical 20-cm diameter thruster currents) K_e/K_a up to 16 was maintained in runs of several hours duration at 90°C. This experiment proved the importance of the mercury losses by splashing. In addition, it indicated (by the measurement of K_e/K_a up to 16 in the presence of splashing) feasibility of efficient LM cathode neutralizer operation at the temperatures required for use in space, provided a nonmechanical igniter is used. The subsequent use of an electrical pulse igniter immediately resulted in stable neutralizer operation without the frequent arc extinctions experienced earlier. The following typical performance was observed under these conditions: neutralizer current = 600 mA; discharge voltage in diode operation = 20 V; $K_e/K_a \approx 53$; number of spontaneous extinctions during 4-hour run (automatically reignited) = 2. For more details on these experiments, see Quarterly Report No. 3, Contract NASW-1404.

izer power. This auxiliary circuit permitted the voltage to rise to a value an order of magnitude higher than in the main neutralizer circuit whenever an arc spot started to decay; this increased the probability that a new spot would form by increasing the power density of ion bombardment of the cathode surface.

The performance of the neutralizer during the 500 hour life test increment is summarized in Fig. 35, which shows (from top to bottom) the voltage between neutralizer and collector, the neutralizer expellant-flow, the average effective operating time, and whether the auxiliary discharge was used. The horizontal bars in the expellant-flow graph indicate the performance obtained during shorter periods with frequent readjustment of the flow rate; as can be seen, the goal of $< 3\%$ of the thruster flow rate was reached during these periods. Therefore, it can be concluded that the same performance should be available continuously with flow control by an automatic feedback loop. The graphs also demonstrate that the neutralizer power consumption was always less than one-third of the goal of 1W per 10 mA of neutralizer current, and that the use of an auxiliary discharge led to no advantage when the flow rate was accurately controlled.

The neutralizer run was terminated at 474 hours instead of the intended 500 hours when the igniter was blocked by back-sputtered material; details are given below.

4. Effects of the Test Environment

While most of the ion beam from the thruster impinged on the collector which had been provided for this purpose, the fraction of the beam which impinged on the cryowall-protecting baffles had a very noticeable effect; because of the greater proximity between baffles and thruster, back-sputtered material from these baffles reached the thruster in proportionately much larger quantities than from the collector.

When the life test was started, the baffles were of copper and the collector material was stainless steel. Consequently, the layer of back-sputtered material which formed on the shield surrounding the thruster and on parts of the ion extraction system was a mixture of copper and stainless steel. This material started to peel off rather rapidly, making it necessary to clean the ion-optical system and the vacuum chamber at the intervals shown in Fig. 29.

Although this was troublesome, it was tolerable because the test was affected only when the backsputtered layer had grown too thick and started to peel off. However, after the neutralizer had been mounted on the thruster for the first experiments, it was found that the backsputtered copper had the additional, intolerable effect of forming a layer on the molybdenum neutralizer face; the face thus became permanently wettable by mercury, and the mercury surface was prevented from assuming its proper

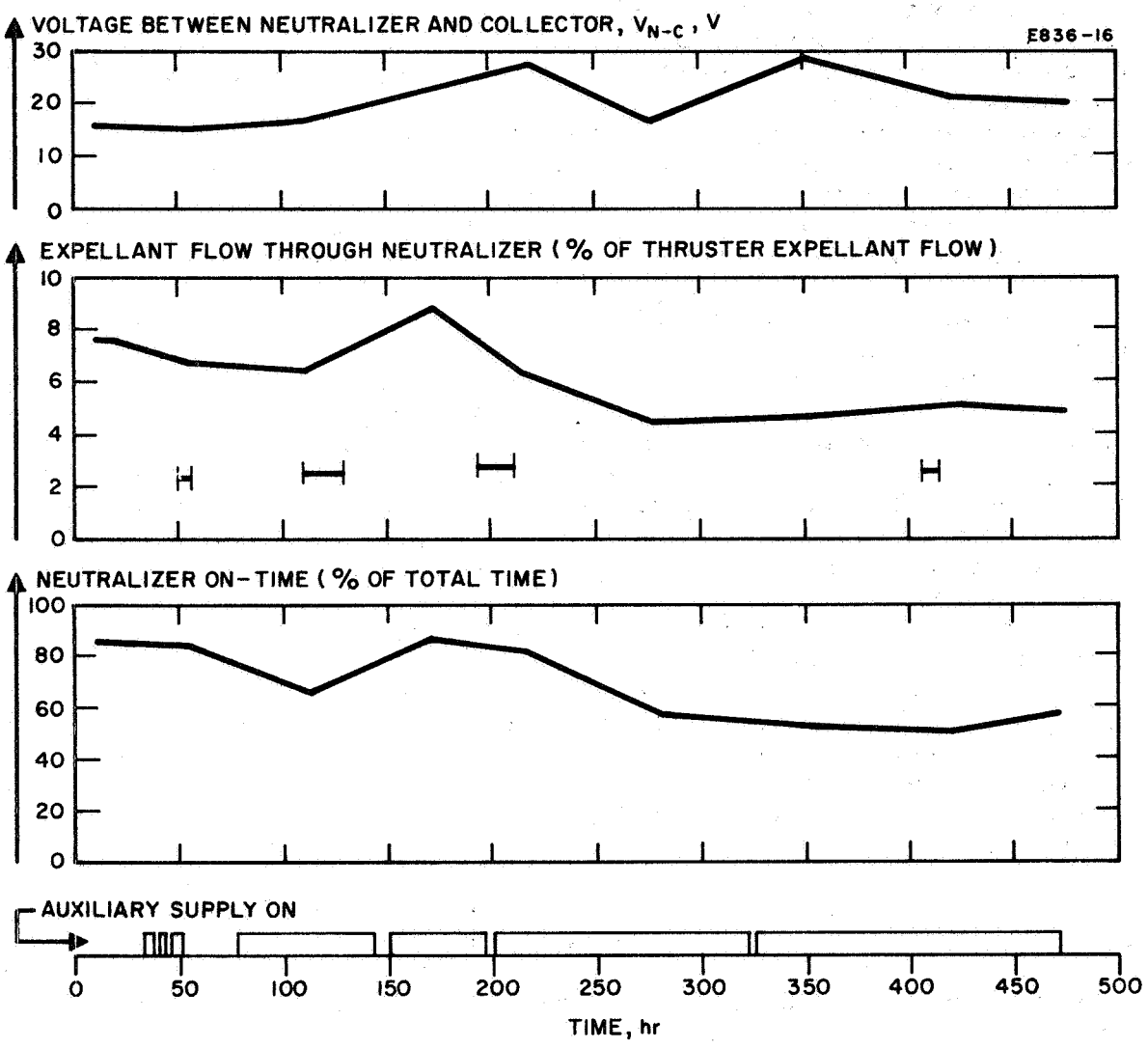

Fig. 35. Neutralizer life test performance.

position in the neutralizer pool-keeping structure. To remedy this situation, the copper baffles were replaced by stainless steel ones for the balance of the test, permanently eliminating this neutralizer test problem. The only detrimental effect of stainless steel backsputtering on the neutralizer was that 26 hours before the end of the final test increment a peeled-off stainless steel flake mechanically blocked the actuator pivot and kept the neutralizer igniter in its "out" position, thus preventing reignition of the neutralizer arc after its next extinction. Figure 36 shows the thruster with neutralizer after termination of the life test, with stainless steel peeling off the "spacecraft skin."

Concurrently with the change in the material of the vacuum-chamber baffles, the discharge chamber baffle was modified to have a central opening, thus leaving the main thruster cathode unprotected against impingement of backsputtered material. After 536 hours of operation under this condition, the thruster was shut off because the cryowall had developed a leak. (In order to conserve funds, the thruster was also shut off routinely during weekends without suffering any adverse effects.) When we attempted to restart the thruster after this interruption, we found that only 10% of the normal mass flow rate could be obtained at the maximum feed system pressure available. Therefore, the cathode was disassembled and inspected; the throat of the pool-keeping structure was found to be clogged with a black substance (Fig. 37). This substance was removed from the throat by pushing it out from the upstream side with a wire. The blackish plug produced in this fashion had a volume of $\approx 10^{-3}$ mm^3 and was subjected to x-ray diffraction (powder pattern) and neutron activation analysis. Because of the extremely small sample size, both methods of analysis could only be performed with great difficulties, and their results have a tentative character.

The Debye-Scherrer diffraction diagram revealed the presence of a face-centered cubic cell with a lattice spacing of 3.6 A. On this basis the major component of the sample was identified as austenitic stainless steel. However, because of the small sample volume, only the line spacing could be used for the identification. The line intensity ratio of the diffraction pattern could not be determined with sufficient accuracy to lend additional support to the analysis.

The neutral activation analysis established the following upper limits for the amounts of certain elements present in the sample:

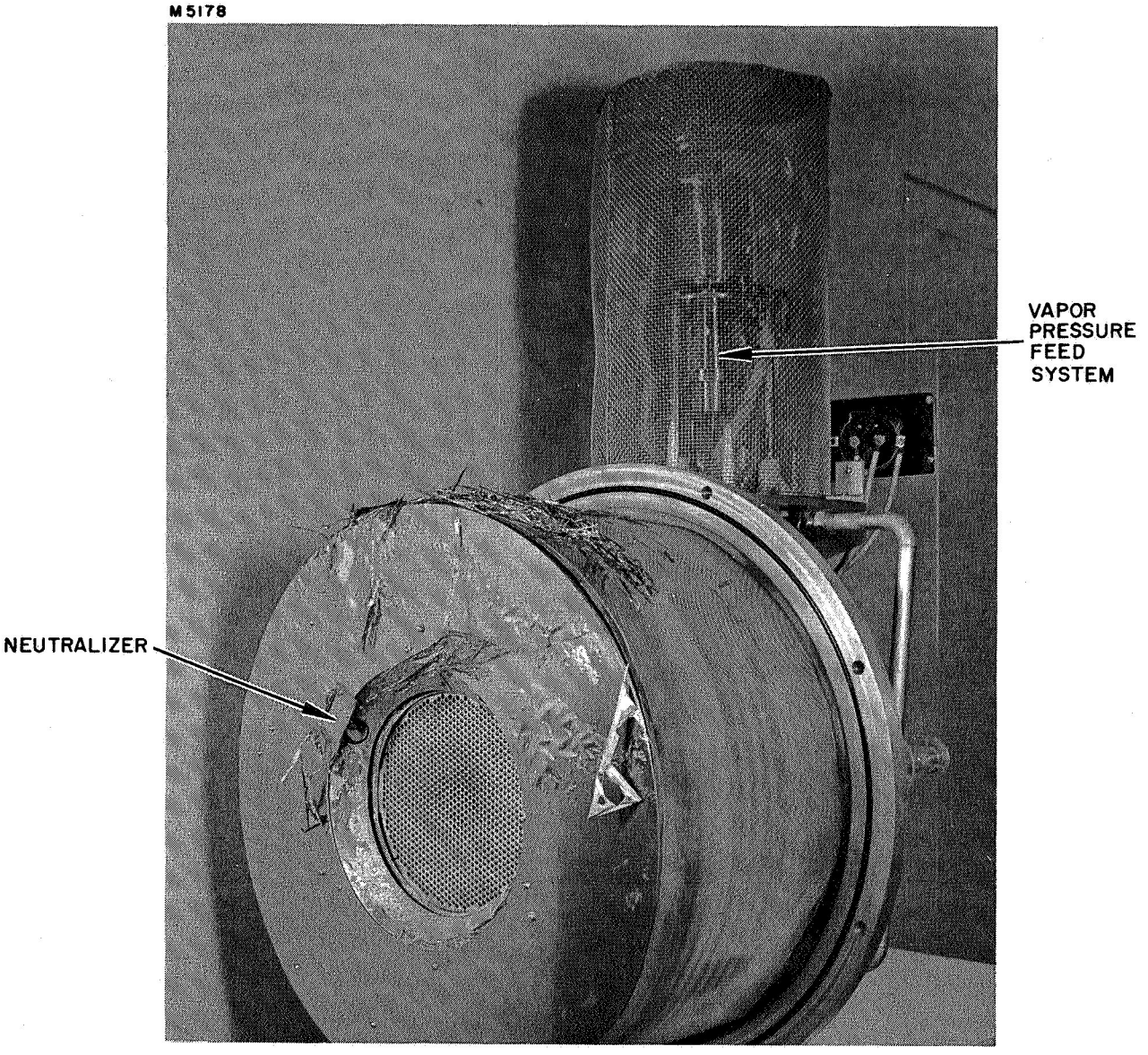

Fig. 36. Thruster with neutralizer and vapor pressure feed system after termination of life test.

Fig. 37. Pool-keeping structure of LM cathode with black deposit after 536 hours of unprotected operation.

Iron	$< 4.78\ \mu g$
Molybdenum	$\leq 2.16\ \mu g$
Mercury	$< 1.20\ \mu g$
Copper	$\sim 0.558\ \mu g$
Nickel	$< 0.158\ \mu g$
Chromium	$< 0.008\ \mu g$
Manganese	$\sim 0.002\ \mu g$.

The result is interpreted as follows: Significant amounts of stainless steel constituents (mainly iron, nickel, and chromium) from the beam-collecting surfaces, as well as some molybdenum from the ion extraction system, were sputtered into the mercury pool during the 536 hours of operation with the unprotected cathode. Some of this material went into solution in the liquid mercury, and when the mercury in the pool-keeping structure evaporated during the five weekend shutdowns of this operating period, the dissolved materials collected on the walls of the pool-keeping structure in the region where the mercury disappeared last - at the throat. Once solidified, these precipitates may or may not have dissolved again when mercury reentered the cathode; in either case, their concentration continued to increase until, after another shutdown for vacuum reasons, sufficient material had accumulated to clog the cathode throat almost completely.

Because the cathode had been inspected after each preceding increment of the life test, it was known that no similar precipitate had formed previously while the cathode was protected by a central baffle. It was concluded, therefore, that the new zone baffle should be converted from a configuration with center opening to one with an opaque zone in the center, surrounded by an annular opening equal in area to the original center opening. (This baffle is shown in Fig. 27.)

After the precipitate had been removed mechanically, the cathode was reassembled, including the previously used flow impedance, and the test was resumed with the modified baffle. Even better thruster performance was obtained than before (see Table III) and the cathode again remained free from back sputtered material to the end of the test, as shown in Fig. 17.

F. Tests at Elevated Cathode Temperature

While a thermionic cathode must be heated in order to emit electrons, an LM cathode receives a thermal power flux from its dense arc spot plasma; this heat flux must be conducted away in order to keep the cathode at a sufficiently low temperature for operation at the optimum electron-to-atom ratio. As stated in Section II-D, this thermal power was removed from the life-

tested cathode by water cooling, and the cathode was kept at ≈35°C. In space, an LM cathode can be cooled by thermal conduction to the thruster shell, followed by radiation from the shell to space. It was recognized during the contract period that the equilibrium shell temperature of electron-bombardment thrusters operating in space will be considerably above 35°C, unless the thrusters are equipped with special waste-heat radiators (which of course is undesirable from the standpoint of weight). Therefore, experiments were performed to determine the maximum cathode temperature at which satisfactory thruster performance could be obtained.

Most of these experiments consisted of measuring the maximum cathode temperature compatible with the arc currents and electron-to-atom ratios required for thruster operation. Such measurements were performed in diode and Penning discharge configurations using the following cathodes: (a) the life-tested cathode type, (b) a cathode with the same dimensions, but having a platinum-clad nozzle throat, and (c) a cathode differing from type (b) by having a maximum nozzle diameter twice as large. The platinum served to provide better wetting of the nozzle throat by mercury, thereby permitting cathode operation with smaller exposed mercury surface areas and hence with reduced evaporation rates. The following typical results were obtained:

Cathode type	a	b	b	b	c	c	c
Cathode temperature, °C	84	103	113	138	148	152	160
Cathode current, A	8.5	8.5	10	6	9.5	8.5	13.5
Electron-to-atom ratio	13	18	12	12	18	15	13

These data should be compared with the thruster life test requirement of 12···20 electrons/atom at 9···14 A, or with the requirement for operation in a 15-cm diameter thruster at ≈450 mA beam current:

11···17 electrons/atom at 6···10 A.

As expected, cathode type (c), with its larger cross section of the heat conduction path, gave the best results in these tests at elevated temperatures. Therefore, before the life test was begun this cathode was mounted in the modified 20-cm LeRC thruster, and the following performance was observed in a brief run: ≈97% mass utilization at 804 eV/ion and 475 mA beam current, with a cathode temperature of ≈135°C.

While a cathode temperature of 135°C would be useful for operation of a single thruster in space, it is too low when clustering of thrusters and the effects of solar radiation are taken into account. Under the subsequent Contract NASW-1404 these problems have since been studied in detail, and a solution has been provided in the form of an annular (rather than circular) LM cathode which can operate at temperatures up to and above 300°C.* It was demonstrated, for example, that the best performance obtained with the

* For details see Summary Report, Contract NASW-1404, Hughes Research Laboratories, June 1966 to July 1967.

life-tested circular LM cathode operating at 35°C (see Section V-E-1) could be duplicated with an annular LM cathode operating at 250°C. The advantage in thermal conductance (and hence in temperature of the exposed mercury surface)provided by the annular design is best illustrated by Fig. 38.

Figure 38 exhibits the functional dependence between the temperature of the exposed mercury surface T_{Hg} and the temperature of the cathode body at the thermocouple location T_K. Cathodes of annular and circular geometry are considered under typical experimental conditions for a 20-cm thruster. (The thruster is assumed to operate at 90% mass utilization, an electron-to-atom ratio of 12, and a specific thermal input to the cathode of 5 WA^{-1}.) The operating parameters of the thruster establish a proportional relationship between the power delivered to the cathode $P_{K,th}$ and the beam current I_B which is taken here as a parameter.

For zero beam current we have zero discharge power for which no temperature drop develops between the mercury pool and the cathode body. Under this condition the curves for both the annular and circular geometries coalesce along the zero thermal resistance asymptote where $T_K = T_{Hg}$. As the beam (and therefore the discharge power) increases, a temperature drop arises to drive the thermal power (delivered to the cathode by the discharge) from the mercury surface through the cathode body to the thruster shell, where it can be radiated to space. For the circular geometry this temperature drop becomes so excessive for beam currents of the order of 600 mA that the heat is delivered to the thruster shell at a temperature which is insufficient to permit its radiative dissipation under any but the most favorable conditions (single thruster, no solar radiation).

In the annular cathode, the heat load is distributed around the perimeter of the annulus ($\sim$1 cm) rather than being concentrated around the perimeter of the circular mercury pool ($\sim 10^{-2}$ cm for a mercury pool at 300°C in evaporative equilibrium with the mercury feed rate). This decrease in thermal loading density allows the same heat to be transmitted to the thruster shell, with a considerable reduction in the temperature drop required. We see that for a mercury surface temperature of 300°C and a beam current of 600 mA, only a 50°C temperature drop is developed by the annular geometry, compared with the nearly 400°C required by the circular geometry under the same total heat loading.

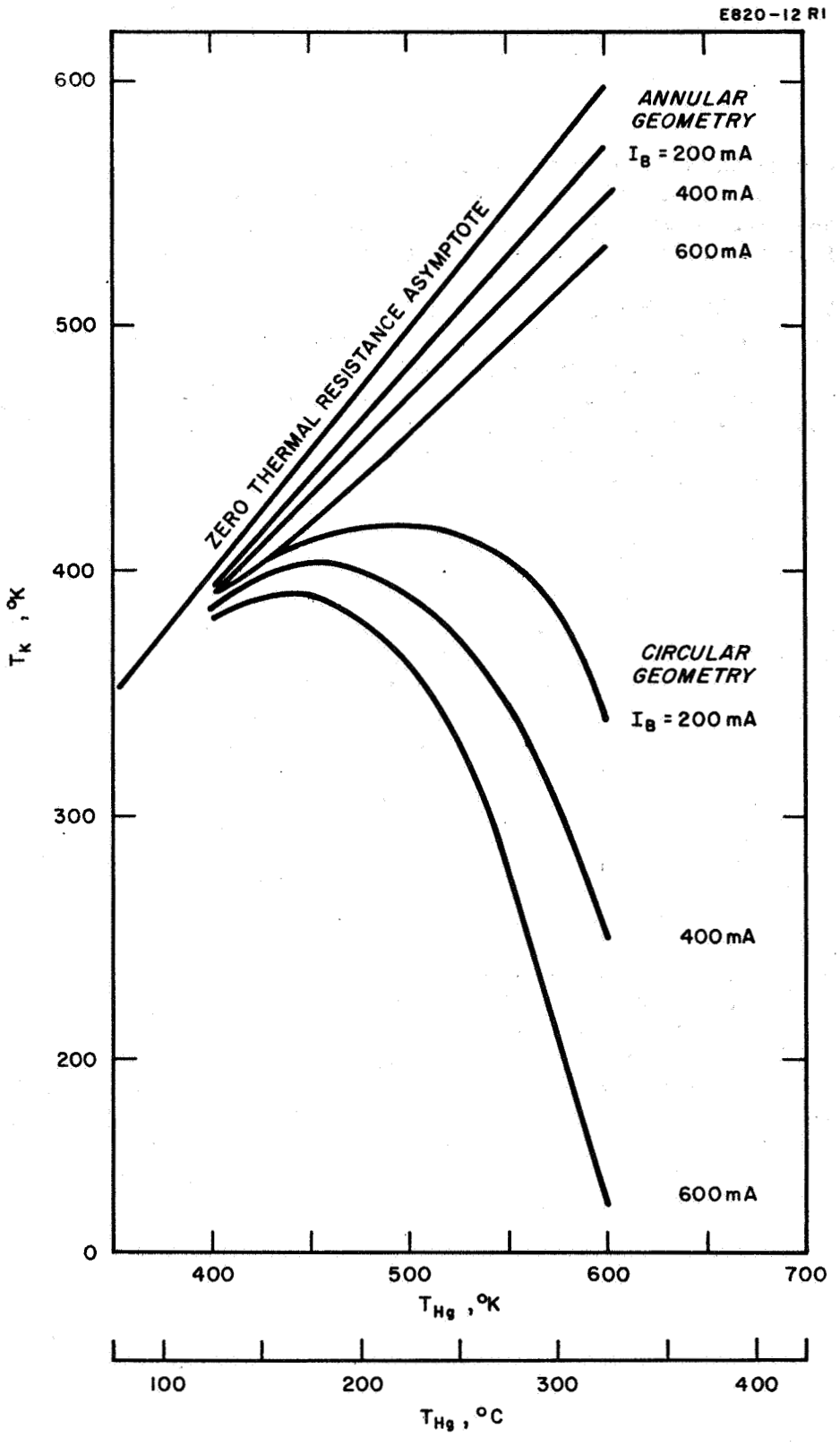

Fig. 38.
Functional dependence between temperature of exposed mercury surface T_{Hg} and temperature of the cathode body at the thermocouple location T_K for annular and circular cathode geometries. ($V_{K,th}$ = 5 W A^{-1}, η_m = 90%, K_e/K_a = 12.) From Quarterly Report No. 3, Contract NASW-1404, Hughes Research Laboratories.

VI. LM CATHODE ELECTRON-BOMBARDMENT DISCHARGE STUDIES

The discharge in an LM cathode thruster differs in three important respects from that in a thruster with a conventional cathode: (1) electron emission takes place with extremely high current densities from a local high-density plasma region, rather than at the relatively low current densities associated with thermionic emission; (2) the electron current drawn from an LM cathode depends only on the applied voltage and the plasma conditions in the discharge chamber, rather than being saturation limited; and (3) both the propellant atoms and the ionizing electrons are emitted by the LM cathode, instead of being introduced into the discharge chamber in separate locations.

Concerning the first one of these points it must be stated that the emission mechanism of liquid-metal cathodes is not satisfactorily understood at present, as evidenced by the many conflicting theories which have been proposed.* Fortunately, however, the purely phenomenological knowledge that we have gained about the emission from LM cathodes (as described in Section II) has proved fully adequate for attaining the objectives of the contract.

The other two points of difference have been the explicit or implicit subject of the theoretical and experimental studies described below. It should be noted that some of our results are also of importance for electron-bombardment thrusters with other cathode types, especially our findings concerning the effects of the magnetic field geometry and of baffles.+ Moreover, our experiments have led us to believe that the consequences of the distinction expressed in point (3) above can be essentially eliminated by a suitable baffle design; because electric and magnetic fields can be utilized for guidance of the charged particle flux while the neutral atom flux is affected only by mechanical interaction with the baffles, we can separately direct both species to a region of optimum entry into the discharge chamber.

---

* The following references are representative of these diverging theories:

1. I. Langmuir, Gen. Electric Rev. 26, 731 (1923) (field-emission theory).
2. S. S. Mackeown, Phys. Rev. 34, 611 (1929) (theoretical application of Ref. (1) to mercury arc).
3. J. Rothstein, Phys. Rev. 78, 331, 1950 (modified thermionic emission theory, involving metallic conduction in very dense vapor region on cathode surface).
4. A. E. Robson and A. von Engel, Nature 175, 646 (1955) (electron emission by means of excited atoms).
5. A. Bauer, Z. Physik 138, 35 (1954), Ann. Physik 18, 387 (1956) (combination of thermionic emission with field-emission theory).
6. K. G. Hernqvist, Phys. Rev. 109, 636 (1958) (electron emission by means of excited atoms, mechanism different from Ref. (4)).

\+ For example, the performance of the NASA-LeRC hollow-cathode SERT II thruster has been improved substantially by incorporation of a baffle and a magnetic shield for the cathode; both components were independently invented and their effectiveness was first demonstrated in the LM cathode thruster programs.

A. Theoretical Model for Discharge

In this section we will describe an attempt to evolve a model of the discharge mechanism in an electron-bombardment type ion thruster. The description given should be considered as a first step only. This first attempt at an analytical description of the discharge mechanism evolved early in the research program. At that time high magnetic fields were required to achieve optimum thruster performance with LM cathodes. Toward the end of the contract period and during the life test extensions of this contract, considerable progress was made in lowering the magnetic field required for optimum thruster performance. Because of the differences in magnetic field, this analytical model is only a first order approximation.

We will consider a cylindrical discharge chamber with an LM cathode, installed in the center of one of the end plates. To make the problem tractable the following assumptions will be made:

1. A mercury arc column exists along the center of the discharge chamber at a potential somewhat higher than the ionization potential of mercury (see Fig. 39).

2. All electrons emitted from the LM cathode are trapped in the discharge chamber and diffuse slowly out to the anode.

3. The diffusing electrons produce electron-ion pairs. The production rate is so small that the number of primary electrons far exceeds the number of secondary electrons.

4. The ions accelerate radially inward and cross the center periodically; at the same time, they drift axially with thermal velocity to one of the end plates.

5. The ion density approximately equals the electron density throughout.

6. Because both ions and electrons can commute freely in the axial direction, the radial potential distribution is essentially independent of the axial position.

7. Because of the small number of ionizing collisions, the primary electrons lose little energy in collisions, and their kinetic energy is taken to be equal to the space potential.

8. The radial drift of the electrons results only from classical cross-field diffusion. Anomalous processes are considered unimportant (because of the small magnitude of the magnetic field).

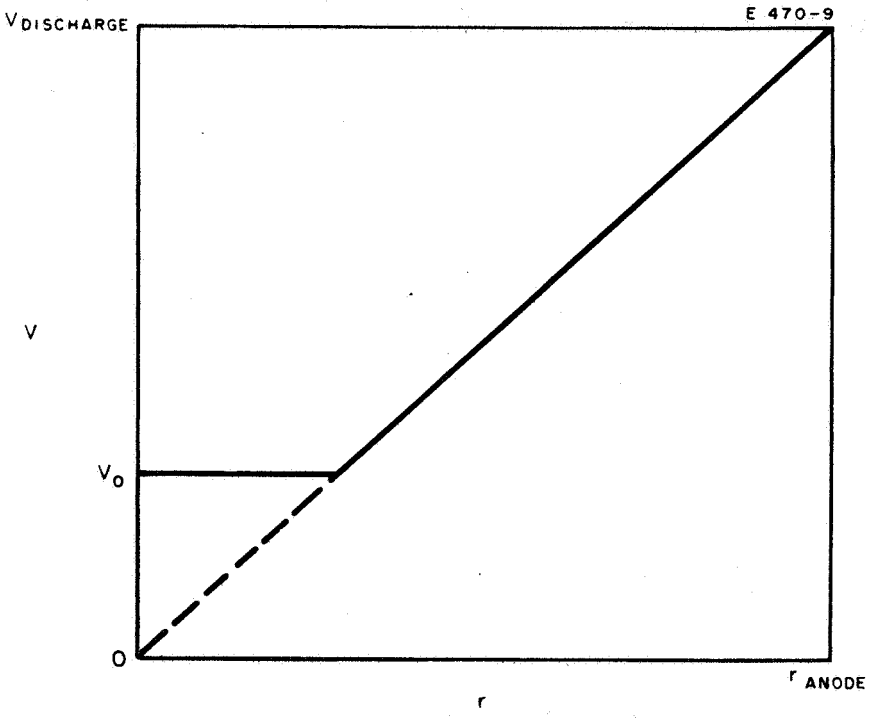

Fig. 39. Assumed radial potential distribution.

The most critical of these assumptions is that relating to the plasma potential distribution. For this reason, the measurement of the plasma potential distribution has been given priority in the experimental investigation of the discharge mechanism.

Under the above assumptions, the radial electron drift velocity can be expressed in MKSA units as*

$$v_d = -\frac{1}{3}\ \frac{m_e^2}{e^2}\ \frac{C_o}{B^2}\ \nu_c\ v^2\ \frac{\frac{d\rho_e}{dr}}{\rho_e}$$

or

$$v_d = -\frac{2}{3}\ \frac{m_e}{e}\ \frac{C_o}{B^2}\ \nu_c\ V\ \frac{\frac{d\rho_e}{dr}}{\rho_e} \qquad (1)$$

where

B	$\equiv$	magnetic induction
C_n	$\equiv$	constants ($n = 0, 1, 2, 3$)
e	$\equiv$	electron charge
m_e	$\equiv$	electron mass
V	$\equiv$	space potential
v	$\equiv$	velocity of electrons corresponding to V
v_d	$\equiv$	radial electron drift velocity
ν_c	$\equiv$	collision frequency of electrons
ρ_e	$\equiv$	electron space charge density.

The radial electron current density is then

$$J = J_o\ \frac{r_o}{r} = -\frac{2}{3}\ \frac{m_e}{e}\ \frac{C_o}{B^2}\ \nu_c\ V\ \frac{d\rho_e}{dr} \qquad (2)$$

* S. Glasstone and R. H. Loveberg, Controlled Thermonuclear Reactions (Van Nostrand, New York, 1960), Chap. 12.

where

J ≡ radial electron current density

r_o ≡ radius of central arc column

J_o ≡ radial electron current density at arc column radius.

We will now estimate the radial potential distribution. We will assume that along the arc column, within a radius r_o, the potential is V_o. At larger radii the potential will be taken to increase linearly with radius

$$V = C_1 r. \tag{3}$$

According to (2), $d\rho_e/dr$ is proportional to $1/r^2$ and

$$\rho_e \propto \frac{1}{r} . \tag{4}$$

We will now determine whether an electron distribution as given by (4) can produce an ion distribution of the same radial dependence — so that neutrality can be preserved throughout. For this purpose we will make two simplifying assumptions. First, we will consider that the ionization frequency ν_i is constant throughout the discharge volume. (Actually, ν_i increases substantially with electron energy and hence presumably with radius. Thus our computation will provide too many ions near the discharge axis.) Second, we will assume that all ions generated within a thin, hollow cylinder of radius r and thickness dr, while moving through the discharge center, will distribute themselves uniformly over the entire cylindrical volume within radius r. (Actually, because the ions move on radial trajectories, they converge more toward the center. Hence, our computation will give a too low ion concentration near the discharge axis. Our two errors thus are in opposite directions and may tend partially to compensate each other.)

The total ion production per unit time in a cylindrical shell of radius r, thickness dr, and length L is

$$q = \nu_i \rho_e 2\pi r L dr.$$

If the charges move to the end plates at velocity v_+, they will accumulate within the cylinder of radius r to a density of

$$d\rho_i = \nu_i \rho_e \frac{L}{r v_+} dr$$

or with

$$\rho_e = C_2 \frac{1}{r},$$

$$d\rho_i = C_2 \frac{\nu_i L}{v_+} \frac{dr}{r^2}.$$

The total ion density at radius r is then

$$\rho_i = \int_r^{r_1} C_2 \frac{\nu_i L}{v_+} \frac{dr}{r^2} = C_2 \frac{\nu_i L}{v_+} \left(\frac{1}{r} - \frac{1}{r_1} \right). \qquad (5)$$

Except close to the chamber wall (at r_1), one can approximate the ion density by

$$\rho_i \cong C_2 \frac{\nu_i L}{v_+} \frac{1}{r} \quad ;$$

therefore, ion and electron densities indeed possess the same variation with radius. In order that their magnitude will also be equal, one must require that

$$\nu_i = \frac{v_+}{L} \quad . \qquad (6)$$

Because ν_i depends upon the average electron energy, eq. (6) can be satisfied by the choice of a suitable discharge potential.

With (2) and (6) we now have two equations which can describe some of the important discharge properties. These two equations predict the following characteristics:

1. According to (2), the discharge can accommodate a wide range of arc currents without a change in discharge potential. This is because as the arc current increases, the charge density increases proportionally, as does the crossed-field diffusion rate. The ratio of ion current to arc current remains independent of the arc current. In actual discharges tested at Hughes Research Laboratories, the discharge voltage indeed varies only slightly with arc current, and at a fixed mass utilization the ion current to arc current ratio is not very sensitive to the arc current.

2. For given discharge potential and arc current, the charge density increases proportionally to the square of the magnetic field. Hence, the ratio of ion current to arc current should increase similarly. In actual discharges, this ratio indeed increases substantially with B.* The fact that the increase is slower than predicted and eventually stops may be attributed to the limited number of neutrals available for ionization.

3. The ratio of ion to arc current can be determined from the following equation, which can be derived from (2) through (5):

$$\frac{I_i}{I_e} = \frac{3}{2} \frac{e}{m} \frac{B^2}{C_3} \frac{\nu_i}{\nu_c} \frac{L}{V_o} r_o (r_i - r_o).$$

With

$$\nu_c \cong 3 \times 10^8 \text{ sec}^{-1} \text{ at } 10^{-2} \text{ Torr}$$

and

$$\nu_i \cong 10^4 \text{ sec}^{-1} \text{ (from eq. (6))},$$

this ratio becomes approximately 1:20, which is relatively close to the observed ratios.

4. The radial variation of the electron and ion density varies as $1/r$, according to (4). A measurement of the extracted ion beam current density gave a curve which closely resembles the $1/r$ variation.

B. Plasma Potential Measurements

From Section VI-A it is apparent that the plasma potential is one of the important parameters which must be known in order that the model proposed for the discharge mechanism of an electron bombardment thruster can be verified. An important consideration in connection with a plasma potential measurement is that the diagnostic tool should not change the potential to be measured. We have investigated two of the various possible measuring techniques: (1) a lithium ion beam probe and (2) a Langmuir probe.

---

* Note that for a fixed discharge chamber geometry and fixed arc current, the discharge voltage also increases with B.

The modulated lithium ion beam probe technique does not perturb the plasma appreciably and does not require that physical probes be placed in the discharge chamber volume. However, no useful potential profiles could be obtained with this method for reasons described below.

The Langmuir probe technique requires the actual insertion of a physical probe into the discharge chamber. Although this must disturb the discharge to some extent, no noticeable deviations of operating conditions were observed as the probe was swept through its range of travel, and the operating characteristics of the discharge chamber with the probe inserted were very similar to those without the probe. Results obtained with this technique are reported in Section VI-B-2.

1. Lithium Ion Beam Probe

Essentially, the modulated lithium ion beam method consists of measuring the time of flight of test charges through the discharge region of interest. The test charges are accelerated to a suitable velocity in a gun by a given potential. The charges then enter the region to be probed. If the potential there is somewhat higher than the potential of the accelerator electrode, the charges will be slowed down. Thus, their flight time is longer than it would be if no retarding potential existed. A value for the average potential along the path of the test particle can be determined by measuring the time delay. This measurement then gives an average potential in the axial direction at one given radial location. In order to obtain the potential profile, measurements must be made at several radial positions by moving the ion gun in the radial direction.

Because the lithium ion beam current was small and the random currents in the mercury plasma were large, a serious signal-to-noise ratio problem arose. To help overcome this problem, the lithium ion beam was density modulated at a high frequency and the detected signal was phase-sensitively detected. This modulation essentially discriminated against the random fluctuations of the plasma. The measurement then consisted of finding the phase shift of the ion beam signal. Successful experiments were conducted, providing potential profiles of the "vacuum" condition, i.e., without a plasma present. However, it was not possible to make a potential profile measurement with a plasma present. A probable reason for the lack of signal is scattering of the lithium ion beam and resulting low transmission.

2. Langmuir Probe

A Langmuir probe immersed in a plasma will collect a certain current, depending on the potential of the probe and its physical shape. When biased strongly negative with respect to plasma potential, the electrons of the plasma are repelled from the probe and saturation ion current is drawn by the probe from the plasma. As the negative bias is reduced to zero, even the slowest of the plasma electrons are collected by the probe, so that ad-

vancing to a positive probe bias creates no further increase in the electron current collected by the probe. The current-voltage characteristic exhibited by a Langmuir probe is distinguished by an electron-repelling region in which the electron current changes markedly with respect to probe potential, terminated by a transition to an electron-saturation region which exhibits no variation in electron current as a function of probe potential.

Under conditions where the dimensions of a Langmuir probe are large with respect to the plasma Debye length, the transition from the electron-repelling region to the electron-saturation region of the current-voltage characteristic is quite abrupt and can be used to determine the value of the plasma potential. For the case of interest in our experiment, however, we wish to use the smallest probe possible to avoid disturbing the properties of the plasma which we wish to measure. Because this plasma has a relatively low number density and a relatively high electron temperature, the probe diameter cannot be much larger and in fact is comparable in size to the Debye length. This condition results in a rounding of the knee which marks the transition between the electron-repelling region and the electron-saturation region, thereby obscuring the exact value of the plasma potential. Nevertheless, the value of the plasma potential can be determined accurately by the use of thermionically emissive probe.

A Langmuir probe may be heated so that it will emit electrons thermionically. If such a probe is biased positively with respect to the plasma potential, the thermionic electrons are not able to leave the probe and no emission current results. When the probe is biased negatively with respect to the plasma potential, thermionic electrons are emitted, causing a major change in the current-voltage characteristic from the form exhibited by a nonemitting probe. By comparing the current-voltage characteristic of an emitting probe with that of a nonemitting probe it is possible to determine the probe potential at which the electron emission first decreases; the location of this point determines the plasma potential. To obtain a clear indication of plasma potential by use of the emissive probe technique, it is desirable to thermionically limit the electron emission current I_t to a value which is less than the amount which can be neutralized by the plasma's random ion current I_i in the vicinity of the probe:

$$I_t < I_i \sqrt{\frac{m_i}{m_e}}$$

Then, so long as the probe is negative with respect to the plasma potential, the total emitted electron current (within the above limit) flows freely from the probe into the plasma without setting up a space charge barrier. As the probe is biased positive with respect to the plasma, the emitted current decreases at an exponential rate, providing a clear indication of plasma potential.

Once the plasma potential has been determined at a given position, the probe can be moved to some other point in the region and another determination can be made. After several measurements have been made in a given plane in the discharge chamber, a potential profile for that plane can be drawn.

The actual probe (see Fig. 40) consisted of a U-shaped 75-μm diameter tungsten wire; the U was 1.5 mm high, with legs 0.75 mm apart. This probe was supported by 0.25-mm diameter tungsten wire legs, enclosed in a ceramic insulator. The outside diameter of the tube was 1.25 mm. The probe was mounted on a movable feedthrough to permit measurement of the potential at various locations within the discharge chamber. For the case of the thermionic cathode, using an argon or mercury plasma, the probe was moved linearly across half the discharge chamber in a plane 2.5 cm from the discharge-chamber end plate. For the LM cathode, the probe projected approximately 7 cm into the plasma, making a 45° angle with the axis of the discharge chamber. The probe was rotated about a line parallel to the discharge chamber axis but displaced along a radius toward the anode. It was thus possible to scan across the complete diameter of the discharge chamber at the midplane.

The electronic circuitry for the probe was extremely simple. The probe was heated by a floating power supply. The probe voltage was referenced to the discharge chamber end plates, and probe current and voltage were recorded on an X-Y recorder.

When data were taken, the emissive characteristic was plotted first; the probe heater power then was decreased so that no emission took place, and the characteristic was retraced. The probe was kept warm at all times so that the surface remained clean.

A typical result is the potential distribution shown in Fig. 41 for an argon discharge with a thermionic cathode operating at an arc voltage of 30 V, an arc current of 0.85 A, and a magnetic field of 10 G. In this case the plasma potential is relatively uniform across the discharge chamber, dropping off to anode potential near the anode surface.

A typical potential profile for a simulated 15-cm ion thruster operating with an LM cathode is shown in Fig. 42. This case is for an LM cathode recessed into a magnetic shield and operating with a centered floating baffle at an arc voltage of 30 V, an arc current of 8 A, an electron-to-atom ratio of 26, and a magnetic field of 120 G. Here the potential profile is depressed on the axis with a relatively small potential gradient at the center and a large potential gradient going toward the anode. The potential profile is relatively insensitive to changes in the electron-to-atom ratio, and the potential depression increases when the applied magnetic field increases. The potential depression also increases when the arc current decreases. In the limit of zero arc current, where no

M 4157

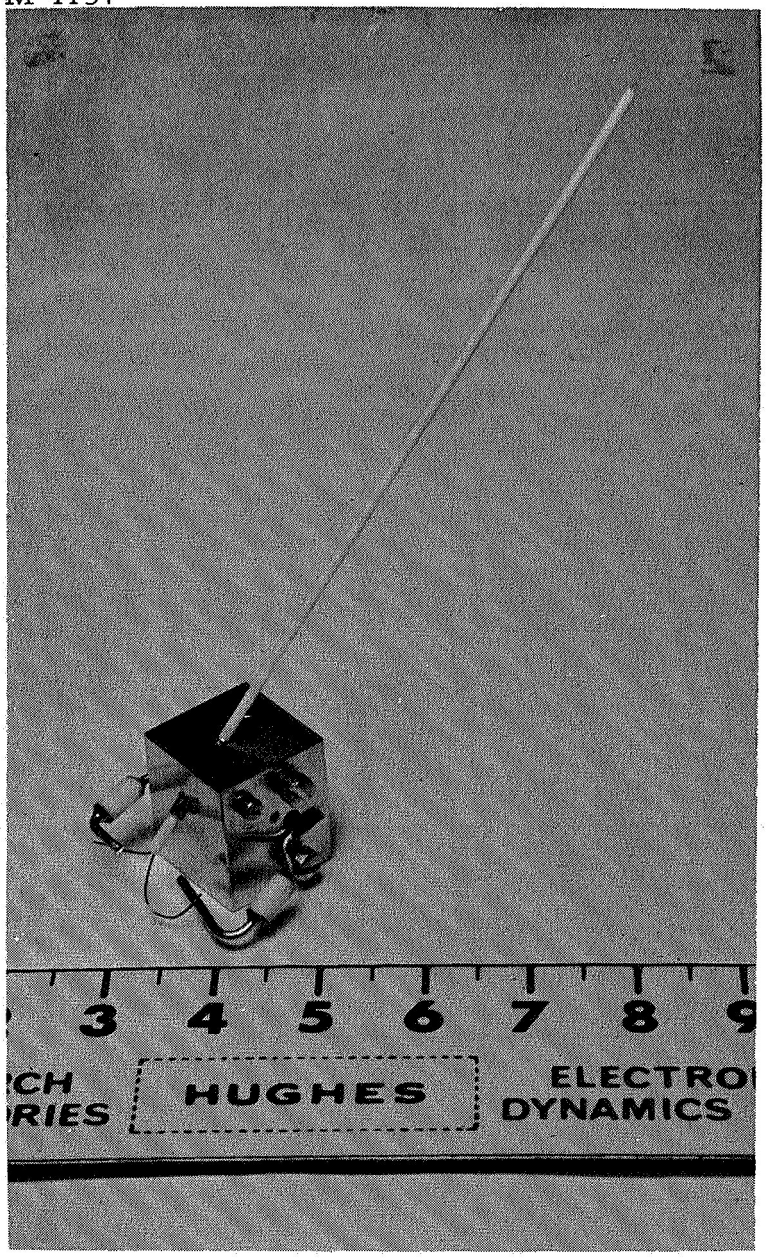

Fig. 40. Plasma potential probe.

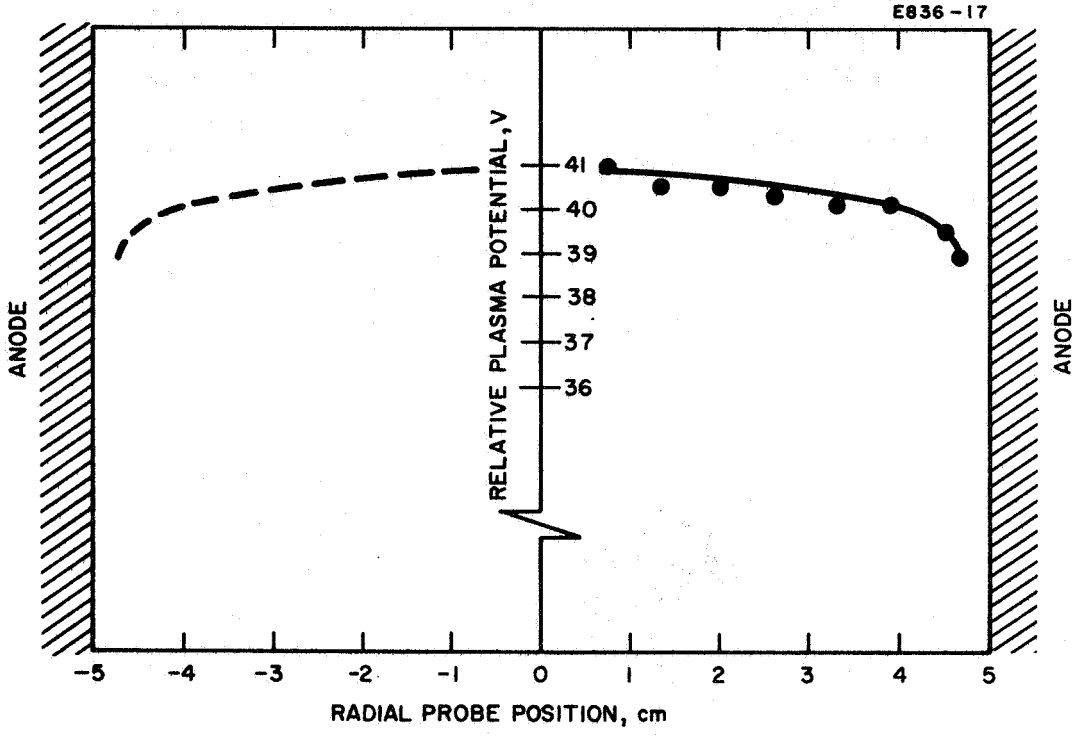

Fig. 41. Typical plasma potential profile for ion thruster operating with thermionic cathode.

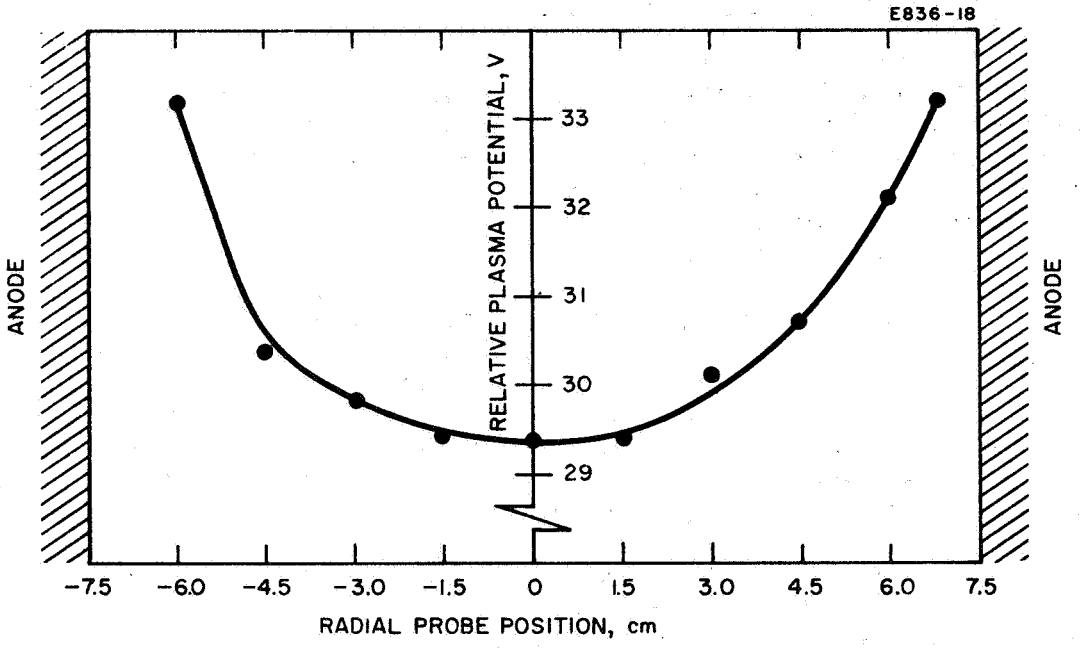

Fig. 42. Typical plasma potential profile for LM cathode ion thruster.

plasma exists, the vacuum potential profile is obtained; comparison with the theoretically expected profile can serve as a test for the measuring technique.

C. Experimental Study of Configuration Effects

The thruster geometry used at the beginning of the contract period was identical to that of the conventional Kaufman thruster, as implemented in the 20-cm NASA-LeRC unit. The most important modification in improving performance with an LM cathode was the insertion of a baffle, as described in Section V. While the first part of the life test was in progress, additional experiments were performed on laboratory-type thrusters of flexible geometry, with the following results:

In a thruster with permanent-magnet type geometry (i.e., with a soft-iron upstream end plate) it was found advantageous to use the baffle to shield the plasma region magnetically immediately downstream from the cathode. This provided a cyclotron radius larger than the baffle for the electrons in the low field region between the cathode and baffle, allowing them to diffuse around it more readily; this decreased the arc resistance and the source energy per ion expended in the discharge chamber.

The influence of the magnetic field geometry was investigated using a thruster equipped with Helmholtz coils, a segmented anode, and a beam scanning device. In all configurations tested, the best performance (high mass utilization, low source energy per ion) resulted when nearly all (> 90%) of the arc current was collected on the anode segment nearest the extraction electrodes. This was possible only with magnetic fields which diverge in the downstream direction. With convergent magnetic fields the major fraction of the cathode current was collected on the farthest upstream segment of the anode, resulting in very poor performance. It was also found that the anode segments which did not collect appreciable fractions of the current could be run at cathode potential with no change in performance or discharge voltage. However, if an anode segment which was collecting current was run at cathode potential, the beam current changed only slightly while the discharge voltage increased, because the electrons were forced to cross more flux lines to reach the active anode.

The effect of the magnetic field divergence is demonstrated by the ion beam profiles shown in Fig. 43. It is seen that the ion current density distribution becomes much more peaked as the field is changed from divergent to convergent.

Figure 44 shows beam profiles taken with a divergent magnetic field with and without a central-disk baffle. The baffle flattens the distribution while raising the beam current by nearly a factor of two in the

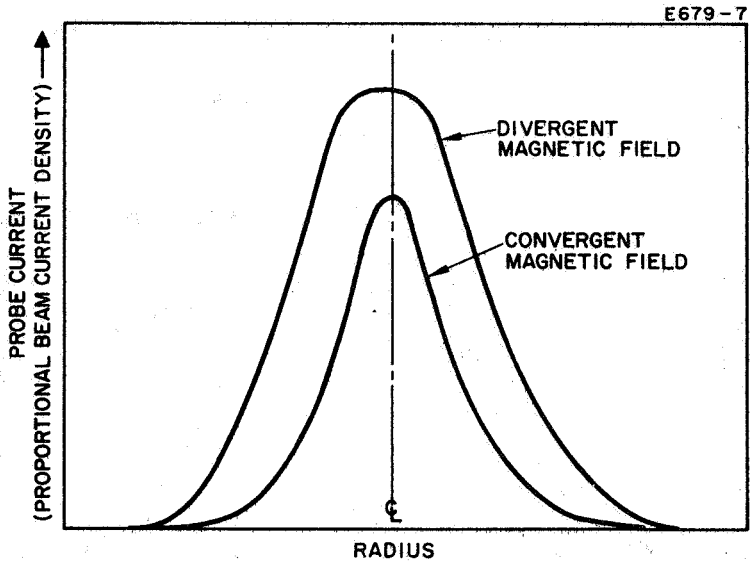

Fig. 43.
Effect of magnetic field divergence on beam profile measured 3 cm downstream of accel electrode. The total width of the graph represents 25 cm diameter; the thruster diameter was 20 cm.

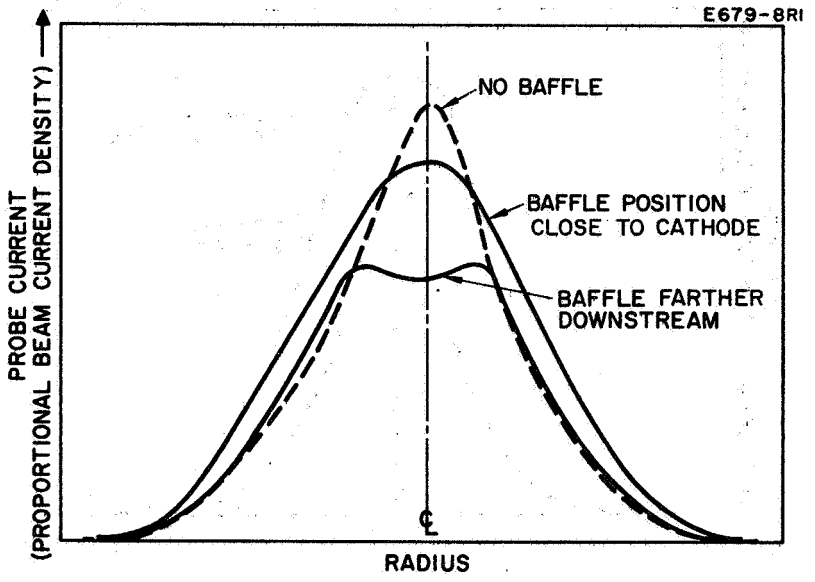

Fig. 44.
Effect of the central-disk baffle on beam profile measured 3 cm downstream of accel electrode. The total width of the graph represents 25 cm diameter; the thruster diameter was 20 cm.

example given. (Note that because of the rotational symmetry, an integration over the entire extraction area will weight the off-axis contributions to the beam current in proportion to their distance from the axis.)

When the baffle is moved downstream (with a divergent magnetic field), the distribution becomes double peaked. This results because under these conditions the energetic primary electrons (which contribute heavily to ion generation) cannot travel far enough between baffle and extraction system to have a sufficient probability for diffusing into the "magnetic shadow" of the baffle.

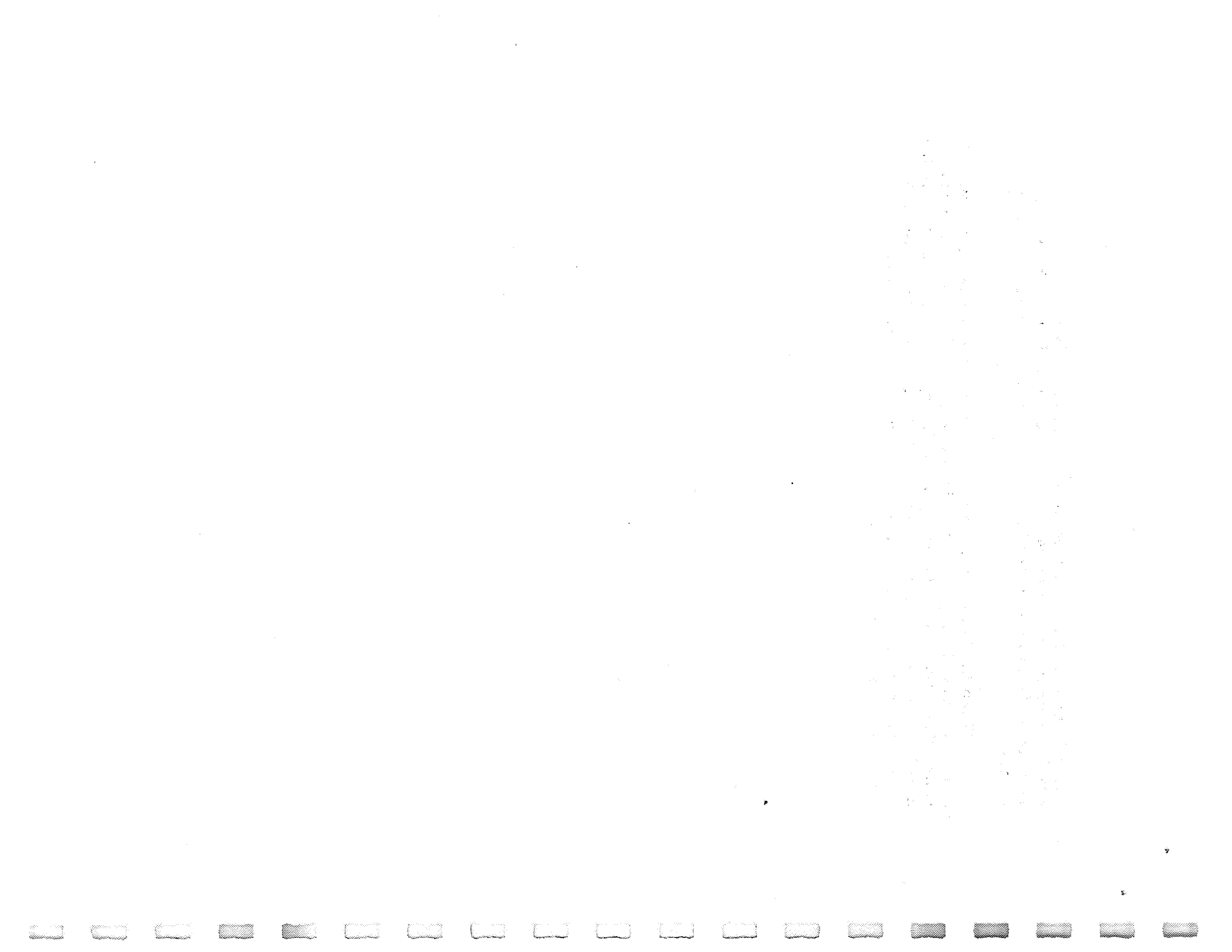

PRECEDING PAGE BLANK NOT FILMED.

VII. RELIABILITY AND QUALITY ASSURANCE

The LM cathode and thruster components which were fabricated for the life test were carefully constructed to stringently controlled dimensions and processing techniques as specified by controlled drawings released by the project engineer. Complete inspection of critical dimensions was invoked when necessary to insure adherence to the drawings. Material purchased for use on the test items was reviewed by receiving inspection and submitted to the project engineer for approval before release to the fabrication areas.

Certificates of compliance and chemical and physical analyses of raw materials were placed on file, after acceptance, with the purchase orders in the receiving department. The following process specifications were utilized during the fabrication and assembly of the LM cathode and thruster prior to and during the tests.

1. IPD-PR-003 Cleaning Procedure for Stainless Steel Parts
2. IPD-PR-014 Dry Hydrogen Firing Moly Parts
3. IPD-PR-015 Dry Hydrogen Firing Stainless Steel Parts
4. IPD-PR-016 Cleaning & Firing of Ceramic Parts
5. IPD-PR-026 Stress Relieving Moly Electrodes
6. IPD-PR-027 Cleaning Moly
7. IPD-PR-031 Cleaning of Swagelok Fittings

The equipment and data logs, as submitted and approved by the NASA Project Manager, were utilized for documenting all significant data and happenings associated with the unit, including assembly, inspection, testing, and operating time. These forms were used throughout the life test. All discontinuances of the test which occurred and are noted in the log were due to the ground test environment and to periodic preventive maintenance of the vacuum facility. These are discussed in detail in Section V-E-4 of this report. The ground environment effects were not under test as specified by the contract; therefore, failure reports and corrective action were not initiated. It should be noted that no intrinsic failure of cathode, thruster, feed system, or neutralizer occurred during the entire test period.

Operating procedures were designated by the responsible program manager and consisted of rigid processing or operating rules. These precautions insured the uniformity of applied procedures necessary to run the

test for long periods of time.

Throughout the testing program the Hughes Primary Standards Laboratory provided calibration of all measuring equipment on a periodic basis. This calibration was done with equipment directly traceable to the National Bureau of Standards. In addition to the periodic inspection, the equipment was calibrated both before and after the life tests.

VIII. PRESENT STATUS AND CONCLUSION

While the life test was performed with an LM cathode kept at $\approx 35^{\circ}C$, LM cathodes which are designed for temperatures of $\approx 300^{\circ}C$ have since been operated successfully in our laboratory under Contract NASW-1404. Performance equalling that of the life-test thruster has been achieved using such high-temperature LM cathodes and a light-weight permanent magnet thruster, thus eliminating the magnet power and the associated system weight. Thruster designs have been developed in which the cathode is cooled by radiation from the structural elements of the thruster itself. A purely electrical ignitor with no moving parts has also been demonstrated and would replace the one shown in Fig. 22 in a flight-type thruster.

These above developments and the following results of the life test -

- the absence of any cathode degradation after $>5,000$ hours of operation
- the complete stability of the thruster characteristics over $>4,000$ hours of test
- the extrapolated accelerator lifetime of $>10,000$ hours
- the complete insensitivity of thruster and cathode to intermittent operation and exposure to air (even by catastropic vacuum failure)
- the demonstration of 85% mass utilization at a power expenditure of 393 eV/Hg ion, with further drastic performance improvements in sight*

- permit the conclusion that thruster systems based on the LM cathode are competitive with any present electric propulsion system and attractive for actual space missions.

---

* Note added in proof: Since this report was written, some of the expected performance improvements have already been achieved at our laboratory. 85% mass utilization at a total power expenditure of ≈ 250 eV/ion (recall that no heater or vaporizer power is required with this cathode) has been obtained as a result of work under Contract JPL 952131, Subcontract under Contract NAS 7-100 (Task Order RD-26).

PRECEDING PAGE BLANK NOT FILMED.

APPENDIX—INVENTIONS AND NEW TECHNOLOGY

A. Patentable Inventions

During the investigations reported here, three inventions believed to be patentable have been reduced to practice for the first time. Two of these inventions were implemented with contract funding and are described in Patent Disclosures which have been forwarded to NASA Western Operations Office for further processing. The third invention was conceived and its feasibility demonstrated during a Company-funded program carried out simultaneously with the life-test extensions of the subject contract.

The patent docket numbers, titles, names of inventors, and dates of first drawing or written description of these inventions are listed below; also shown are the sections of this report describing the use of these inventions.

PD 67063 "Large Length to Diameter Ratio Filter or Impedance," by J. A. Snyder, March 23, 1966 (Section III-D of this report)

PD 67064 "Liquid Metal Propellant Refill System," by T. A. Planz, August 14, 1965 (Section III-C of this report)

PD 7025 "Liquid-Mercury Flow Meter," by H. J. King, W. O. Eckhardt, and J. A. Snyder, April 28, 1966 (Section III-E of this report).

B. New Technology

All experimental results described in this report have been obtained without requiring the use of new technologies beyond those developed and reported under the preceding Contract NAS 3-4118.

DISTRIBUTION LIST

	Number of Copies
National Aeronautics and Space Administration Washington, D. C. 20546	
Attention: RNT/James Lazar	1
RNT/J. Mullin	1
National Aeronautics and Space Administration Lewis Research Center 21000 Brookpark Road Cleveland, Ohio 44135	
Attention: Spacecraft Technology Procurement Section, MS 54-2	1
Technology Utilization Office, MS 3-19	1
Technical Information Division, MS 5-5	1
Library, MS 60-3	2
Spacecraft Technology Division, MS 54-1	
C. C. Conger	1
J. Sovey	1
R. R. Nicholls	5
H. R. Hunczak	1
Electric Propulsion Laboratory, MS 301-1	
W. Moeckel	1
H. R. Kaufman	1
E. A. Richley	2
Report Control Office, MS 5-5	1
National Aeronautics and Space Administration Scientific and Technical Information Facility P. O. Box 33 College Park, Maryland 20740	
Attention: NASA Representative RQT-2448	6
National Aeronautics and Space Administration Marshall Space Flight Center Huntsville, Alabama 35812	
Attention: Ernest Stuhlinger (M-RP-DIR)	1
I. Dalins	1
National Aeronautics and Space Administration Ames Research Center Moffett Field, California 94035	
Attention: Library	1

National Aeronautics and Space Administration
Langley Research Center
Langley Field Station
Hampton, Virginia 23365
Attention: Technical Library — 1

National Aeronautics and Space Administration
Goddard Space Flight Center
Greenbelt, Maryland 20771
Attention: Mr. W. Isley, Code 734 — 1

National Aeronautics and Space Administration
Western Operations
150 Pico Boulevard
Santa Monica, California 90406
Attention: Mr. F. A. DiLorenzo — 1

Research and Technology Division
Wright-Patterson AFB, Ohio 45433
Attention: AFAPL (APIE) Major P. E. Peko — 1

AFWL
Kirtland AFB, New Mexico 87417
Attention: WLPC/Captain C. F. Ellis — 1

Aerospace Corporation
P. O. Box 95085
Los Angeles, California 90045
Attention: Library/Technical Documents Group — 1

Jet Propulsion Laboratory
4800 Oak Grove Drive
Pasadena, California 91103
Attention: Mr. D. Kerrisk — 2
Technical Library — 1

Electro-Optical Systems, Inc.
300 North Halstead
Pasadena, California 91107
Attention: Mr. R. C. Speiser — 1
Mr. G. Sohl — 1
Mr. J. A. Wolters — 1

TRW Inc.
TRW Systems
One Space Park
Redondo Beach, California 90278
Attention: Mr. D. B. Langmuir 1
Mr. E. Cohen 1
Mr. D. Goldin 1

Westinghouse Astronuclear Laboratories
Electric Propulsion Laboratory
Pittsburgh, Pennsylvania 15234 1

General Electric Space
Flight Propulsion Laboratory
Cincinnati, Ohio 45215
Attention: Mr. M. L. Bromberg 1

United Aircraft Corporation
Research Laboratories
East Hartford, Connecticut 06108
Attention: Mr. R. G. Meyerand, Jr. 1

Colorado State University
Fort Collins, Colorado 80521
Attention: Mr. L. Baldwin 1
Mr. W. Mickelson 1

U. S. Atomic Energy Commission
P. O. Box 62
Oak Ridge, Tennessee 37831
Attention: Technical Information Service Ext. 1

Republic Aviation Corporation
Plasma Propulsion Laboratory
Farmingdale, Long Island, New York 11735
Attention: A. Kunen 1

United States Air Force
Office of Scientific Research
Washington, D. C. 20025
Attention: Mr. M. Slawsky 1

Case Institute of Technology
10900 Euclid Avenue
Cleveland, Ohio 44106
Attention: Dr. Eli Reshotko 1

Gruman Aircraft Engineering Corporation
Bethpage, Long Island, New York 11101
Attention: Mr. I. Tobias — 1

Northrop Corporation
Hawthorne, California 90250
Attention: P. Lenn — 1

General Electric Company
Missile and Space Division
Space Sciences Laboratory
P. O. Box 8555
Philadelphia, Pennsylvania 19101
Attention: Dr. P. Gloevsen — 1

The Royal Institute of Technology
Stockholm 70, Sweden
Attention: B. Agduv — 1

University of Washington
Department of Electrical Engineering
Seattle, Washington 98105
Attention: Mr. H. Golde — 1

Bell Telephone Laboratories
Murray Hill, New Jersey 07971
Attention: Dr. Buchsbaum — 1

University of Sheffield
Department of Electrical Engineering
Mappin Street
Sheffield 1, England
Attention: Mr. A. L. Cullen — 1

Services Electronics Research Laboratories
Baldock, Herts, England
Attention: Dr. Boot — 1

Standard Telephone Laboratories
Harlow, Essex, England
Attention: Mr. E. A. Ash — 1

The University
Department of Electrical Engineering
Mayfield Road
Edinburgh 9, Scotland
Attention: Dr. B. Meltzer — 1

Rome Air Development Center
Headquarters--Air Force Systems Command
Griffis AFB, New York 13442
Attention: RALTP 1

Swiss Federal Institute of Technology
Zurich, Switzerland
Attention: The Library 1

Nagoya University, Chikusa-ku
Institute of Plasma Physics
Nuclear Fusion Research Group
Research Information Center
Nagoya, Japan
Attention: Mr. Y. Y. Terashima 1

LTV Aero Space Corporation
Adv. Sys. Astro. Div.
P. O. Box 6267
Dallas, Texas 75201
Attention: Mr. F. T. Esenwein 1

Cornell Aeronautical Lab., Inc.
Buffalo, New York 14221
Attention: Prof. A. S. Gilmour, Jr. 1
Mr. D. Lockwood 1